Millennial Indian Monsoon variability and forcing during the Holocene as revealed by the Qinghai Lake, Yunnan Province Record

Cairns Harrison
Project Supervisor: Professor Jaime Toney
BECS Research Group

Submitted in fulfilment of the requirements for the
Degree Master of Sciences by Research

School of Geographical and Earth Sciences
College of Science and Engineering
University of Glasgow

October 2018

Abstract

The Indian Summer Monsoon (ISM) is an incredibly influential climate system, with many developing nations and over 1 billion people reliant upon favourable monsoon conditions. A suite of organic paleoclimate proxy biomarkers was extracted from sediment core samples retrieved from Qinghai Lake, Yunnan Province, southwest China in order to reconstruct various climate parameters at high-resolution in the region throughout the Holocene. The main aim of the project is to investigate changes caused by the ISM. The upper 145cm of the core were analysed covering an age range of 8877 cal yr BP (calibrated years before present) to -16 cal yr BP (cal yr BP denotes calibrated years before present hereafter). The results indicate several distinct climatic regimes, often separated by abrupt changes in climate. From 8877 cal yr BP to 6895 cal yr BP multiple proxies imply a prolonged period of warm, wet climate and thus an intense ISM system during this period which likely represents the Holocene Climatic Optimum (HCO). Between 6895 cal yr BP and 3240 cal yr BP the climate becomes much more chaotic with several distinct drops and spikes in temperature and changes in precipitation illustrated by the average chain length (ACL) and short to long-chain acid ratio. Overall, during this period the climate was more arid with a weaker monsoon in the Yunnan province than during the HCO, but there was a high degree of variation in monsoon intensity indicated by almost all proxies with rapid changes in precipitation. ACL values sharply spiked to high values similar to the HCO period from 3540 cal yr BP to 3240 cal yr BP. Following on from 3240 cal yr BP to 1130 cal yr BP, a high value ACL plateau along with P_{Wax}/P_{Aq}, and acid ratio data indicates a warm, wet period and the return of strong monsoon intensity during the Roman Warm Period (RWP). A brief cool, dry period with a weaker monsoon followed by a rapid rise in temperature and monsoon intensity between 1133 cal yr BP-755 cal yr BP likely represents the Medieval Warm Period (MWP). Over the final 755 cal yr BP to -16 cal yr BP period of this record the ACL, carbon preference index (CPI), acid ratio and P_{Wax}/P_{Aq} record suggests progressively cooler and increasingly intense monsoon conditions during the Little Ice Age (LIA) towards the present in the Qinghai Lake region.

Contents

List of Tables

List of Figures

Acknowledgements

There are several acknowledgments I must make to the many who helped me towards completing this body of work. Firstly, I owe a huge debt of gratitude to the Leverhulme Trust, and my employers at Sainsbury's who helped me massively towards funding the costs of this project. I want to thank Professor Toney for giving me the chance to study such an interesting topic as part of the BECS group and for her help along the way. I would have been unable to complete this project without the guidance of Ali Salik, an excellent lab technician who taught me the majority of the processes undertaken in this project and provided a tremendous amount of assistance throughout this research masters. The knowledge and input from PhD candidates Charlotte Slaymark, Bianca Cavazzin, Mike Zwick and Postdoctoral Research Associate Dr Julien Plancq was invaluable in helping me understand the context of aspects of lab work and various processes involved in biomarker research. In particular, Mike sacrificed a great deal of his time to help me with several technological problems and he has imparted a great deal of wisdom in the process. I am very thankful for his kindness and help as he saved me a great deal of time and stress. I also want to thank my fellow master's student Anca Amariei for her advice and help throughout.

Of course, I owe a great deal to my parents, and like most people I cannot express how grateful I am for them, nor thank or repay them enough for the unconditional support they have provided for me. Finally, I want to thank my partner Eilish, who has also consistently and unconditionally supported me through the most difficult periods of this master's. No matter how moody or frustrated I became with the work, she persistently, and always positively, encouraged me towards finishing.

Declaration

I declare that, except where explicit reference is made to the contribution of others, that this thesis is the result of my own work and has not been submitted for any other degree at the University of Glasgow or any other institution.

1 Introduction

The Indian Summer Monsoon (ISM), part of the collective Asian Summer Monsoon climate system, is one of the most anticipated, geographically widespread and historically well documented examples of weather phenomena in the world. Despite this, it remains a notoriously chaotic and unpredictable weather system (Goswami and Ajaya Mohan, 2001) that demands further research due to the significant influence it exerts on the economic, environmental and social sectors of several nations in southeast Asia (Gautam *et al*., 2009; Ghosh *et al*., 2016; Xavier *et al*., 2007). Despite its nomenclature, the ISM range spans much wider than India's borders. Southeast Asia is one of the most densely populated regions in the world (Gautam *et al*., 2009), with well over 1 billion people living in areas that are affected annually by the Indian/Asian Summer Monsoon, which includes regions of Bangladesh, Bhutan, China, India, Nepal, Pakistan and Vietnam among other nations. Any deviance from 'normal' or 'desirable' summer monsoon conditions in terms of precipitation can have disastrous consequences on the communities that live under the influence of the ISM (Ghosh *et al*., 2016). A deficit of precipitation causes droughts, while a surplus causes flooding. Extreme variation from the most desirable monsoon conditions on either end of the spectrum, often takes a particularly harsh toll on the agricultural sector of afflicted nations (Xavier *et al*., 2007). A year of extreme monsoon conditions can leave communities unable to grow crops. There is still a relatively high proportion of families living a subsistent lifestyle in the developing nations within the ISM range, and these extreme variations cripples their ability to feed themselves. Outside of subsistence communities, these extremes of monsoon conditions damage the local and national economies respectively, as many countries' economies in the ISM region rely heavily on their agricultural sectors. For example, over 600 million people living in the Gangetic Plains depend upon the hydrological and agricultural resources influenced by the monsoon (Gautam *et al*., 2009). In India, around 58% of the working population are employed in the agricultural sector (from industrial to subsistence farming), which makes up around 17% of the GDP compared to UK's 0.6% in 2015/17 (IBEF, 2018; Madhusudhan, 2015). Flooding from the monsoon causes the most damage and takes the highest toll on effected nations. During the 2017 ISM, over 1.5 million homes in Bangladesh and India were destroyed or badly damaged by the flooding, with almost 1300 confirmed deaths and likely over 45 million people directly affected (UNICEF, 2018). Therefore, understanding ISM variation through time is vital to assisting those who are so reliant on it producing favourable conditions, and anticipating the future of the ISM in a rapidly changing global climate.

Included in the regions that are affected by the ISM, is the Yunnan Province in southwestern China. This project will utilise a range of biomarkers extracted from a 1.56m section of a 22.5m sediment core from Lake Qinghai (25°07′57″N, 98°34′18″E,

Figures 1 and 2) to reveal changes in paleoclimatic factors that will provide insight to alterations in the ISM throughout most of the Holocene period. Specifically, this project aims use biomarkers to reconstruct factors that infer changes in the character of the ISM such as precipitation and lake temperature. These factors are strong indicators of the character of the ISM and increases in both can indicate a stronger ISM. Biomarkers are chemical compounds produced by biological processes in living organisms. They can be used to infer changes in environmental parameters that influence the biological processes within these organisms. One type of biomarker that has been proven as robust is a class of lipids known as n-alkanes, which are slow degrading biomarkers that derive from plant leaf waxes (Eglington and Hamilton, 1967). These n-alkanes enable investigation into changes in vegetation that subsequently infer changes in temperature, precipitation and quality of organic matter preservation with the use of various equations to calculate parameters such as the n-alkane average chain length, proportion of terrestrial/aquatic material input and the carbon preference index (Baker *et al*., 2016; Zhou *et al*., 2005). These parameters when calculated allow further inferred analysis of changes in the ISM.

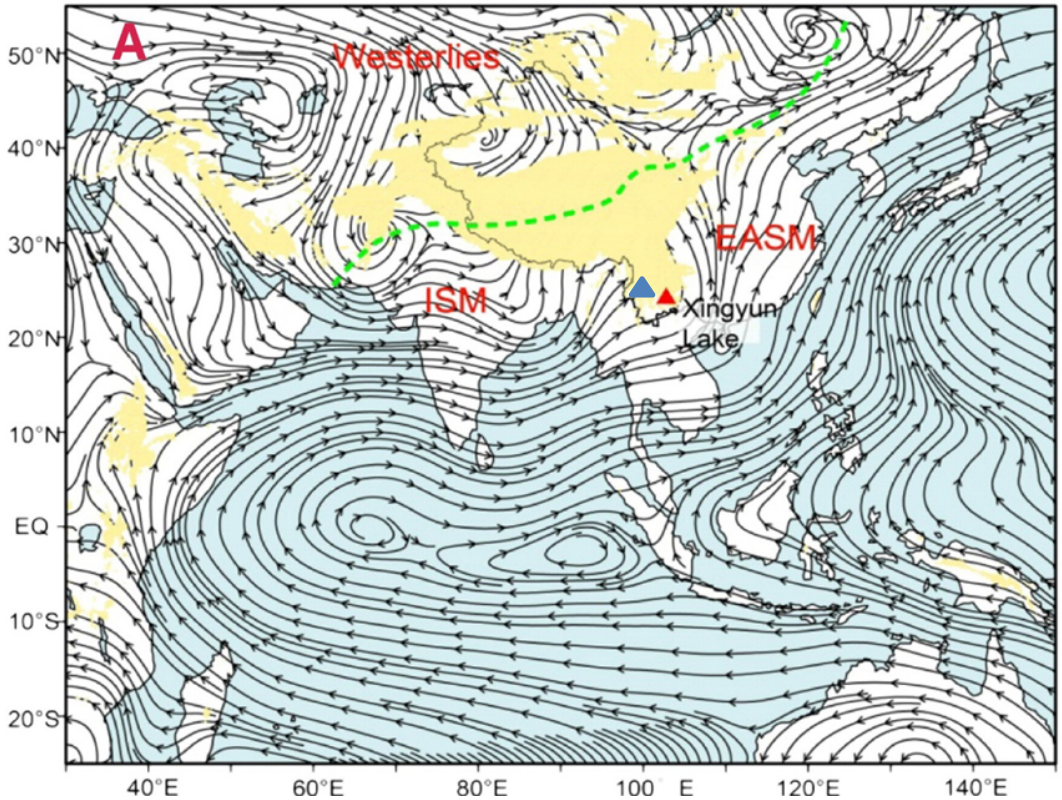

Figure 1: Revised, annotated average 850hPa streamline data during June-July-August based on the National Center for Environmental Prediction/National Center for Atmospheric Research reanalysis. Black lines indicate atmospheric circulation systems, showing the transport of moisture from the Bay of Bengal towards the study regions, the blue triangle indicates the approximate location of Qinghai Lake (Modified from Chen *et al*., 2014).

Figure 2: Annotated satellite image of Qinghai Lake and the surrounding catchment area (Google Maps, 2018).

Several comprehensive studies have shown that alkenones can act as a very effective proxy for lake surface temperature reconstruction. Haptophyte algae have been shown to produce different ratios of di-, tri- and tetra-unsaturated alkenones, which are measured and used in an alkenone index to calculate temperature in marine systems (Brassell *et al*., 1986; Muller *et al*., 1998). Species-specific calibrations are needed for accurate temperature calculations, particularly in lacustrine environments due to wider algal genetic diversity (Theroux *et al*., 2013), but if found alkenones will be a valuable tool. The same can be said of long-chain diols, which also act as a proxy for lake surface temperature change (Rampen *et al*., 2014a) using the long chain diol index developed by Rampen *et al.* (2012). But again, care must be taken in lacustrine environments, diols are a particularly new proxy and therefore require more research before becoming completely reliable. Sterols and hopanes may provide insight to human influences, and further hopanes can point to terrestrial soil bacterial input to the lake system and therefore precipitation rates but neither proxy will be a major focus of biomarker analysis. Finally, long-chain and short-chain fatty acids can enable investigation of vegetation surrounding the lake and also provide insight to precipitation changes through the ratio of short to long chain acids (Hou *et al*., 2006).

This suit of proxies when used in combination with one another can unveil likely changes in climate, qualitatively and quantitatively, to help improve our collective understanding of the ISM throughout the Holocene. This project will specifically focus on biomarker analyses, providing insight from previously living, organic sources. In the future this body of work may be compared to inorganic, paleomagnetic and elemental analyses completed by our colleagues at Sun Yat-Sen University to investigate whether these different forms of analysis corroborate each other and work synergistically to add value to characterising the ISM in parts of China.

There has been significant attention paid to the monsoon system with many similar climate reconstructions undertaken in the Yunnan Province in the past (Cook *et al*., 2012; Shen *et al*., 2006; Xiao *et al*., 2014, 2015; Xu *et al*., 2015; Yang *et al*., 2016). However, any additional data is a positive contribution towards understanding the monsoon. It has been noted in other research that much of the paleoclimate reconstruction work undertaken in Yunnan Province has occurred in the northwest of the region (Yang *et al*., 2016) in Lake Erhai/Shudu/Tiancai, for example, while Qinghai Lake lies in the southwest of the province, an area from which relatively few reconstructions have been produced.

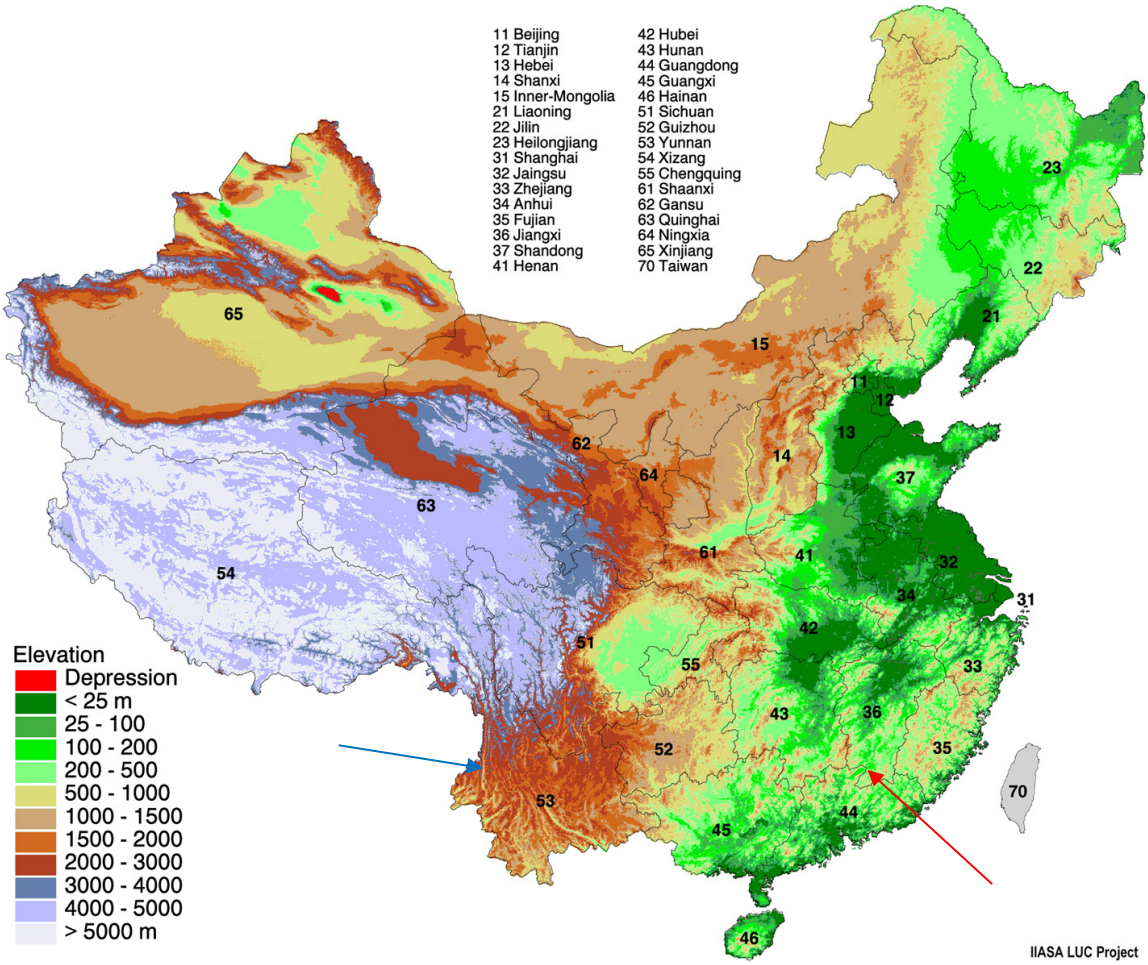

Figure 3: Elevation map showing the location of provinces within China with bracketed elevations indicated by different colours. The Dingnan peat sequence lies just north of the '44' label marked by the red arrow, with Qinghai Lake's location indicated by the blue arrow. This illustrates the Yunnan province and Qinghai Lake lie at high elevation between (1500 and 2500 m)(U.S. Geological Survey, EROS Data Center, 2018).

The Qinghai Lake region is fairly high elevation (on average over 1500-2500m elevation, Figure 3), lying to the southeast of the Tibetan Plateau in the western Gaoligong mountains. Qinghai Lake is situated at 1849m above sea level. The lake is fed by groundwater and precipitation with no in/outflowing river system contributing

to lake level change (Wang *et al.*, 2002). This makes it sensitive to responding to changes in the monsoon, as lake level changes are solely influenced by precipitation and evaporation. The primary control of climate in the Yunnan province is the ISM and the pressure systems which drive it (Figure 1). Here we present the results of this multi-proxy, biomarker, sediment core record of Holocene climate in southwest China, along with interpretations of the various climate events they represent and potential causes.

2 Methodology

The methodology used in this experiment from gathering samples in the field, to lab preparation of samples and the eventual analysis and processing of sample results is detailed in this section. The methodology was split into three main sections with a small fourth section. The first will cover the fieldwork carried out by project supervisor Professor Jaime Toney and a colleague, Professor Xiaqiang Yang from Sun Yat-Sen University, Guangzhou, China. The second section will cover the Biomarkers for Environmental and Climate Science (BECS) wet lab processes undertaken here at Glasgow University that were crucial to preparing the samples for analysis. The third section will cover the analysis of the samples in the Gas Chromatography (GC) Lab, also located in the Gregory Building at Glasgow University, the equipment used in this analysis and the processing of results. The fourth and final section will cover the core age dating process.

2.1 Fieldwork:

The fieldwork section of this project was carried out by project supervisor Professor Jaime Toney in collaboration with Professor Xiaqiang Yang from Sun Yat-Sen University, Guangzhou. The aim was to retrieve a sediment core from the deepest section of Qinghai Lake (25°07′57″N, 98°34′18″E, Figure 2), near Tengchong city, within Tengchong county (Figure 4), in Yunnan Province, south west China.

Figure 4: Illustrates the location of Tengchong County, marked by the red boundary within Yunnan Province, in reference to other major Chinese cities such as Guangzhou and the Myanmar border, which lies in on the western side of Tengchong County. The approximate location of Qinghai Lake is marked by the red triangle (Google Maps, 2018).

This is not to be confused with the much more famous Qinghai Lake in Qinghai Province, which is the largest lake in China. The deepest section of the lake, at around 5.9m depth (Yang et al. 2016) is preferential for core extraction as this is where the sediment is least disturbed and most well focused, and therefore the sediment layers will have the best structure and representation of changing climate parameters through time.

The coring platform used for this operation included a large bamboo, built-for-purpose platform (Figure 5), which provided a stable base for drilling into the sediment from above. The percussion drill included up to 23m of metal core pipeline to extract the sediment core, and used a diesel engine. In total, the sediment core collected from Qinghai Lake was over 22m in length. However, only the top 1.56m of the core was taken for analysis in this project. The remaining 20.5-21.5m section of the core will be utilised in a related PhD project.

Figure 5: Image displays bamboo platform used for core extraction from Qinghai Lake.

The 1.56m core for this project was taken to Sun Yat-Sen University for further processing. Here the core was sampled in to 1cm sections, producing 156 separate 1cm sediment samples available for analysis. These samples were then freeze-dried at -50°C, 0.006mbar pressure in a freeze-dryer overnight. This process removes any water from the sediment samples through sublimation which prevents heating of the sample that could alter the biomarker lipids. Water would interfere with processing with organic solvents. The samples were transported back to Glasgow where the BECS wet lab processes could begin, as well as my personal involvement in this project.

The decision was made that a total of 46 individual sediment samples would be an appropriate sample quantity for this project, and the sample range taken would be dispersed as evenly as possible throughout the 1.56m sediment core. This was achieved by taking samples at 3cm intervals, with a couple of exceptions to widen the range closer to covering the full 1.56m. The shallowest sample was taken at 1cm and the deepest sample was taken at 146cm. The selected sediment samples were assigned a BECS ID number and noted in the BECS ID lab book.

2.2 BECS Wet Lab Processes:

At this stage of the sample processing, I was trained by Lab Technician Ali Salik, as well as, by Professor Jaime Toney.

Firstly, I observed the appropriate health and safety procedures in the BECS wet lab to learn how to handle where solvents, materials and equipment. I became familiar with health and safety risks and signed the relevant COSHH forms. PPE (including lab coat, latex gloves and if necessary, goggles) was worn during processing samples, which started from the unrefined sediment up to samples separated into organic compound classes, and clean-up for GC analysis. The BECS Wet Lab processes can be broken down in to several distinct stages; furnacing glassware, Accelerated Solvent Extractor (ASE) Preparation, runs and cleaning, Extraction of the Total Lipid Extract (TLE), weighing and splitting the TLE, Acid/Neutral Separation, Clean-up and derivitisation of the Total Acid Fraction (TAF), clean-up and further separation of the Total Neutral Fraction (TNF), Bis(trimethylsilyl) trifluoroacetamide (BSTFA) Derivitisation, and finally, Sample and Standard Preparation for GC FID/MS runs. Most of the key stages in this process are illustrated in Figure 6. Each of these stages is important to preparing the samples for analysis on Gas Chromatography with Flame Ionisation Detector (FID) or Mass Spectrometer (MS). The following is a description of each of these BECS protocols.

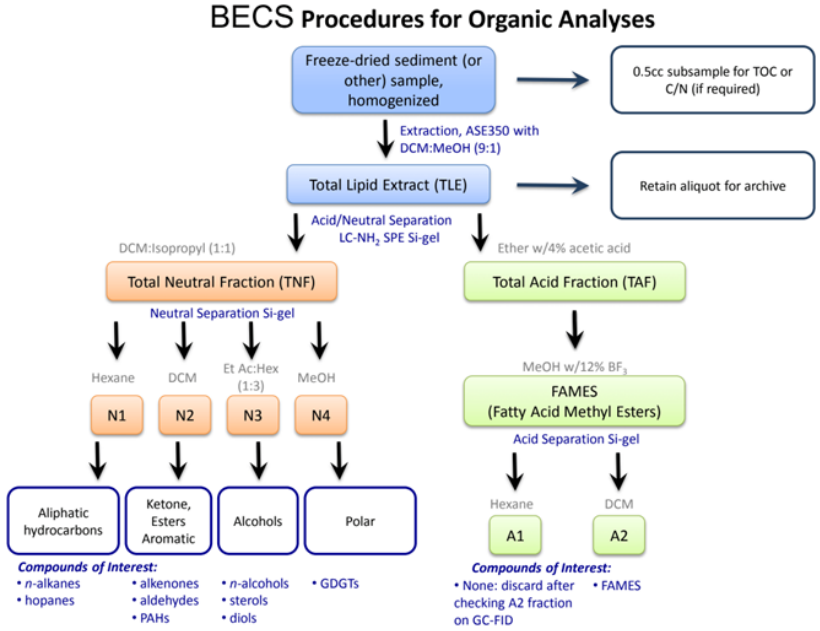

Figure 6: Depicts most of the key stages involved in the BECS wet lab sample processing procedure (from head of research group, Toney).

2.2.1 Furnacing Glassware:

All ASE filters, sand and glassware used during BECS Wet Lab work in this project were sterilised by combustion in a Carbolite CWF1200 combustion furnace at 450°C for 8 hours prior to use. All glassware used was previously soaked in 1 part Decon 90

to 9 parts hot water overnight and then cleaned prior to combustion. The solvent-free and dry glassware was wrapped in tin foil and carefully positioned in the furnace.

2.2.2 ASE Preparation, Runs, and Cleaning:

The initial processing procedure began by removing all the non-sediment bound lipid content from the Qinghai Lake sediment samples. This leaching of the total lipid content (known as the Total Lipid Extract), from the sediment samples, was executed by an Accelerated Solvent Extractor (ASE) Machine, Thermoscientific Dionex ASE 350 (Figure 7). It operates by adding a solvent mix 9:1 by volume of dichloromethane (DCM) and methanol (MeOH) to the sediment sample and holding it at pressure (1500 psi) and temperature (110°C) in an ASE cell. The solvents absorb to the lipid content, which is collected in 60ml glass vials along with the TLE in the ASE collection chamber. However, before the ASE could be operated the ASE cells, vials and samples were prepared.

Figure 7: Image shows the Thermoscientific Dionex ASE 350 used for the extraction of organic lipids from sediment samples.

Pre-cleaned 10ml ASE cells were brought to a DCM-wiped and tin foil covered work surface. One ASE cell is necessary per sample, and ASE runs would include between 13-18 samples in this project, with the exception of learning samples and pilot

samples. Pre-prepared ASE glass fibre filters that have been combusted are stored ready in a covered glass jar, alongside a covered jar of pre-combusted, Fisher chemical, low iron sand. Two pair of tweezers were sterilised with a DCM rinse and used to extract a glass fibre filter from the jar and place this filter precisely in a slot at the base of each ASE cell cap. Once both caps have had their filters added, the ASE cell is screwed into one of the ASE caps. At this stage, the ASE cell cap (with filter) and body are weighed using Fisher Scientific SG-402 scales. This allows for the future calculation of the sediment sample mass. Once weighed the cell cap and body were taken back to work surface. A specialized ASE cell funnel was cleaned with DCM, then once dry is used to funnel the sediment sample in to the ASE cell body. Now the ASE cell cap (with filter) and body loaded with the sample were reweighed to calculate the sediment sample mass. After the sediment sample was loaded and weighed, the remaining cell body space is filled using combusted sand. Any residual sand at the top of the cell body is wiped away. The top cell cap and filter was then screwed on to the cell body tightly, and the top of the cap is labelled, using a sharpie, with the samples BECS ID. Blanks were prepared the same way as samples except the entire cell body is filled with combusted sand.

The ASE cells are now prepared and ready. One 60ml glass vial per sample was taken and the top was covered tightly with tin foil. The vials have been sterilised beforehand by cleaning and overnight combustion. An ASE vial cap was screwed tight on to the top of vial and the vial was labelled with its BECS ID, again using a sharpie. Before loading cells onto the ASE machine, the ASE machine was turned on, the nitrogen was turned on from a stored tank outside, and an ASE rinse was performed to ensure there is no sample contamination. Once the rinse is completed the ASE cells containing samples/blanks were loaded in numerical order, hanging vertically, into the numbered cell holders with the labelled cap at the top, and the 60ml vials were loaded into the corresponding numbered slots in the ASE chamber. Blanks were routinely inserted at the start and end of each run to check for ASE contamination. One final check was conducted to ensure the sample cells and vials were in the correct locations, and to confirm that there is enough of the respective solvents in the storage tanks (generally over 1200ml is acceptable). The run was then initiated and each sample takes 45 minutes to be processed.

Once the ASE run is completed and the cells have been allowed time to cool down the clean-up of the ASE cells can begin. Clean-up is a crucially important stage to avoid contamination of future samples. The cells were disassembled, firstly the top cell cap was removed and the contents of the cell body, sample and combusted sand, can be tipped out and restored in plastic bags or disposed of. The remaining cell cap was removed and sediment was cleaned from the body, before the ASE filters were

removed from the cell caps using the tweezers. Any remaining sediment was rinsed and scrubbed out of the cell caps and body.

The stainless-steel ASE cell caps were placed in a small Teflon jar, while the cell bodies were placed in a large Teflon Jar. Both jars were filled until all cell caps and bodies from a run were completely submerged in Rinse 1 solution (used Acetone). There is an additional large Teflon Jar if needed for larger ASE clean-ups. The jars lids were screwed on and then they were placed in a Branson 5510 ultrasound bath and sonicated for 30 minutes. Post sonication the jars are removed and the Rinse 1 solution was disposed in to the flammable waste liquids bin in a fume cupboard using a glass funnel. The jars were then filled to the same point with Rinse 2 (Fresh Acetone), capped and were sonicated again for 30 minutes. Post sonication the jars were removed but this time the Fresh Acetone Rinse 2 is recycled into the Rinse 1 Jar as used acetone for future rinses. The Rinse 1 Used Acetone Solution can technically be used up to 3 times before it is disposed of. Once the Rinse 2 acetone had been completely strained out the jars were filled to the same point, submerging all cell parts, with Rinse 3 solution (a deep cleaning DCM:MeOH (methanol), 2:1 solution), capped and were re-sonicated for 30 minutes in the ultrasound bath. Post sonication, the jars were again removed and the Rinse 3 solvent can be either disposed or recycled. Like the Rinse 1 solution, Rinse 3 can be used up to 3 times before it must be disposed of. Rinse 3 was disposed of in a separate chlorine waste bin, found in the fume cupboard, as the rinse contains DCM.

Once Rinse 3 is completely strained out the clean ASE cell parts were organised. Two metal trays were covered in fresh tin foil in the fume cupboard. The ASE cell caps were all position on one tray to dry, while the cell bodies are placed on the other. Both trays were quickly covered with fresh tin foil to prevent contamination. The tin foil was labelled with a sharpie, noting that the cell parts are cleaned, alongside the date on which they were cleaned, concluding the cleaning procedure.

2.2.3 Weighing and Splitting the TLE:

The TLE must be weighed before continuing with further processing. This is due to the fact that the TLE used must not be over 10mg mass as it is crucial for proper separation and the sample concentrations may be too high otherwise. The 60ml vials containing the TLE for each sample were removed from the ASE chamber. The caps and tin foil covering were removed and they were placed in a Calibre Lifesciences TurboVap LV for drying. The nitrogen tanks outside were turned on and the TurboVap was set to dry the TLE samples for 15minutes. The samples remained in the TurboVap until completely dry. While waiting for the TLE to dry, one pre-combusted 8ml vial per sample was labelled with a sharpie then weighed. Once dried the samples in the 60ml vials have as small volume as possible of DCM added to re-dissolve the TLE. If

necessary, sonication of the vials is used to re-dissolve the TLE. Pre-combusted glass columns (Borosilicate Pasteur pipette, one per sample) with rubber teats were used to extract the re-dissolved TLE and transport the sample to each respective 8ml vial.

With all samples transferred into 8ml vials, the TLE can be re-dried so that the vials can be re-weighed to calculate the TLE mass. The 8ml vials were placed into vial slots in a Techne Dri-Block DB-3 machine. The gas nozzles are lowered into each vial and the nitrogen is turned on to dry the TLE. Once dried the vials are re-weighed on Mettler Toledo digital scales, and the TLE was calculated for each sample. If the TLE is over 10mg, it is split using a known volume of DCM, calculated to dilute the sample appropriately. Sonication is used if necessary to re-dissolve the sample. A Hamilton Glass syringe is then used to remove the appropriate, calculated volume of dissolved TLE that will leave slightly under 10mg TLE in the 8ml vial once it is dry again. The extracted TLE is then archived in 2ml pre-combusted GC vials. The Hamilton syringe was cleaned thoroughly between sample extractions with DCM to prevent contamination. The remaining TLE in 8ml vials is re-dried under nitrogen. If the TLE was under 10mg it was not split and the vials were stored, covered for the next stage.

2.2.4 Acid/ Neutral Separation:

Appropriate quantities of 2ml GC vials, 8ml vials, boron pipettes and low iron sand were combusted in preparation for this stage.

A work surface was prepared, wiped down with DCM and covered in fresh tin foil. 3 column stands were set up and the columns used to separate the acid and neutral fractions were prepared. First the columns were shortened using a glass cutting pen to remove a few cm off the bottom of the pipettes. One column per sample were placed in the column stands. Two pairs of metal tweezers were sterilised with a DCM rinse and used to take small wads of quartz glass wool and insert them at the top of the columns. A long boron pipette was used to push the glass wool down towards the shortening tip of the column until it fits correctly. The fit must be tight enough that it prevents any silica or sand from falling through, but not so tight that it restricts the flow of solvent. A sterilised spatula was used to load LC-NH_2 SPE Si-gel in to a modified funnel. The modified funnel was then used to insert 4cm of LC-NH_2 SPE Si-gel in each column. This gel is expensive and also very dangerous if inhaled so care was taken not to spill any. The columns are tapped with a spatula to allow the silica gel to settle. The modified funnel was then used to insert a small mass of combusted sand in each column to cover the top of the silica gel to prevent it from drying out.

The columns were now prepared and must be rinsed before use to sterilise them. A 100ml 1:1, DCM:ISO (Isopropyl alcohol a.k.a Isopropanol, Propan-2-ol) solution was prepared in the fume cupboard. Each column was rinsed with 3 bed volumes (5-10ml)

of DCM:ISO solution. The solvent was collected in 8ml vials and disposed of in a disposal flask. New 8ml vials were taken and labelled TNF with respective sample BECS IDs, then weighed and placed numerically under each column. Each TLE sample in the 8ml vials was then re-dissolved with a small volume of DCM:ISO solution (200µl-400µl), extracted and loaded numerically into each column using a boron pipette and rubber teat. The samples were left to seep into the silica gel. A solution of ether with 4% acetic acid was prepared by pouring 96ml ether and 4ml acetic acid in to a measuring column in the fume cupboard.

The TNF was then eluted by inserting and eluting a total of 4ml of 1:1 DCM:ISO solution, 1ml at a time using a Hamilton Glass syringe. The TNF, which was collected in the 8ml vials, were removed and dried under nitrogen. The TNF vials were replaced by new 8ml vials labelled as TAF with the respective correct BECS IDs. Each column was then eluted with 4ml of ether with 4% Acetic Acid, 1ml at a time, to extract the TAF. The TAF was collected in the vials and then dried gently under nitrogen. The TAF and TNF once dried, were ready for further processing. The dirty columns are disposed in a waste column jar, left to dry and waste silica is disposed in a special tub. Used pipettes are disposed in the glass recycling Used 8ml vials were cleaned with Decon 90 baths.

2.2.5 Clean-up and Derivitisation of the TAF:

The TAF samples require methylation prior to being run on the GC instruments. The 8ml glass vials that the TAF samples were stored in were specifically selected as they had no chips in the glassware. This ensures that Teflon caps can fit tightly to the vials, creating a proper seal during derivitisation. 100µl MeOH with 12% BF_3 (Boron Trifluoride) was added to each 8ml vial and the vials were capped tightly with the Teflon caps, placed in a Memmert UN30 drying oven at 70°C and left for one hour to derivitise the samples. After an hour the vials are removed and dried gently under nitrogen.

While the samples were drying, a work surface was prepared with DCM and foil so columns could be prepared. 3 column stands were set up and combusted boron pipettes were again shortened with the glass cutting pen and one per sample was set up in the stands. Glass wool was loaded in and then the modified funnel was used to load 3cm of 230- 400 mesh/35- 70micron regular silica gel in to each column. The columns were tapped to settle the gel and a thin layer of combusted sand was loaded in to each sample. 8ml vials were then placed under and each column was cleaned by elution of 4ml of Hexane which was collected and disposed of. New 8ml vials were labelled as TAF HEX along with respective BECS IDs and were placed numerically under columns. A small volume of hexane (300-500µl) was used to re-dissolve each TAF

sample and sonication was used if necessary. The samples were then loaded numerically in to the columns using one boron pipette per sample and a rubber teat.

The TAF hexane fraction was then eluted using 4ml Hexane and collected in the 8ml vials. This fraction is not necessary for FAME (Fatty Acid Methyl Ester) analysis but is retained and archived to check methylation works properly. New 8ml vials are labelled as TAF DCM alongside respective BECS IDs and were placed numerically under the correct columns. The TAF DCM fraction is then eluted using 4ml DCM and collected in the 8ml vials. The TAF DCM fraction was dried gently under nitrogen. It is important not to blow down nitrogen too aggressively with TAF samples as methyl esters of some fatty acids are highly volatile and may break down or escape. GC vials were labelled for each sample with a label printer and weighed on digital scales. The TAF DCM samples were then re-dissolved in 300µl of DCM, with sonication if necessary, and were transferred to a GC vial using a Hamilton syringe (which was thoroughly cleaned between sample extractions). The sample were dried in the GC vial Techne Dri-Block under nitrogen, and once dry, were re-weighed to calculate the mass of the TAF. Columns were disposed the same way as previously. All Glassware undergoes the same cleaning processes.

2.2.6 Clean-up and further Separation of the TNF:

The TNF requires further separation into 4 separate chemical fractions known as N1-N4 by using four separate solvents. This process separates out aliphatic hydrocarbons in N1, ketones, esters and aromatics in N2, alcohols in N3 and polar compounds in N4 respectively. This is carried out in order to isolate various biomarkers for analysis in each separate fraction.

New columns were prepared and shortened with the glass cutting pen at the clean work station. The columns were set up and glass wool was loaded in to each column and positioned. A sterilised spatula and the modified funnel was used to load 5cm of regular silica in to each column. The columns were tapped to settle the silica gel and a thin layer of combusted sand was added. At this point all the 8ml vials necessary are labelled and all the necessary solvents were topped up and prepared. Each column was cleaned before use by eluting 4ml hexane through each, which was collected in vials and disposed.

Each dry TNF sample is then re-dissolved in a small volume of hexane (600µl), with sonication if necessary. The samples are then loaded numerically in to each column using a boron pipette and rubber teat. N1 labelled vials for each sample with BECS ID are placed numerically underneath the correct columns. The N1 fraction is then eluted using 4ml Hexane and collected in the 8ml vials. The process of switching vials correctly occurs three more times for each respective fraction. The N2 fraction is

eluted using 4ml DCM and collected. The N3 fraction is eluted using 4ml of a pre-prepared ethyl acetate:hexane, 1:3 solution and collected. The N4 is finally eluted using 4ml MeOH and is collected. All four fractions were then dried under nitrogen.

2ml GC vials were labelled with a label maker for each sample in each fraction and then one spring coil was inserted into each GC vial. One pre-combusted 200µl glass GC insert per sample was then inserted into the top of each spring coil within the GC vials. These inserts hold the sample. Each GC vial, with label, spring coil and insert was weighed on digital scales. Each N1 and N2 dry fraction sample was re-dissolved with a small volume of 150-200µl DCM, sonication was used if necessary. The samples were then transferred in to their corresponding GC vial insert using a Hamilton Glass syringe, which was cleaned thoroughly between sample extractions. The N1 and N2 samples were dried and re-weighed. At this point the N1 and N2 samples were ready for final preparation before GC analysis, and were stored in cryoboxes until being run. However, the N3 and N4 samples require further derivitisation before GC analysis, and are left in their 8ml vials for the next stage. Clean-up of glassware and columns follows the same procedure as previously.

2.2.7 Bis(trimethylsilyl) trifluoroacetamide (BSTFA) Derivitisation:

N4 fractions were not used in this project and therefore only the N3 fraction underwent derivitisation. N4 fraction samples were re-dissolved and transferred with DCM to their respective GC vials, then archived. The N3 fractions require derivitisation with bis(trimethylsilyl) trifluoroacetamide (BSTFA). This process is necessary as the silication of samples allows for alcohols to be detected properly in GC analysis. The samples were always derivitised no more than 48 hours prior to GC analysis.

The samples were dried under nitrogen in 8ml vials before a Hamilton syringe was used to add 30µl BSTFA and 40µl pyridine in to each sample. The vials were capped with Teflon caps and placed in the drying oven, which was pre-heated to 80°C, and left for 2 hours. Post derivitisation, the N3 sample vials are removed and allowed to cool to room temperature before being dried under nitrogen. 200µl of DCM was then used to re-dissolve the derivitised N3 samples, which were then transferred to their respective GC vial inserts with a Hamilton glass syringe. The syringe was washed between samples the same as previously to prevent contamination. The samples were then re-dried under nitrogen before being re-weighed in GC vials with spring coil and insert. Once weighed the N3 samples were ready for final preparations before GC analysis.

2.2.8 Sample and Standard Preparation:

Prior to running samples, they must be diluted in a known volume of DCM and standards were prepared. If the samples were in GC inserts either 150µl or 200µl was used to dilute them. If the samples were just in GC vials 500µl was added. The GC vials were capped with GC caps and the samples were ready for analysis. Standards were prepared with varying volumes of DCM and pre-prepared BECS Standards mixes in GC inserts. Three GC vials with spring coils and inserts were prepared per run and labelled. 100µl (alternatively 150µl) of BECS standards solution was added using a Hamilton glass syringe to make a 10µg/ml Standard. A 5µg/ml BECS standard was prepared with the same process but with 50µl:50µl DCM: BECS Standards solution mix (or 75µl:75µl). Finally, a 2.5µg/ml BECS Standard was prepared with a 25µl:75µl BECS Standard solution: DCM mix (or 37.5µl:112.5µl BECS Standard: DCM mix). The Standard vials were capped with GC caps and were ready for GC analysis.

2.3 Gas Chromatography Analysis:

N1, N2, N3 and TAF fraction samples were run on GC instruments to identify and quantify concentrations of the respective biomarkers required in this project. The department has three GC instruments, of which two, an Agilent 5977 GC-MS (Gas Chromatography Mass Spectrometer) and an Agilent 7890 GC-FID (Gas Chromatography Flame Ionization Detector), were utilised in this project (Figure 8). These instruments have varying functions and sensitivities. The FID is used for biomarker quantification, it is a very robust machine that is not prone to damage by high sample concentrations, and so can analyse large batches. The GC-MS however, is a highly sensitive machine that is fantastic at identifying compounds but can be damaged by samples with high concentrations. A general pattern of procedure is followed with GC analysis. First, entire sample batches were run on the GC-FID to check the concentration of samples is adequate for analysis but not so high that it may damage the GC-MS. Samples (generally only a few, especially if concentrations were too high) were then run on the GC-MS for biomarker identification. Specific biomarkers Retention Times (RTs) were identified from GC-MS results and noted. This then allowed for analysis of the FID results, where biomarkers were re-identified using the RTs (as well as surrounding peak patterns) and quantified.

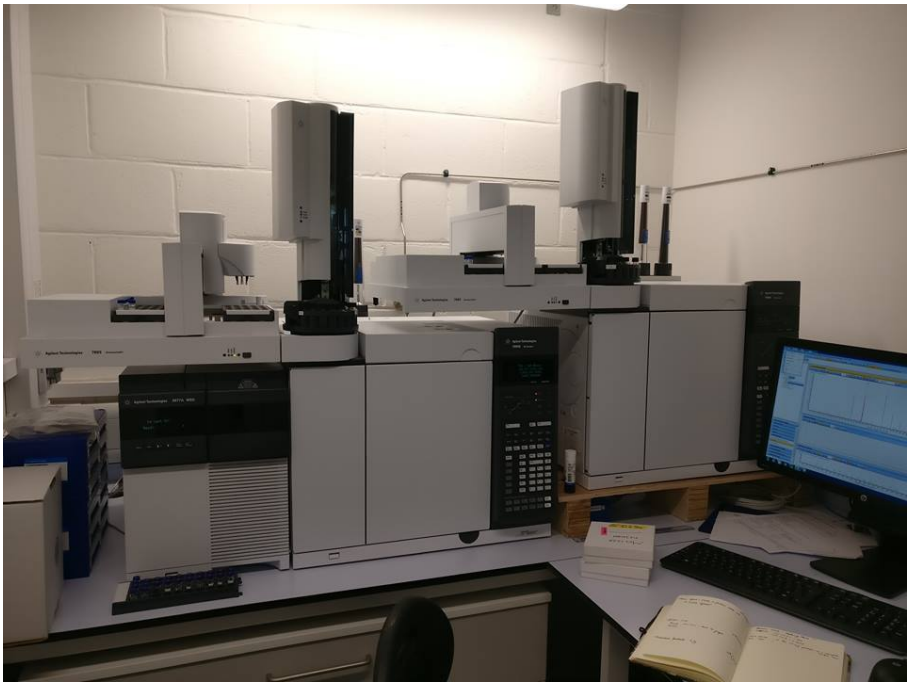

Figure 8: Figure shows the Agilent GC-MS (left) and GC-FID (right) used in this project for analysis of samples.

Although most samples were analysed following this procedure, there was one exception in the N3 samples, which required both compound identification and quantification via the GC-MS.

The GC-MS Agilent 5977 run method details are the following: GC-MS runs for identification were set within the range of 50- 600 m/z (mass/charge ratio). A 60m long HP-1-MS column with a 0.25mm internal diameter and a 0.25µm film thickness was used. The initial oven temperature of 600°C was retained for 2 minutes at the start of the run before increasing by 300°C/minute until it reached 1200°C. Following on the oven temperature was increased by 50°C/minute until the temperature peaks at 3050°C. The total run time for each sample was 56 minutes, with the first results detected after 10 minutes (i.e. gas cut-off after ten minutes). The front inlet temperature was 3100°C, with interface temperatures between the Mass Spectrometer and source also at 3100°C. The temperature of the source itself was 2300°C and the MS quad temperature was 1500°C. The system purge time was 0.705 minutes, and the purge flow at 50 minutes. The column flow was 1.2ml/minute with a flow velocity of 28.4cm/second. The method used constant flow. The injection volume per sample was 1µl. Helium was used as the carrier gas, with a flow of 25ml/minute.

The GC-FID Agilent 7890 run methods are the following: GC-FID runs for quantification did not require a m/z setting and used a 60m long RTX-1 Restek column with an internal diameter of 0.25mm and a film thickness of 0.25µm. The initial oven temperature program is the same as the GC-MS. However, once the GC-FID oven

reaches 1200°C, the temperature increased by 50°C/minute until it peaked at 3300°C and this temperature was sustained for 15 minutes. The front inlet used spitless injection at a temperature of 3200°C. The system surge time was 0.705 minutes and the purge flow at 50 minutes. The total run time per sample was 61 minutes. The flow rate was 1.2ml/minute, with a flow velocity of 30.4cm/second. The method used constant flow, with changing pressure (psi). Hydrogen was used as the carrier gas, with a flow of 40 ml/minute.

2.3.1 Processing results:

Once run the sample results were analysed and processed to allow for quantification of relevant biomarkers. These quantifications could then be further used in relevant equations for calculation of various changing climate parameters, e.g. n-alkanes concentration used in the Average Chain Length (ACL) equation. This section is split into fractions, so each fraction and its respective analysis techniques and biomarker/s processing procedure after analysis is explained.

2.3.1.1 N1 Fraction

The N1 fraction was analysed following the general procedure, to identify and quantify n-alkanes and hopanoids. Large batches of 13, 15 and 18 samples respectively were analysed on the GC-FID, with a few samples run on the GC-MS. Both of the types of biomarkers were identified using the GC-MS and their RTs were noted. The FID results were then used to quantify the concentration of the respective n-alkanes and hopanoids. The process of quantification (to calculate the dry mass of each respective biomarker in µg's per gram of the samples sediment mass) begins by extracting and recording the peak area of the respective n-alkane/hopane peaks on the FID computer. Calibration curves were calculated using the three standards from one of the runs. Separate calibration curves from 3 different standard n-alkane peaks were used to calibrate concentrations for peaks within certain RT sections. A C_{16} calibration was used for n-alkane peaks before 25minutes RT. A C_{23} calibration was used for n-alkane peaks between 25- 35 minutes, while a C_{30} calibration was used for all n-alkane peaks after 35 minutes. The same calibrations are used for all other N1 biomarkers within these respective retention time 'windows'.

The C_{16} calibration equation with intercept, re-arranged in the correct form to calculate the concentration by incorporating peak area, is $x = \frac{y}{28.257}$ where x is the concentration, and y is the peak area of the biomarker being analysed. The R^2 value was 0.9582.

The C_{23} calibration equation with intercept, re-arranged correctly to calculate concentration was $x = \frac{y}{14.545}$ with an R^2 value of 0.9442.

The C_{30} calibration equation with intercept, re-arranged correctly to calculate concentration, was $x = \frac{y}{13.038}$ with an R^2 value of 0.932. All R^2 values for the calibration curves were much higher and move favourable without the intercept, but they remain acceptable.

Once the concentration of the N1 biomarkers was calculated using the respective calibration curve equations, it requires further adjustment. First, the result is then corrected for the dilution of DCM for each sample with the equation $\left(\frac{x}{1000}\right) \times y$ where x is the concentration previously calculated and y is the dilution volume. It is then corrected to convert from mg/l to mg/g of the samples sediment mass with the equation $\left(\frac{1000}{(x \times 1000)} \times y\right)$ where x is the sample sediment mass (g) and y is dilution correction value previously calculated. Finally, the result is scaled up to µg/g by multiplying by 1000. The final µg/g concentration values of the respective n-alkanes (C_{16}-C_{35}) were used for ACL, CPI (Carbon Preference Index), P_{aq} (Proportion of aquatic plant material input) and P_{Wax} (Proportion of terrestrial plant material input) calculations.

2.3.1.2 Average Chain Length:

The ACL was calculated using the ACL equation from Häggi et al (2016). The ACL equation used was $\mathrm{ACL} = \frac{(27 \times cC27 + 29 \times cC29 + 31 \times cC31 + 33 \times cC33)}{(cC27 + cC29 + cC31 + cC33)}$ where c represents the final scaled up concentration calculation in µg/g of the respective n-alkanes in each sample. This equation covers terrestrial plant (odd number) n-alkanes from C_{27}-C_{33}. Two other ACL graphs were produced with the equations altered to include C_{25} and then C_{25} and C_{23} respectively into the equation, in case any of the terrestrial plants around Qinghai lake had lower chain lengths (most are C_{27} or higher) and to compare graph trends. Ultimately the C_{27}-C_{33} ACL equation and graph were considered most representative.

2.3.1.3 Carbon Preference Index:

The CPI was calculated using a modified version of the CPI equation from Häggi et al (2016). The equation was modified to remove both C_{28} and C_{29} values. This was done because no C_{28} values could be extracted from the N1 FID results, as they were obscured by large phthalate contaminant peaks. CPI graphs were produced for equations with the C28 removed and both the C_{28} and C_{29} removed.

Due to the phthalate contaminant peaks obscuring the C28 peaks in N1 samples FID analysis, the CPI equation had to be modified to remain functional, as equal numbers of corresponding odd and even n-alkanes are needed in this equation. Therefore, 2 modified versions of the CPI were calculated to investigate which was most suitable for use, one with solely the C28 removed, and one with the C28 and corresponding C29 removed from the equation. Results show that the best CPI dataset is that with

the C28 and C29 removed, with less skewed results (see page 32). This is surely most accurate, as removing a numerator and denominator from the equation provides more representative results than simply just removing a denominator, which skews results to higher values, unfairly indicated better preservation. Therefore, the CPI without C28 and C29 was described and used in the results, while the other was discarded.

Therefore, the equation used was $CPI = 0.5 \times \left(\frac{cC27+cC31+cC33}{cC26+cC30+cC32} + \frac{cC27+cC31+cC33}{cC30+cC32+cC34}\right)$ where c was the concentration in µg/g of the respective n-alkanes in each sample.

2.3.1.4 Proportion Aquatic Material and Proportion Terrestrial Material:

The proportion of aquatic materials was calculated using the equation from Baker et al (2016). This equations formula was $P_{Aq} = \frac{cC23+cC25}{cC23+cC25+cC29+cC31}$, where c was the concentration in µg/g of the respective n-alkanes in each sample. The proportion terrestrial material equation effectively shows the inverse of the aquatic version, and the equation also came from Baker et al (2016). The equation used was $P_{Wax} = \frac{cC27+cC29+cC31}{cC23+cC25+cC27+cC29+cC31}$, where c was the concentration in µg/g of the respective n-alkanes in each sample.

2.3.1.5 N2 Fraction

N2 samples were analysed following the same method as N1 samples using the GC-MS for alkenone identification and GC-FID for compound quantification. Samples were to be calibrated in the same manner as N1 samples using the same peaks for a calibration curve, as the N2 samples were run alongside the N1s.

Any alkenones detected by the GC-MS require identification (of the alkenone type and the source algal species), FID quantification, further processing to adjust the concentration value to mg/g or µg/g in the same style as the N1 samples and a species-specific calibration to calculate quantifiable changes in lake surface temperature.

2.3.1.6 N3 Fraction

The N3 fraction was analysed in large batches (13, 15 and 18 samples respectively) using the GC-MS to identify and quantify any diols and sterols present in the sediment samples. Conducting quantification of diols requires samples to be run in the regular TIC (Total Ion Current/Chromatogram) mode and SIM (Selective Ion Monitoring) mode. The SIM mode samples were always analysed in the same GCMS run as the TIC mode samples and TIC and SIM runs for the same sample were run straight before/after each other respectively. This was done to avoid RT shifts between TIC and SIM samples (this has been noted to happen when batches are run several weeks/months apart), which can make identifying the correct SIM peaks for quantification difficult and sample TIC/SIM runs were arranged specifically to

prevent sample solvent evaporating after the initial TIC run GC cap penetration, for a fair comparison. The SIM mode was set to search for a particular suite of ions associated with long chain diols. These ions are used to detect the presence of hydrocarbon fragments from the breakdown of specific diol isomers. The specific ions searched for were the 299, 313, 323, 327, 341, 345, 355, 359, 369, 373 and 387 ions.

Once runs were completed, N3 results were analysed on the Agilent Quantitative Analysis programme. Peaks were scanned using the 'NIST' programme to search for sterols, with care taken to investigate potentially co-eluting peaks. Any sterols found consistently appearing at the same RT in most samples can be quantified on the FID using sterol peak areas and a calibration curve constructed using BECS standards from the same runs. Any diols located require quantification via the GC-MS using the sample TIC and SIM runs. The process of diol identification and quantification involves several steps. First the diols are located with the TIC scan results by investigating the ion signature of the peaks around specific known RTs. For example, the C_{32} diol generally appears around 51 minutes RT. Therefore, the search for the C_{32} diol involves scanning the peaks around 51 minutes RT using the spectrum preview until the correct ion profile is located. This involves checking that 73, 149 and other important accessory ions are present for the specific diol being searched for, confirming the presence of the diol. Once the diol is located the RT is noted to aid finding SIM mode peaks and the same diol in other samples in the future. Then, work shifts to the SIM graph to continue quantification. Firstly, a right click of the mouse on the SIM graph is used to open up a tab of options, and the option 'Extract Chromatogram' was selected. This opens up another window where settings were altered. The 'Type' was changed from TIC to SIM and then 'OK' was clicked. This produced a series of SIM chromatograms, one for each of the individual ions established in the SIM run parameters. This allows for isolated analysis of the different ions and therefore isolated quantification of the fragments representing different diol isomers through extracting the respective peak area data. At this stage, using the previously identified diol RTs, all available data (isolated SIM ion peaks) was gathered for the respective diol isomers, at the correct RTs for each diol identified.

With guidance from PhD candidate, Bianca Cavazzini, I identified the C_{28} peak in the TIC scan and further the 1,13 diol isomer peaks in SIM mode needed for the LDI. In particular, we were able to identify the correct peaks using the C_{28} compound's ion signature with strong 75 and 143 ion concentrations (Versteegh *et al*., 1997). As a note, the identification of diols, especially the C_{28} diol in my samples was challenging because there were multiple peaks near the RT of C_{28} and it was not clear in the TIC. I initially indicated the C_{28} values as 0 and with Bianca's help was later able to obtain peak areas presented here.

With the peak area data gathered it could now be further processed to provide quantitative lake surface temperature change data. The total sum of the 1,15 C_{30}, 1,13 C_{30}, 1,13 C_{28}, and 1,15 C_{32} diol isomers was calculated. Each of the individual diol isomers listed above were then divided by the total sum of all these isomers, to provide the fractional abundance of the individual isomers relative to the others. These values are then used in the Long Chain Diol Index (LDI) developed by Rampen et al (2012). This index's equation is the following

$\text{LDI} = \frac{(fC30,1,15\ diol)}{(fC28,1,13\ diol + fC30,1,13\ diol + fC30,1,15\ diol)}$ where f represents the fractional abundance of the respective diol isomer.

Once the LDI is calculated, the equation showing the relationship between the LDI and SST can be rearranged to calculate SST values for samples. The original equation developed by Rampen et al (2012) is $\text{LDI} = 0.033 \times SST + 0.095$

This equation was rearranged to $\text{SST} = \frac{(LDI - 0.095)}{0.033}$ and lake surface temperatures in °C could then be calculated. This method of extracting SIM chromatograms was chosen over alternative methods because isolating ions removes any interfering ion data known as 'background noise' that may skew data towards less representative results.

2.3.1.7 TAF Fraction

The TAF samples were analysed the same way as the N1 samples using GC-MS for fatty acid methyl ester identification and the GC-FID for quantification. The only real difference was that all TAF samples were run in the same batch. The samples were also calibrated in the same manner as the N1 samples using the same peaks but from a different, newer set of BECS standards (as the calibration is most accurate for the sample set when standards are analysed in the same run, or at a similar, close date) as the TAF samples were run several weeks after the N1s.

The C_{16} calibration equation used with intercept, re-arranged in the correct form to calculate the concentration by incorporating peak area, is $x = \frac{y}{24.45}$ where x is the concentration and y is the peak area of the acid being analysed. The R^2 value was 0.9988.

The C_{23} calibration equation used with intercept, re-arranged correctly to calculate concentration was $x = \frac{y}{11.857}$ with an R^2 value of 0.9977.

The C_{30} calibration equation used with intercept, re-arranged correctly to calculate concentration was $x = \frac{y}{9.2076}$ with an R^2 value of 0.9855.

The calibration curves were used to calculate concentration of peaks, in the same ranges as the N1 calibrations. The concentrations results were then further processed and adjusted in the same manner as the N1 samples to convert to µg/g of sample sediment mass.

The short vs long chain acid ratio was calculated using the following equation: Short vs Long Chain Acid Ratio $= \frac{(cC16+cC18)}{(cC28+cC30)}$ were c is the concentration in µg/g of the respective acids. C_{16} and C_{18} acids were chosen as representative of the short chain aquatic acids, while C_{28} and C_{30} were chosen because they are two of the highest concentration, long chain terrestrial acids detected and recorded.

2.4 Core Chronology

At the time of writing this thesis, our colleagues from Sun Yat-Sen University in Guangzhou, China, have not yet acquired the radiocarbon and palaeomagnetism dating on our core (Core TCQH17A), and so directly dated ages for the sediment core are unavailable. However, the best alternative solution to this problem has been adopted to provide approximate ages for the samples. We assumed that sedimentation rates for a nearby sediment core Core QH4, which was collected three years previously in 2014, would be similar to our core. We used the radiocarbon and palaeomagnetism chronology for Core QH4, which was retrieved using the same methods from Qinghai Lake and from an adjacent location within the lake. Professor Toney has advised that for now, use of the QH4 core data will suffice for dating the TCQH17A samples, until it can be updated with relevant data from the TCQH17A. As such, we acknowledge that prior to publication of this record, radiocarbon dates sampled from the TCQH17A core will need to be analysed (sent to BETA Analytical) and a more robust chronology applied.

Windows Excel was used to process the data acquired from the QH4 core. We received 4 calibrated radiocarbon dates from QH4 (Table 1), and used these to extrapolate ages for each centimetre of core in between these ages. To create the tentative age model, we assumed that the top of sediment core TCQH17A represents the year that it was retrieved – 2017.. Therefore, the age at 0 centimetres is -67 cal yr BP, in reference to 1950 AD. Age uncertainties were provided for the 4 dates received (Table 1), but because this is not our final age model, we have chosen to use a simple linear interpolation between points rather than propagate the age uncertainties to each centimetre. Again, this is a tentative age model until we have dates returned for our sediment core.

Table 1: Chronology data provided by colleagues from Sun Yat-Sen University on the related QH4 core via radiocarbon dating. This data was then used to extrapolate dates for each centimetre of Core TCQH17A.

Depth (cm)	Age (Calibrated Years Before Present)
0	-67
20.6	992.5 ±62.5
74	6355 ±55
137	8355 ±35
220	13170 ±85

Ages between each depth parameter provided from the QH4 core were calculated using linear interpolation between depths, with x = depth and y = age. The equation used for each centimetre between 0cm and 20.6cm was $y = 51.432 \times x - 67$

The equation used for depths between 21cm and 74cm was $y = 100.42 \times x - 1076.2$

The equation used for depths between 74cm and 137cm was $y = 31.746 \times x + 4005.8$

The equation used for depths between 137cm and 146cm was $y = 58.012 \times x + 407.35$

These equations yielded results that indicate that the 146cm long section TCQH17A used in this project has an approximate age range between -67 cal yr BP and 8877 cal yr BP, although sampling began at 1cm so the sampling age range was from -16 cal yr BP to 8877 cal yr BP (see appendices). These dates were used to create the secondary y-axis for the plots of biomarker results. The age axis created is not linear and a note is made in the Figure captions. Dates referred to in the text assume a linear interpolation between these dates.

3 Results

3.1 N1 Fraction

3.1.1 n-Alkanes

Concentrations of n-alkanes in µg/g of sample sediment mass were calculated for all n-alkanes detected in samples from C_{16}-C_{35}, with the exception of C_{28} which could not be calculated as the C_{28} peak was overprinted in all samples by large phthalate contaminant peaks that we expect were introduced during the coring process (Figure 9).

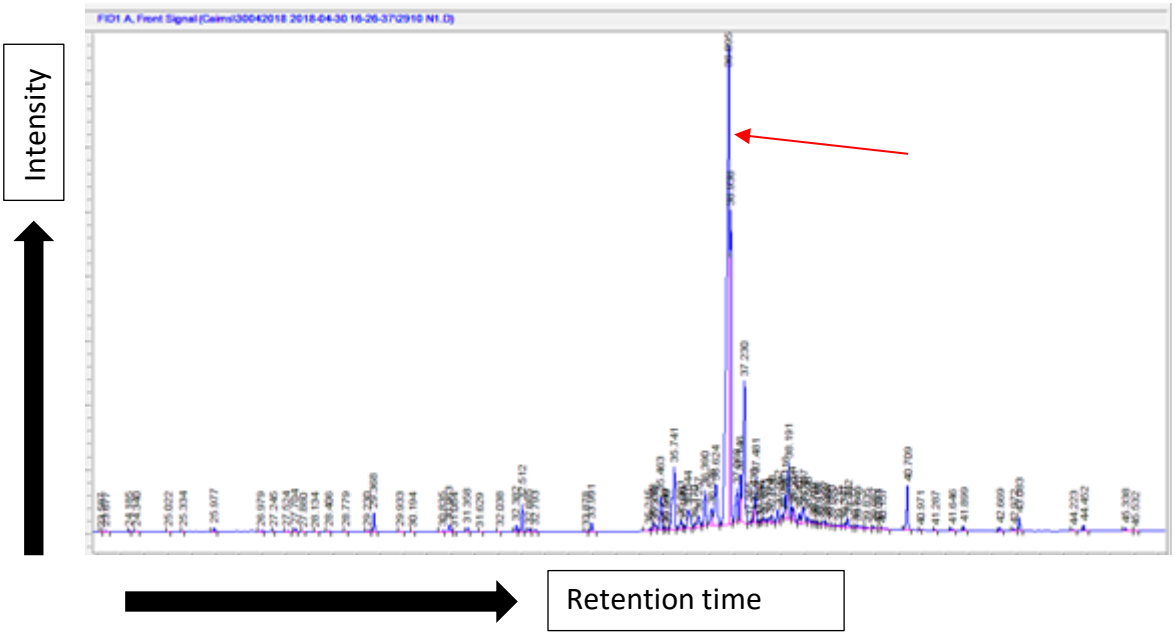

Figure 9: Annotated image shows example of FID chromatograph with large phthalate contaminant peak overprinting C_{28}, indicated with red arrow.

Most of the n-alkanes display a general trend in concentration fluctuations through the core with four distinct initial peaks (n-alkanes C_{22} and smaller generally display 3 distinct peaks with the 31cm being the largest) with concentrations spikes at 4cm, 13cm, 31cm and 43cm core depth, and corresponding troughs flanking the peaks at 7cm, 19cm, 34cm and 46cm core depth with the 31cm and 46cm peaks showing the highest concentrations. In most n-alkane profiles, deeper than 46cm the concentration values generally plateau at low values between 0.1µg/g and 1.1µg/g for even numbered n-alkanes (varies depending on alkane chain length) with slight oscillations and some occasional, outlying minor peaks. In odd numbered n-alkanes the same low plateau is observed across odd n-alkanes but with much greater variation across different odd chain lengths, with the lowest plateau averages of approximately 0.1µg/g in C_{17} (46cm to 146cm), while C_{29} has the highest plateau averages of 9.6µg/g. There are a couple of minor exceptions to these general descriptions of n-alkane profiles.

n-Alkanes with an even number of Carbon atoms have much lower concentrations than uneven chains. The highest n-alkane type concentrations were generally detected in C_{29} and C_{31} (43cm peak concentration of 35.4 µg/g and 30.4µg/g respectively), with concentration values becoming progressively lower towards the low and high extremes of n-alkane chain length (C_{16}, C_{17}, C_{34}, C_{35} etc, Figure 10). C_{17} has a 31cm highest peak value of 0.6µg/g, which is almost 33 times smaller than C_{29}'s 4th highest 31cm peak at 20.1µg/g.

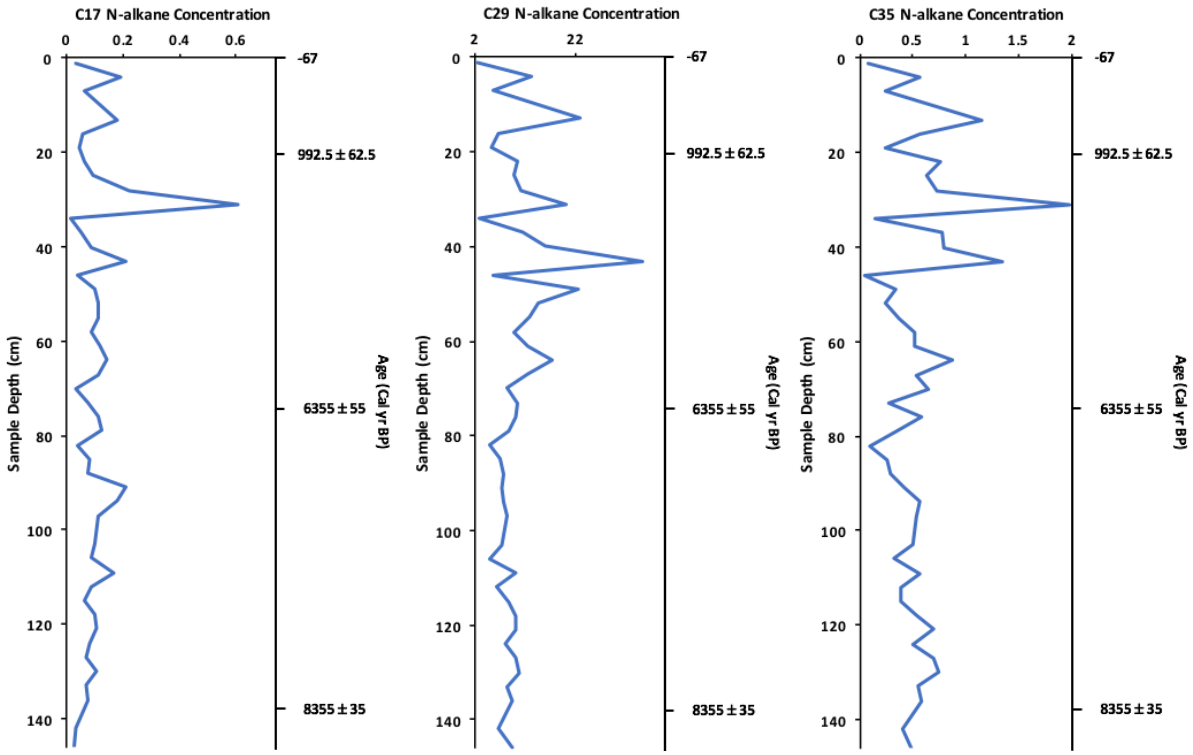

Figure 10: Image illustrates how n-alkane concentration values change dependent on chain length, with the highest values observed for C_{29} and concentrations decreasing with shorter/longer chain lengths. Note: the secondary y-axis shows depths of calibrated radiocarbon ages from an adjacent sediment core and this axis is non-linear.

3.1.2 Hopanes

The hopane results display a distinctive trend, with highly oscillating concentrations through the top 30cm, a largest peak at 43cm (with distinct surrounding trough lows at 34cm and 46cm), and a fairly oscillating but more stable concentration range, from 49-146cm, and a note able low concentration trough at 82cm in all hopanes. The concentration variation through this 49-146cm section of core is at its most minimal (relative to max hopane concentration) in the C_{29} BA Hopane, with concentration ranges from 0.7292µg/g (55cm) to 0.1499µg/g at 82cm (Figure 11). However, irrespective of max hopane values, concentration becomes slightly less varied, but remains at fairly similar values, with increasing hopane carbon chain length, with the exception of the C_{31} Hopane. The same scenario occurs with the average values across this 49-146cm section, except with slightly greater decrease in value with increasing chain length (averages of 0.440µg/g in C_{29}BA, 0.3952µg/g in C_{29}BB and 0.3227µg/g in C_{30}), until C_{31}. The C_{31} BB Hopane has the highest max concentration of 2.016µg/g, and it also has the highest overall averages (0.732µg/g) which are significantly higher than all other hopanes analysed (0.4299µg/g in C_{29} BA, 0.405µg/g in C_{29} BB, and 0.2968µg/g in C_{30} BB) and over twice as high as the lowest C_{30} BB hopane averages (0.8238µg/g).

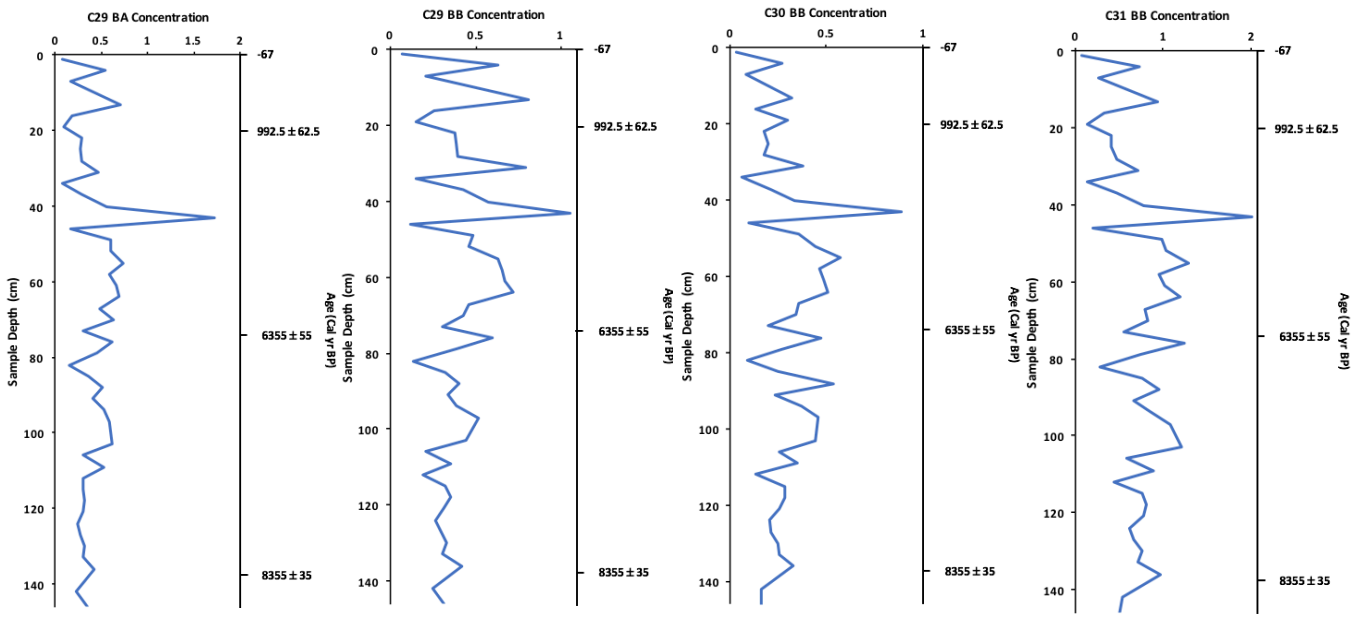

Figure 11: Figure displays concentrations for the four respective hopanes detected, graphed against sample depth in the core (cm) and age (years before present). Distinctive features can be observed, such as the 43cm peak hopane values and 49-146cm plateau, which is particularly prominent in the C_{29} BA hopane.

3.1.3 ACL

Three Average Chain Length graphs were produced for three respective ranges of mid-long chain, odd numbered, terrestrial n-alkanes; C_{23}- C_{35}, C_{25}- C_{35} and C_{27}- C_{35} respectively. All three graphs display general trends such as a steady rise ACL before a sharp drop at 19cm depth, followed by two other periods of ACL fluctuating inflation from 19cm-43cm and from 46cm-70cm depth with deep troughs showing a rapid decrease in ACL at 46cm and 82-85cm. However, the C_{23}-C_{35} and C_{25}-C_{35} show more scattered and dispersed results due to the increased range of concentrations, and therefore the C_{27}-C_{35} equation from Häggi et al (2016) is used as they represent the ACL results with the smallest range distribution (Figure 12).

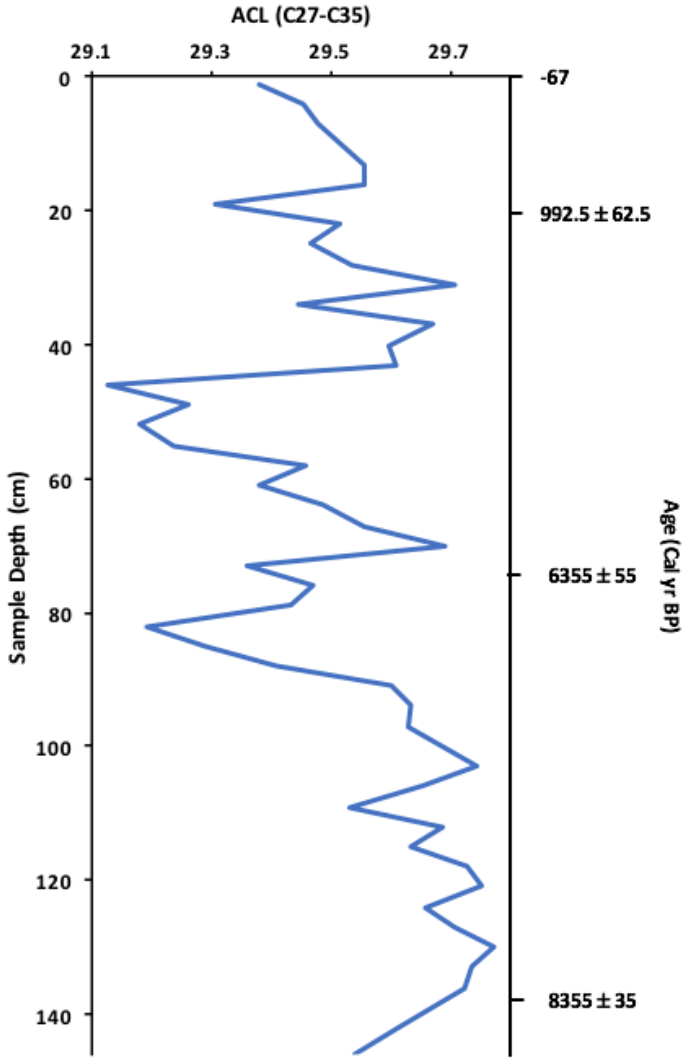

Figure 12: Graph displays the ACL values for the n-alkane range from C_{27} to C_{35} graphed against sample depth (cm) and age (cal yr BP).

The bottom 146cm-130cm of the core display a gradual rise in ACL values from 29.5 to 29.8. From 130cm to 91cm the results display a generally slightly oscillating but gently sloping plateau with ACL values slowly decreasing up core from 29.8 to 29.6. There is one distinct exception with a sharp trough at 109cm with ACL values dipping

to 29.5. Moving up core from 91cm, the ACL decreases rapidly to its second lowest value at 82cm of 29.2. Following on from this in the middle section of the core, the ACL rises quickly from 91-70cm, with one oscillation peak at 76cm on the way up to the 70cm peak value of 29.7 (Figure 12). From 70- 46cm the ACL declines slightly more gradually with a couple of oscillation peaks through the decline at 58cm (29.5) and 49cm (29.3) until it reaches this records lowest ACL value of 29.1 at 46cm. The ACL then spikes markedly quickly from 46cm-43cm from 29.1 up to 29.6. Further up core at 37cm depth, the ACL value rises further to 29.7 before quickly declining to 29.4 at 34cm and spiking again to 29.7 at 31cm depth. From this major peak at 31cm, the ACL drops steeply to 29.3 in a distinct trough at 19cm depth with one minor oscillation peak at 22cm depth (29.5). From this low, the ACL again rises quickly to 29.6 at 16cm depth. The top 16cm of the C_{27}-C_{35} ACL result shows a gradual ACL decrease from 29.6-29.4 from 16-1cm respectively, towards the present day (Figure 12). The mean ACL value across all sample results is 29.5. The ACL value ranges from 29.1 to 29.8.

3.1.4 CPI

Due to the phthalate contaminant peaks obscuring the C_{28} peaks in N1 samples FID analysis, the CPI equation was modified by removing both C_{28} and C_{29}. A comparison graph was created to check whether a CPI equation with only C_{28} removed, or one with the C_{28} and C_{29} removed was more appropriate. The results show they both follow the same trends, but the equation with the lone C_{28} removed skews CPI values upwards (Figure 13). CPI values for the CPI without C_{28} and C_{29} are described below.

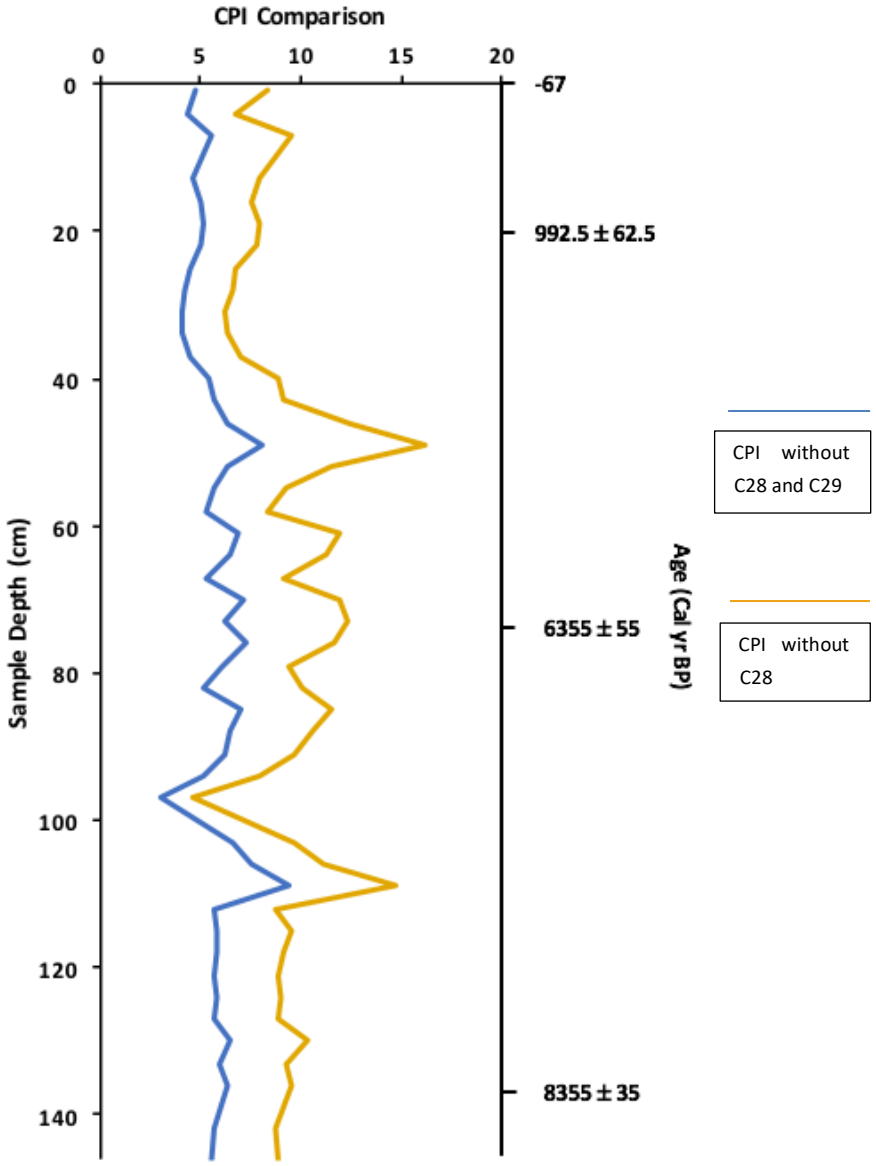

Figure 13: Graph illustrates CPI values plotted against sample depth (cm) and age (cal yr BP). This figure shows that both CPI versions follow the same trend but crucially that removing both a numerator and a denominator provides more accurate data, as removing C_{28} alone drastically increases overall CPI values.

The bottom 34cm of the CPI core results from 146cm- 112cm depth show a gently oscillating plateau of CPI values ranging from 5.6 (146cm depth) to 6.5 (130cm depth), with average values of 5.82 across this 34cm section at the core's base (Figure 13). The CPI value then spikes rapidly to the overall highest CPI value detected, from 112cm- 109cm, with the value rising from 5.7 to 9.5 during this period. Following on from this peak up core, the CPI value decreases to its overall lowest detected value of 3 at 97cm depth. Over the 12cm section from 109cm to 97cm depth the CPI value drops by 6.5. Moving further up core the CPI sharply rises from 97cm- 85cm depth, with values increasing from 3 to 7.1, a rise of 4.1. From 85cm - 58cm, including the 85cm peak, there is a series of four moderate peaks and corresponding troughs in CPI values, with the lowest value of 5.1 at 82cm depth and the highest peak of 7.3 at 76cm depth. From the 58cm trough value of 5.3, the value up core rises to one final, major peak with a CPI of 8. Following on up core, from 49cm the CPI value drops steeply, then more gradually to a low of 4.1 at 34cm depth. CPI values then gradually rise back up slightly from 34cm- 19cm, with the CPI increasing from 4.1 (34cm) to 5.1 (19cm). Across the last 19cm at the top of the core, the CPI value decreases slightly up core, before fluctuating up to a minor peak and down to a final trough before rising to 4.8 at 1cm depth (Figure 13). Across the whole core record, CPI values range from 3 to 9.5, with an average CPI value of 5.8.

3.1.5 Proportion of Aquatic Material

The P_{Aq} results display a series of sharp shifts and plateaus in the relative input of aquatic plant material to the Qinghai Lake system throughout the Holocene/last 9000 years shown by core. Moving from the base of the core up, the first 28cm from 146cm-118cm depth illustrates a gradual, fluctuating decline in P_{Aq} values from a high of 0.29 at 43cm to a low of 0.21 at 118cm (Figure 14). From this trough up core, the value then increases, from 118cm- 109cm to a peak 109cm value of 0.31. Further up core, from 109-91 cm the P_{Aq} value decreases slightly between 109cm and 106cm, dropping from 0.31 to 0.29. From 106-91cm however, the values maintain a gently fluctuating plateau, with averages of around 0.29. From 91cm- 85cm the P_{Aq} value rises sharply to a distinct peak out the plateau, with values climbing from 0.28 (91cm) to 0.36 (85cm). At 82cm depth, the P_{Aq} value drops to 0.29 before jumping up slightly at the edge of the plateau to 0.31 at 79cm depth. The value drops again between 76-73cm depth from 0.3 (76cm) to 0.2 at 73cm. The values maintain a short, low trough plateau from 73-67cm until the value spikes from 0.19 (67cm) to 0.26 (64cm) and back down to the overall lowest P_{Aq} value detected of 0.18 at 61cm depth. From here the value increases sharply up core, rising from 0.18 (61cm) to 0.26 at 55cm. Further up core, from 55-43cm, the values decline with one oscillation en route to the second lowest P_{Aq} detected of 0.18 at 43cm. From 43cm- 34cm, the P_{Aq} sharply rise to its highest detected value of 0.41 at 34cm depth. Further on from 34cm to 16cm, the P_{Aq} values

display a gently sloping plateau, decreasing slightly in value up core, with a couple of minor troughs at 28cm and 22cm depth. The P_{Aq} values then drops rapidly from 0.38 at 16cm to 0.24 at 13cm, then to 0.23 at 7cm. At 4cm depth the value rises back up slightly to 0.3 before dropping again to 0.27 at 1cm, towards the present day (Figure 14). The average P_{Aq} value across the core is 0.28, with values ranging from 0.18 (61cm) to 0.41 (43cm).

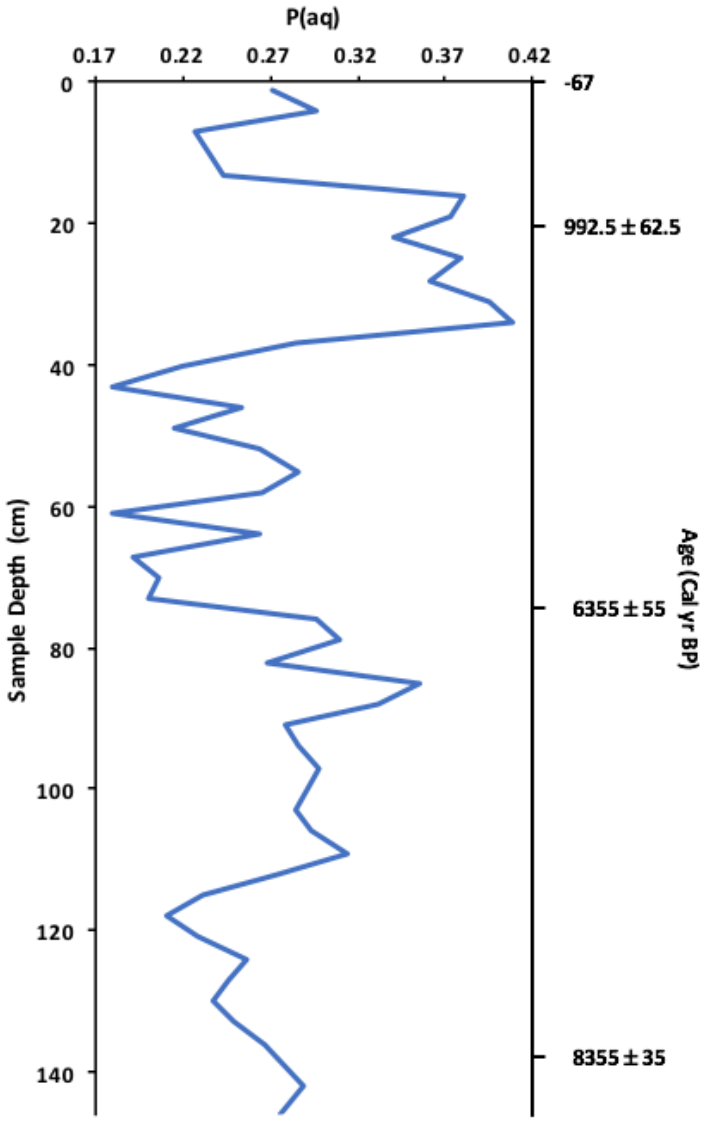

Figure 14: Graph shows P_{Aq} values plotted against sample depth (cm) and age (cal yr BP).

3.1.6 Proportion Terrestrial Material

The P_{Wax} results are effectively an opposing, asymmetric but mirror set of results to the P_{Aq} as reflecting the relative changes in proportion of terrestrial material directly infers changes in P_{Aq}. These results display the fact that the P_{Wax} values were significantly greater than P_{Aq} values, in fact they were almost 3 times more concentrated on average (0.28 in P_{Aq} and 0.78 in P_{Wax}).

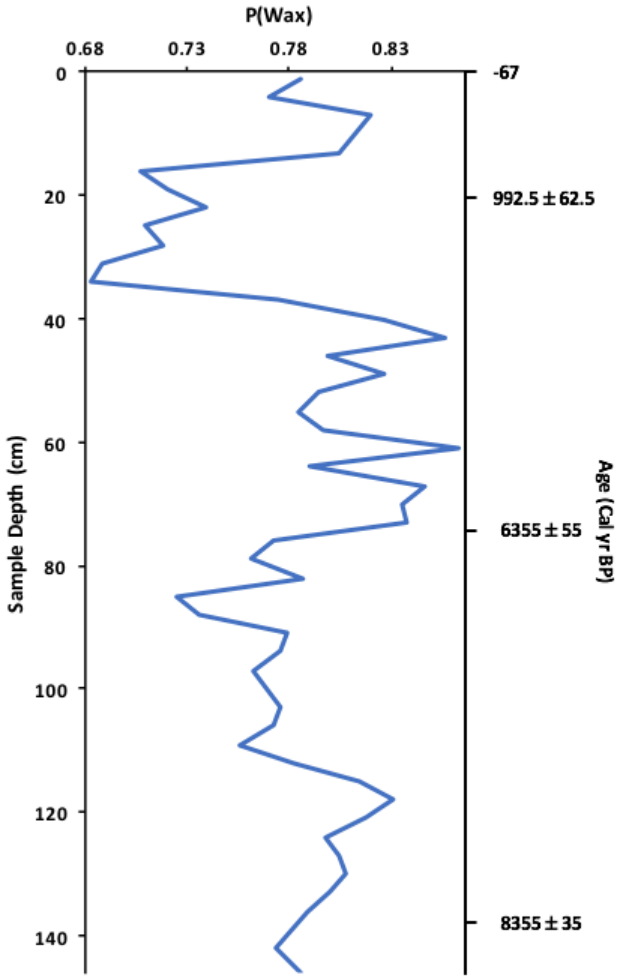

Figure 15: Graph displays P_{Wax} values plotted against sample depth (cm) and age (cal yr BP).

Describing the core from the base up, the first 28cm section from 146cm to 118cm depth, mimics the P_{Aq} reverse results, displaying a gradual rise in P_{Wax} from 0.78 (142cm) to 0.83 (118cm). From 118-109cm the P_{Wax} values drops down from 0.83 at 118cm to 0.76 at 109cm (Figure 15). Moving further up core, from 109cm to 76cm depth the P_{Wax} values maintain a fairly flat plateau, with values decreasingly slightly up core, and one noticeable trough which bottoms with a P_{Wax} of 0.72 at 85cm, the opposite of the distinct peak P_{Aq} 85cm value. From 76cm to 73cm the P_{Wax} rises rapidly from 0.77 to 0.84. From 73cm to 67cm, there is a fairly short, stable high value plateau in P_{Wax} values before dropping to 0.79 at 64cm and spiking quickly back up to 0.86 at 61cm depth. Beyond this up core, from 58cm-46cm the P_{Wax} values retain another stable plateau, with values in this 12cm section averaging 0.8. AT 43cm depth however, the P_{Wax} values spikes up slightly to 0.86, before dropping down rapidly to the lowest detected P_{Wax} value of 0.68 (34cm) from 43 to 34cm, reflecting the terrestrial opposite of the P_{Aq} value rise at this point. Moving further up through time towards the present, from 34cm to 16cm depth the P_{Wax} values show high variability superimposed on a plateau with values rising slightly up core, and average across this 18cm, low plateau of 0.71. This reflects the corresponding terrestrial input data of the high P_{Aq} plateau. Over the final top section of the core, the P_{Wax} value initially jumps from 0.71 at 16cm, to 0.8 at 13cm depth. It continues to gradually rise to 8.2 at 7cm

before dropping to 0.785 at 1cm nearest the present day (Figure 15). The P_{Wax} values range from 0.68 (34cm) to 0.86 (61cm), with a previously mentioned average of 0.78.

3.2 N2 Fraction

Unfortunately, despite scanning all 46 samples and double checking, no alkenones were detected by the GC-MS in the Qinghai Lake Sediment (Figure 16). A few FID scans were also analysed with the same results. Therefore, the lack of alkenones completely inhibits any chance of using alkenone calibration techniques to calculate lake surface temperature changes and no calculations have been undertaken.

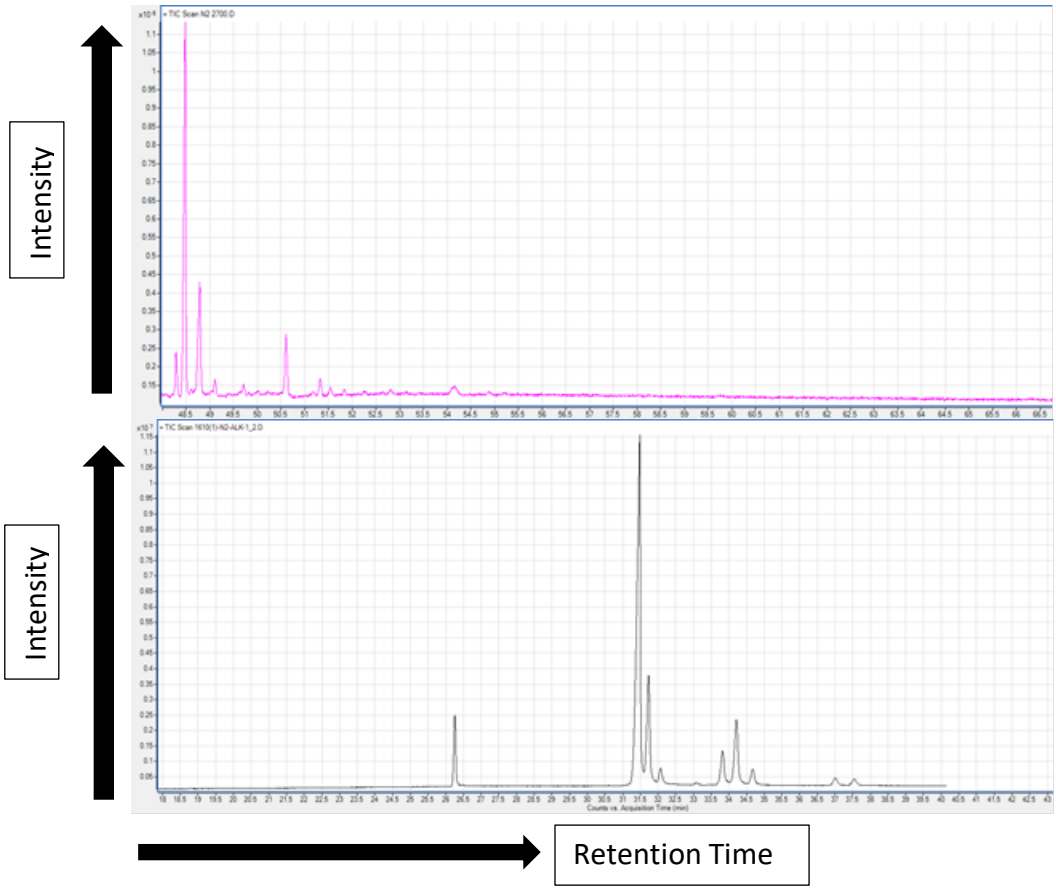

Figure 16: Figure shows two separate GC-MS chromatographs. The top chromatograph is an example of a typical N2 sample profile from Qinghai Lake, at the correct retention time, displaying no alkenones, which should appear in the middle section of the chromatograph. For comparison, the bottom is an example of a sample provided by Dr Julien Plancq showing a typical alkenone profile. Note, the bottom chromatograph used a different method so the retention time is different, but the profile shows subtle differences in peaks (in comparison to the top chromatogram) indicating the detection of alkenones.

3.3 N3 Fraction

Four pilot samples were run near the end of 2017, prior to the significant GC-MS issues occurring and provided an opportunity to gather some data on the N3 fraction, including sterols and long-chain diols. The issues will be further examined and explained in depth in the discussion section (pages 56 and 57).

The GC-MS TIC and SIM chromatograph results of N3 pilot samples 2368, 2369, 2370 and 2371 are fantastic and show clean, easily identifiable diols in both modes, with distinct ion signatures in TIC mode spectrum preview (Figure 17). In particular, pilot sample 2369 shows the classic diol characteristic chromatographs signature, with intense TIC diol peaks that have distinctive ion signatures allowing for easy diol identification and very pronounced diol peaks in SIM mode (Figure 18). In comparison to the much messier and distorted results of the main batches (Figure 19), these pilot results are almost ideal. The SIM data extraction method provided peak areas for the C_{28}, C_{30} and C_{32} diol isomers in the pilot samples. The peak areas were used to calculate the fractional abundance of the four diol isomers in each pilot sample used to calculate the LDI, which allowed the subsequent calculation of the LDI (Table 2) and then temperature for each sample.

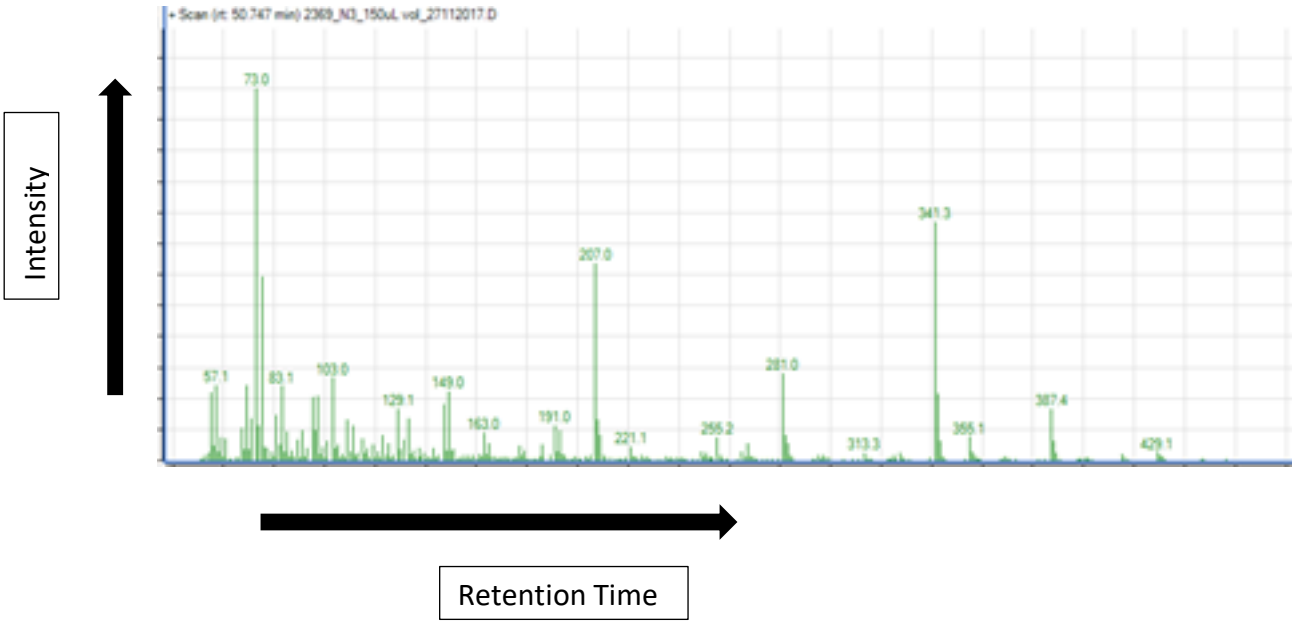

Figure 17: Chromatograph displays spectrum preview of a typical, strong ion signature for the C_{32} diol in sample 2369. This example displays high concentrations of key ions included 73, 149 and 341. Other ions are more significant in different diols but in this C_{32} example these are key indicators.

Figure 18: Annotated GC-MS chromatographs from pilot sample 2369, with the top graph showing the TIC sample, and the bottom showing the SIM sample. Note the clear SIM mode peaks indicated by red arrows illustrating the presence of diols.

Figure 19: Example of typical GC-MS chromatographs from batch samples. The top graph shows the TIC scan and the bottom shows the SIM scan. It is notably different to the pilot sample chromatograph results, and this issue persists in all samples, suggesting a GC-MS problem. Potentially a tuning issue or a dirty column may have caused these problems.

Table 2: Conveys the calculated LDI's and subsequent calculated lake surface temperature values for the respective pilot samples.

Pilot Sample Number, and Age (cal yr BP)	LDI	Temperature (°C)
2368- 1936 cal yr BP	0.52	12.83
2369- 3945 cal yr BP	0.67	17.41
2370- 7180 cal yr BP	0.74	19.56
2371- 8530 cal yr BP	0.92	25.13

The temperature results, despite the significantly low resolution, indicate an overall decline in temperature from the base of the core up, with an initial high temperature near the base of the core of 25.13°C calculated at 140cm depth, followed by a steady decrease in temperature up core to a calculated temperature of 19.56°C at 100cm depth. Between 100cm and 50cm the temperature change appears more gradual, declining from 19.56°C to 17.41°C. Over the last two samples available, the temperature appears to drop more rapidly again, with approximately a 5°C drop over 20cm from 17.41°C at 50cm depth to 12.83°C at 30cm depth (Figure 20). Stigmasterol was detected in all four pilots and lanosterol was detected in sample 2368.

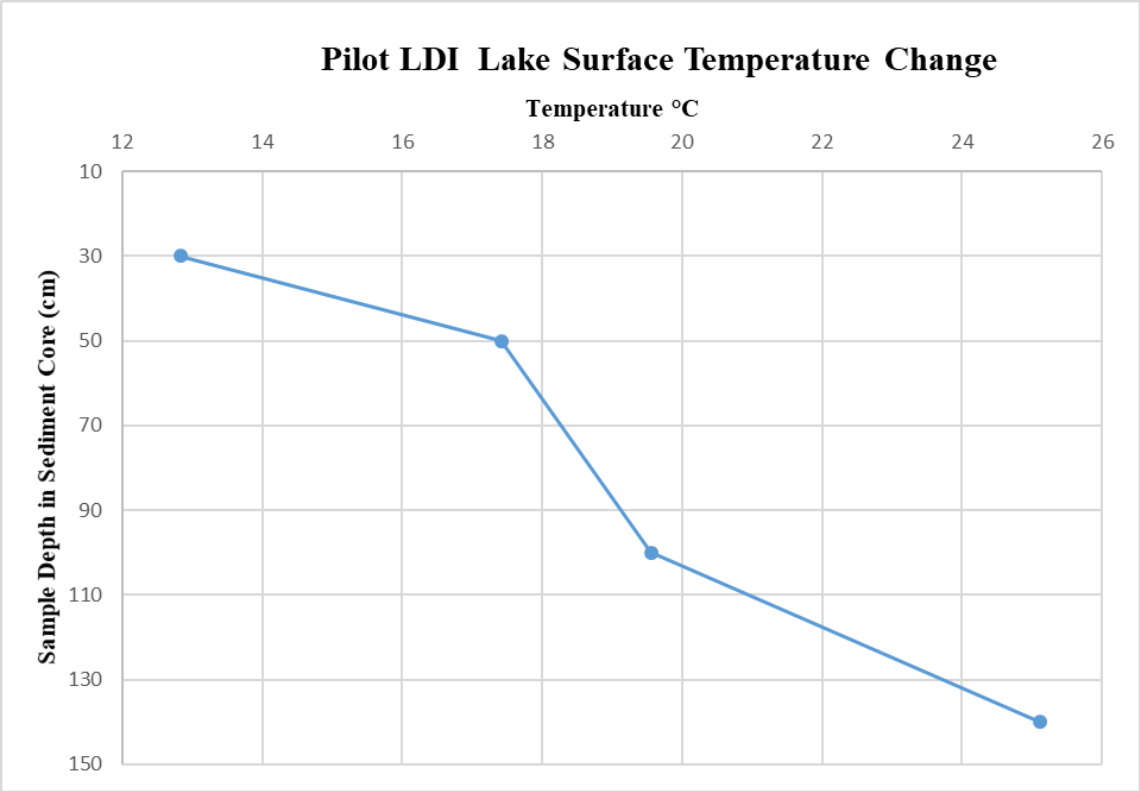

Figure 20: Graph illustrates the calculated pilot sample lake surface temperature plotted against sample depth.

3.4 TAF

TAF sample concentration results were gathered for all fatty acids detected, which ranged between C_{16} and C_{34} in carbon chain length. Of particular interest however, were select acids known to come from certain sources, that are grouped as either short chain acids, mid-chain acids or long chain acids. Results descriptions will encompass the acids included in these groups, and descriptions will be separated based on grouping. In the short chain acids, C_{16} and C_{18} acid results from algal sources will be described. C_{22} acid concentrations predominantly from aquatic macrophyte sources (Hou *et al.*, 2006) and C_{24} from sphagnum and mosses (Baas et al. 2000) comprise the mid-chain acids, which are graphed and described individually to point out differences. The C_{28}, C_{30} and C_{32} acids make up the long chain acid group, produced by terrestrial plants in the epicuticular leaf wax layer (Hou *et al.*, 2006). There are some general correlations shared by all acids in all three groups, such as relatively low concentrations at the base of the core, concentration spikes around 97cm depth approximately, a varying period of low concentrations up core, followed by a rapid spike in concentration and oscillating very high and low concentrations over the last 70-40cm at the top of the core, depending on group chain length (Figures 20, 21 and 22). Each group will be individually described to provide greater detail.

3.4.1 Short Chain Acids

The short chain acids C_{16} and C_{18} have concentrations ranging from 0.73µg/g to 9.27µg/g in C_{16} and from 1.72µg/g to 17.13µg/g in C_{18}, respectively. C_{18} concentrations are consistently higher than C_{16} values, but the concentration changes in each acid approximately mirror each other at each stage (Figure 21). From the base of the core up, over the first 10cm section both acids concentrations rise from 1.56µg/g to 3.27µg/g in C_{16} and from 2.67µg/g to 3.78µg/g in C_{18}. Concentrations then drop to a low value plateau between 133cm-112cm, with average concentration values of 1.84µg/g in C_{16} and 2.21µg/g in C_{18} across this period. Moving up core, from 112cm-97cm depth the concentration spikes from 1.57µg/g to 4.82µg/g in C_{16} and from 1.93µg/g to 7.46µg/g in C_{18}. Following this 97cm peak, concentrations decrease to C_{16}s second lowest recorded value of 1.36µg/g, and C_{18}s lowest recorded concentration of 1.72µg/g at 82cm (Figure 21). From 82-70cm depth the concentration value rises and falls slightly in both acids, before increasing rapidly to the first major peak values of 8.53µg/g in C_{16} and 15µg/g in C_{18} at 64cm depth. From this 64cm peak to the closest sample to the top of the core at 1cm depth, in both acids, the concentration values rise and fall rapidly in a succession of major peaks and troughs. Major peaks are located at 64cm, 43cm, 28cm, 13c and 4cm depth, with corresponding major troughs at 58cm, 46cm, 34cm, 16cm and 1cm depth (Figure 21). The highest C_{16} concentration of 9.273µg/g occurs at 43cm, while its lowest concentration of 0.73µg/g occurs at 34cm depth. The C_{18} acids highest concentration of 17.13µg/g occurs at 13cm depth. The average concentration across the C_{16} record is 3.24µg/g, while in C_{18} the average concentration is slightly higher at 4.68µg/g.

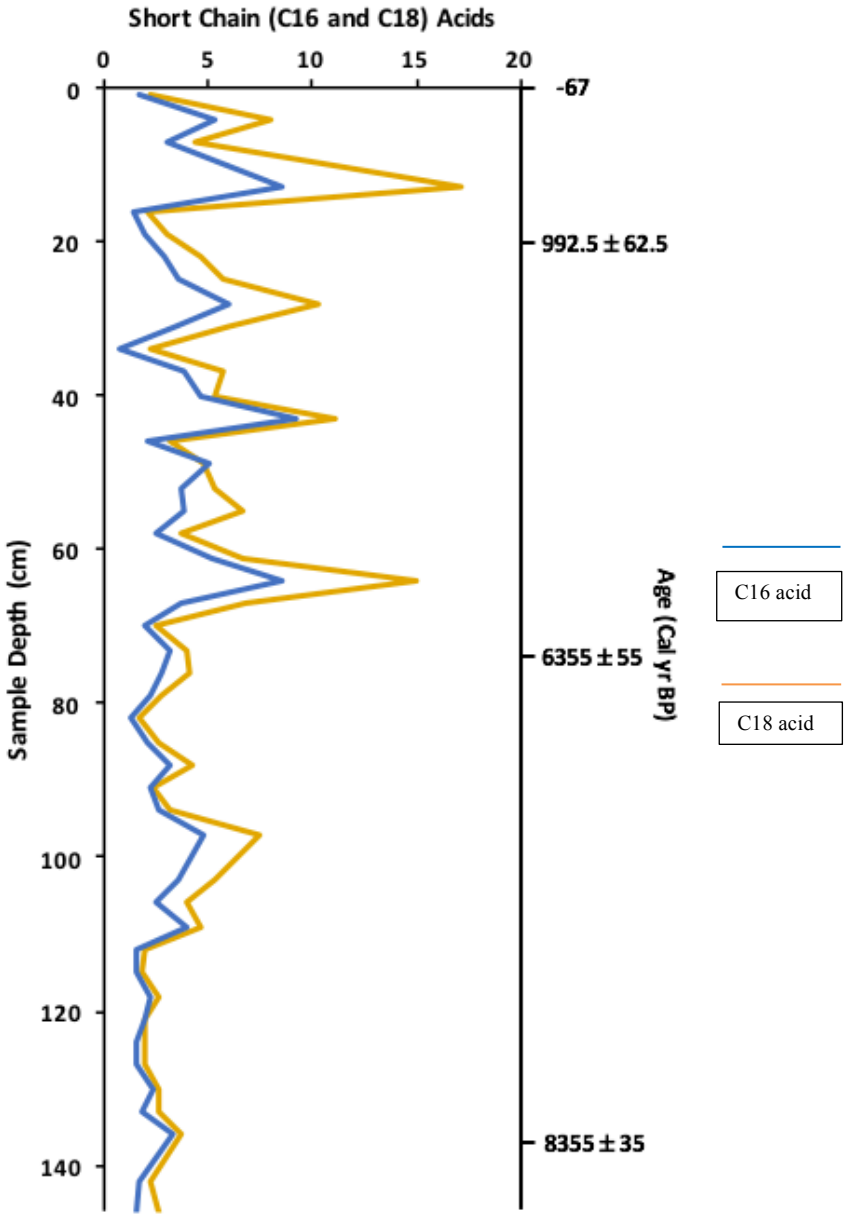

Figure 21: Graph shows the concentrations of C_{16} and C_{18} acids in µg/g plotted against sample depth (cm) and age (cal yr BP).

3.4.2 Mid-Chain Acids

The C_{22} acid concentrations, from the base of the core upwards, show an initial low concentration plateau, with a slight increase in value up core between 146-112cm depth, with an average concentration of 2.25µg/g across this period. Moving up core form 112 to 97cm depth the concentration quickly increases from 1.870µg/g at 112cm to 9.36µg/g at 97cm, the first major peak, before dropping very rapidly to 1.87µg/g at 91cm depth (Figure 22). The concentration value rises again to a minor peak of 5.49µg/g, at 73cm, with a couple slight fluctuations along the way up core. The

concentration then declines rapidly to another trough value of 1.72µg/g at 70cm. Moving up core from 70-46cm, the value oscillates to a couple of minor peaks and troughs, with a notable peak of 8.04µg/g at 52cm, before falling to the 46cm concentration of 4.14µg/g. From this trough, the concentration spikes rapidly to its highest recorded value of 25.22µg/g at 43cm, before quickly falling back to 3.19µg/g at 34cm depth. The pattern of oscillating concentration continues up core with it rising to another minor peak of 7.27µg/g at 28cm, and dropping to 2.76µg/g at 16cm. It spikes again to the second highest value of 17.7µg/g at 13cm, before dropping and rising again to the last major peak of 10.5µg/g at 4cm depth, before decreasing to the value of 3.03µg/g at 1cm, towards the present day (Figure 22). Concentrations range from 1.27µg/g at 142cm, to the highest concentration of 25.2µg/g at 43cm. The average C_{22} concentration across the core is 5.1µg/g.

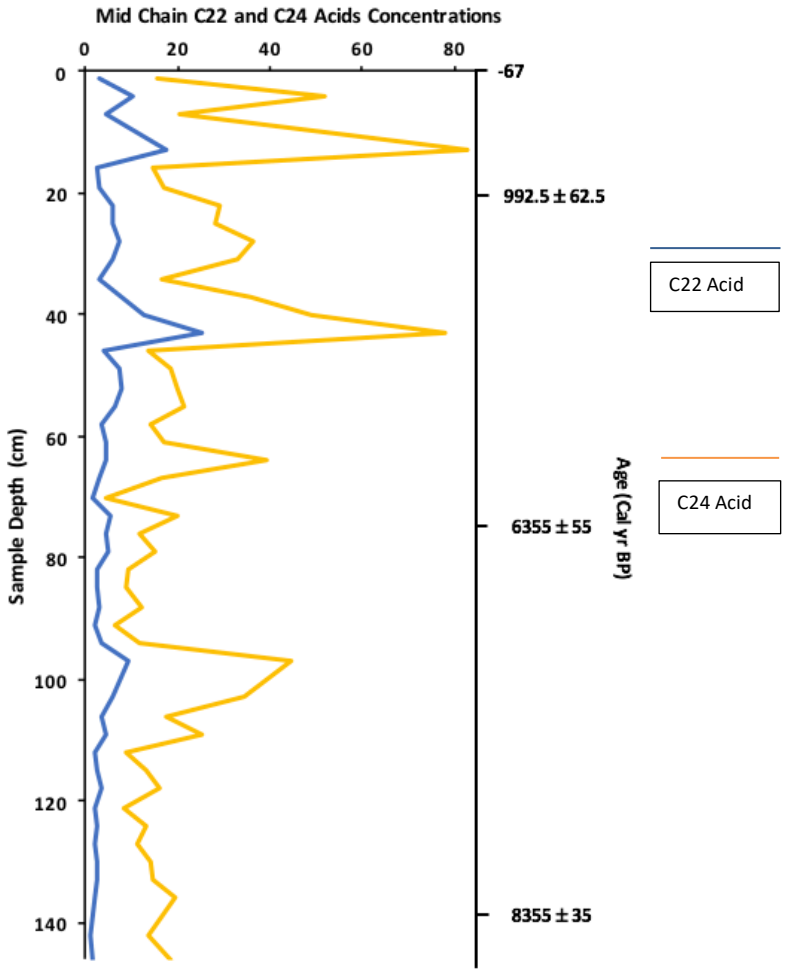

Figure 22: Graph displays concentration in µg/g of mid-chain C_{22} and C_{24} acids plotted against sample depth (cm) and age (cal yr BP).

The C_{24} acid results generally correlate with those of the C_{22} acid. However, there are some differences. Working from the base of the core up, the C_{24} concentration initially decreases (as opposed to it rising initially in C_{22}) from 146-121cm, with values

dropping from 18.44µg/g to 8.26µg/g, respectively (Figure 22). The average concentration across this period of gradually decreasing concentration is 14.15µg/g. The concentration then spikes upwards from 18.44µg/g at 121cm to 44.45µg/g at 97cm depth, with a couple of concentration fluctuations between, up core towards this 97cm peak. Moving further up core, the concentration decreases rapidly to 6.35µg/g at 91cm depth. The concentration then gradually increases again, with a couple of fluctuations in the data up core, to a 73cm minor peak of 19.92µg/g, before dropping quickly to the lowest recorded concentration of 4.4µg/g at 70cm depth. Following on from this low upwards, the concentration rises to a major peak of 39.26µg at 64cm (Figure 22). From this peak up core, the concentration drops to 13.82µg/g at 46cm, before spiking rapidly to 78.22µg/g at 43cm depth. The concentration then decreases quickly to 16.42µg/g at 34cm depth in a major trough, before rising again up core to another major, but smaller peak of 36.44µg/g at 28cm. Moving further up core, the concentration again drops to a trough value of 14.58µg/g at 16cm, then spikes massively and rapidly to the highest recorded C_{24} concentration of 82.85µg/g at 13cm. Over the final 13cm, the concentration quickly falls and rises to another major peak of 51.65µg/g at 4cm, before dropping sharply to the 1cm concentration of 15.36µg/g, towards the present day (Figure 22).

As mentioned previously, there are differences between the C_{22} and C_{24} acids, the first of which is that the C_{24} acid concentration is much higher than C_{22}. From 146-121cm the C_{22} values plateau with a slight increase, while C_{24} values decrease gradually. The 42cm section from 112cm to 70cm of the C_{22} chromatograph is very similar to the C_{24} profile, in particular the relative 97cm peak, 91cm trough, 73 cm minor peak, and 70cm trough concentration values (Figure 22). In the C_{22}, the 64cm peak is very minor, while in the C_{24} acid results, the peak is relatively much more prominent. Although the 43cm and 13cm peaks are both very prominent in both acid result, in C_{22} the 43cm is relatively larger, while in C_{24} the 13cm peak is the most prominent. A final couple of differences near the top of the core is that the 28cm peak concentration is relatively larger in the C_{24} results compared to in the C_{22} (Figure 22). However, the C_{22} results in the final 43cm section at the top of the core are very comparable and similar, relatively, to the C_{24} concentration profile.

3.4.3 Long Chain Acids

In the long chain group, the C_{28}, C_{30} and C_{32} graphed concentration results mimic each other throughout the core record, but at different concentrations (Figure 23). For this reason, C_{30} results will be described to portray how the concentrations change across the core for all acids, and it should be noted that C_{28} concentrations are approximately slightly under double the C_{30} concentration at each sample, while C_{32} concentrations are approximately around half the C_{30} concentrations at each sample (Figure 23). Concentration values range from 2.1µg/g to 126.22µg/g in C_{28}, with an average

concentration of 28.16µg/g. The C_{30} concentrations range from 0.84µg/g to 72.25µg/g, with an average concentration of 16.2µg/g. Finally, the C_{32} concentrations range from a low of 0.28µg/g to 27.59µg/g with an average concentration of 6.49µg/g across the core.

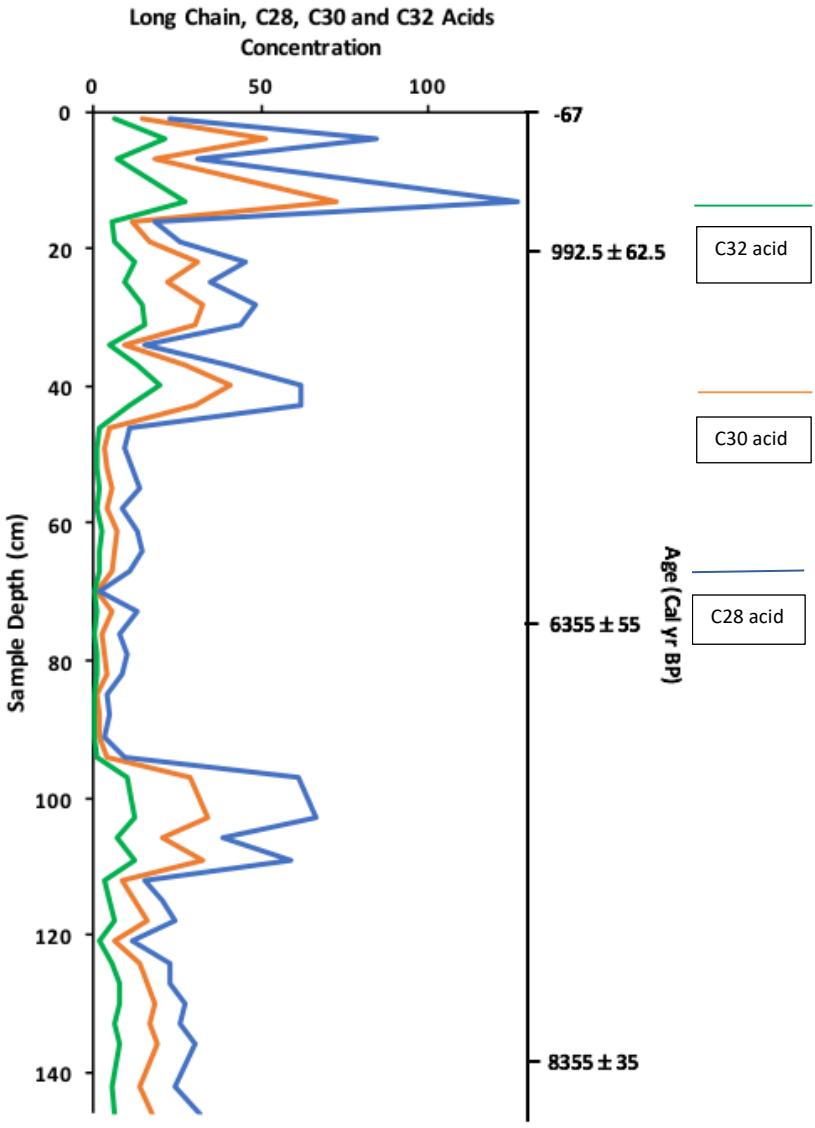

Figure 23: Graph displays the C_{28}, C_{30} and C_{32} acids concentration in µg/g plotted against sample depth (cm) and age (cal yr BP).

From the base of the core working up, the C_{30} concentration from 146-124cm holds a slightly inconsistent plateau with one main dip in concentration to 13.86µg/g at 142cm (Figure 23). The average concentration across this rough plateau for C_{30} is 16.47µg/g. From 124cm to 121cm the concentration drops down from 13.71µg/g to 6.36µg/g, before rising again up to 15.69µg/g at 118cm. From this 118cm minor peak, the concentration decreases from 15.69µg/g down to 8.2µg/g at 112cm depth. Moving up core, the concentration then spikes rapidly to 32.6µg/g at 109cm, before quickly dropping again to 20.57µg/g at 106cm, then rapidly rising again up to 34.0µg/g at

103cm with a further slight concentration decrease to 28.83µg/g at 97cm. The 106cm decrease in concentration is the only anomaly in what otherwise could be described as a 109-97cm concentration plateau. From 97cm up core, the concentration decreases from 28.83µg/g to 4.13µg/g at 94cm depth. From 94cm to 46cm depth, the concentration values hold a relatively stable plateau, with one distinct exception, where concentrations decrease to their lowest values in all three acids, 0.84µg/g in C_{30}. The average concentration across the 94-46cm plateau section for C_{30} is 3.72µg/g. This low concentration plateau is a distinct feature that does not appear in other shorter chain acid group results. Further up core, the concentration spikes from 4.69µg/g at 46cm, to 30.03µg/g at 43cm, then further to 41.03µg/g at 40cm, the first major peak values to appear since those down-core from the low plateau (Figure 23). The concentration then drops down to 9.11µg/g at 34cm, before rising again to another peak of 32.77µg/g at 28cm. From 28 to 22cm the concentration first falls about 10µg at 25cm then rises to 30.75 µg/g at 22cm. From 22cm to 16cm the concentration falls to 11.45µg/g, then from this low it rebounds up rapidly to the highest recorded value of 72.25µg/g at 13cm. All three acids highest recorded concentrations appear at 13cm depth. The concentration drops to 18.46µg/g at 7cm before rising to the final major peak of 51.59µg/g at 4cm. The concentration then decreases towards the present day, with the 1cm concentration dropping to 14.36µg/g (Figure 23). Not only all three acids in this long chain group, but seemingly all acids analysed share the same concentration profile changes with extreme relative similarity over the top 16cm of core samples.

3.4.4 Short to Long Chain Acid Ratio

The ratio of short vs long chain acid ratio was graphed for analysis. From the base of the core working up, initially the ratio holds a very low value rough plateau between 146cm and 124cm depth. The average ratio value across the 22cm section of core is 0.11. From 124cm to 121cm, the value jumps slightly from 0.0995 (124cm) to 0.2192 (121cm), before dropping back down to 0.12 at 118cm (Figure 24). This minor peak is the only slight anomaly in an otherwise low plateau of values from 146cm to 97cm depth. From 118cm to 97cm the plateau ratio value has an average of 0.11. From 97cm to 88cm, the ratio value spikes rapidly from 0.14 up to 1.180, the second highest ratio recorded. Following this major peak up core, the ratio drops back down to 0.25 at 82cm., before quickly rebounding back up again to the highest recorded ratio of 1.53 at 70cm, with one minor oscillation peak between at 76cm. Moving further up core, from 70cm to 49cm depth, the ratio value falls and rises in two more fluctuation to produce two major peaks of 1.15 at 54cm and 0.83 at 49cm, with a large trough between these two peaks, with a lowest value of 0.52 at 58cm depth. From the 49cm peak, the ratio value drops rapidly down to 0.1 at 40cm. Over the top 39cm of core samples, the ratio values again hold a low plateau, with an average ratio from 40-1cm

of 0.13 (Figure 24). There is one very minor peak of 0.2 at 28cm that increases this average slightly.

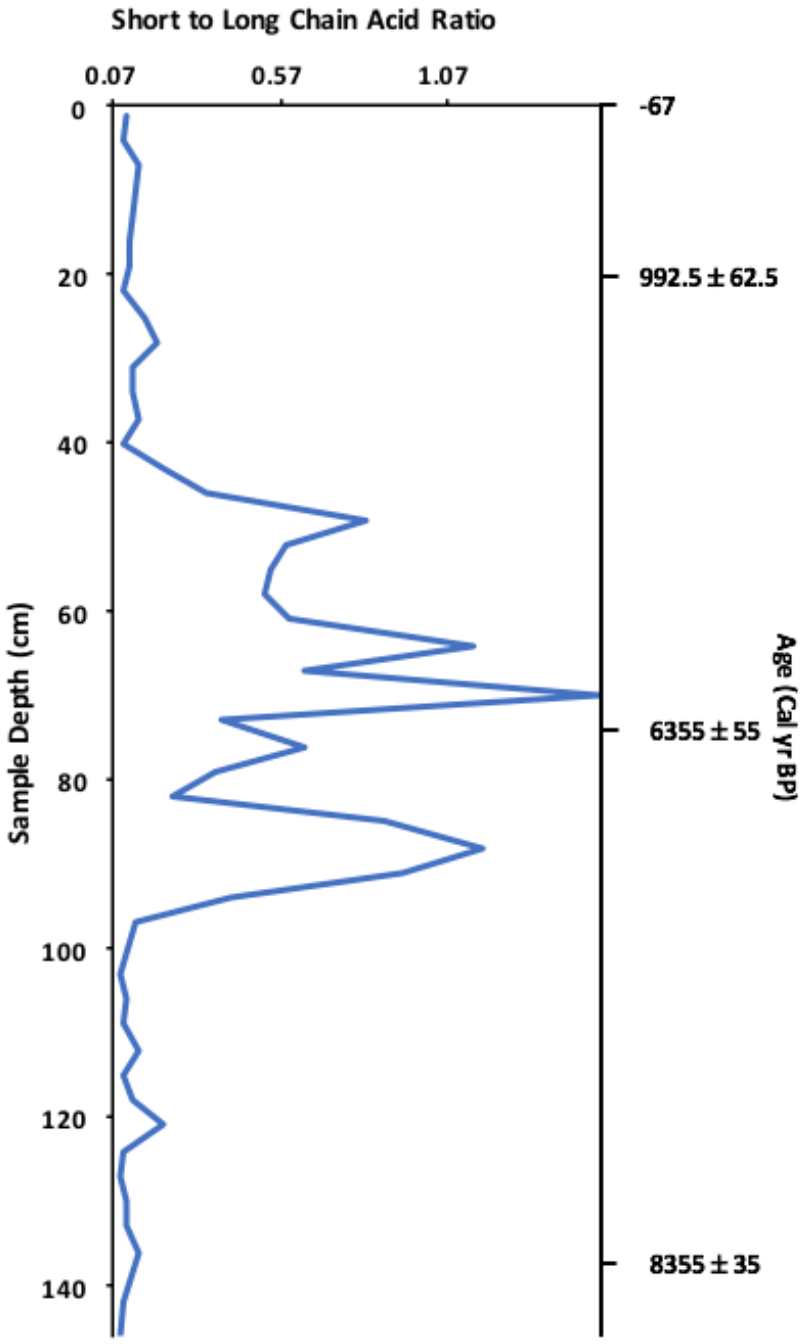

Figure 24: Graph illustrates the short to long chain acid ratio plotted against sample depth (cm) and age (cal yr BP).

4 Discussion

4.1 n-Alkanes and Acids as Biomarkers in Lake Sediments

In this study, the n-alkane biomarkers are used to provide information on how the environment around Qinghai Lake changed over the Holocene. n-alkanes are straight chain hydrocarbons that provide a useful paleoclimate reconstruction tool for a vast variety of reasons. n-Alkanes are produced by bacteria, as well as aquatic and terrestrial plants. They are produced in the epicuticular layer of higher plant leaves, as leaf wax compounds and have a high predominance of odd-numbers of carbon atoms in the hydrocarbon chain when sourced from plants (Eglington and Hamilton, 1967). Crucially, research has proven that n-alkane chain length is diagnostic of their source. Eglington and Hamilton (1967) demonstrated that generally, odd numbered n-alkanes with a very long carbon chain length (between C_{27} and C_{35}) are sourced from terrestrial plants. Meanwhile aquatic plants have been shown to generally produce shorter chain, odd numbered n-alkanes, usually between C_{17} and C_{21} in length (Cranwell *et al*., 1987). This knowledge allows for the implication and quantification of changes in climate based upon the changes in vegetation reflected by n-alkane records. n-Alkanes are very robust compounds, and are preserved well in sediment, making them legitimate tools for analysing climate over many thousands of years (Castañeda and Schouten, 2011). Changes in the average chain length of n-alkanes have been shown to indicate changes in temperature and precipitation (Baker *et al*., 2016; Zhou *et al*., 2005), and alteration in the proportion of aquatic material/proportion of terrestrial material in a lake system can reflect changing water levels and thus infer changes in climate and monsoon intensity (Baker *et al*., 2016; Eglington and Hamilton, 1967; Zhou *et al*., 2005). It can be difficult to know exactly what has caused the changes in n-alkane chain length at times. When a terrestrial plant becomes stressed, whether it be by an increase in temperature or a decrease in precipitation (and thus available water for the plant) it will produce longer chain-alkane leaf waxes to protect the plant from losing water to the external environment. Although it is generally presumed that n-alkane leaf wax production is controlled to a greater extent by precipitation than temperature, the n-alkane results have to reviewed in context with our proxies for greater certainty (Zhoa *et al*., 2003), and may be interpreted differently based upon other proxy results.

Previous studies have shown that higher plants from terrestrial environments produce n-alkanes with a notable odd-to-even carbon chain length predominance (Eglington and Hamilton, 1967). The carbon preference index provides a method that allows the calculation and analysis of the odd to even, molecular distribution preference of n-alkanes. Higher CPI values reflect greater differences in the relative concentrations of odd numbered n-alkanes to even numbered n-alkanes (Rao *et al*., 2009). Furthermore,

Roa *et al*., (2009) postulate that CPI values can reveal changes in temperature. They investigated changes in CPI from varying latitudes and discovered that sub-tropical and temperate regions had higher CPI values than tropical regions, and that CPI increased with latitude, implying that CPI values increase with progressively cooler temperatures. CPI values from two cores from Japan reflect temperature changes in glacial/interglacial cycles with good consistency, and also report that lower CPI values indicating a warmer, wetter climate (Ishiwatari *et al*., 1994; Yamada and Ishiwatari, 1999). However, Roa *et al*., (2009) also cite examples were periods of known warm, wet climate have been recorded alongside low CPI values, so although the CPI has great potential as a paleoclimate tool, more research is needed to refine this methods accuracy of assessing temperature and precipitation changes.

The CPI also provides a tool to analyse and assess the standard of preservation of the organic matter extracted from the core's sediment (Baker *et al*., 2016), with greater values implying the presence of better-preserved n-alkanes, and lower values indicating more degraded n-alkanes. This in turn, allows us to assess how reliable results are from various points within the core, as poorly preserved organic matter may not be entirely accurate in representing changes in climate.

The relative proportion of terrestrial and/or aquatic material present in a lake system can provide insight to climate condition, in particular lake level and therefore precipitation (Baker *et al*., 2016). The general rule is that a higher P_{Aq} value indicates more aquatic material and thus a period of higher water levels and more intense precipitation, inferring a stronger monsoon. The inverse applies to a high P_{Wax} high value, with this indicating low lake water levels and thus less precipitation and a weak monsoon. However, this rule has to be taken with caution, as periods of high precipitation can often wash more terrestrial material in to the lake system with run-off from the surrounding slopes increasing the P_{Wax}, so it is not always strictly correct. Both data sets display the opposite trends of each other (Figures 13 and 14), so only one is necessary for discussion and the P_{Aq} will generally be discussed.

The hopane results can provide some indication of terrestrial input to the lake system and in turn illuminate potential precipitation changes in the region. This is because the majority of hopanes are sourced from terrestrial soil bacteria, and an increase in hopanes detected in the sediment points to an increase in terrestrial soil input caused by increased soil instability as a result of saturation with water (Cooke *et al*., 2008). Therefore, periods of intense monsoon activity may destabilize the surrounding lake slopes and result in an increase of hopanes deposited in the lake sediment via increased erosion, soil slumps and landslides. Increased precipitation can also wash hopanes in to the lake with run-off.

The short to long chain acid ratio effectively displays whether long or short chains are dominant in the lake sediment record at different times. This ratio reveals information about aquatic productivity and precipitation in the surrounding lake Qinghai catchment. This is partly due to the fact that Qinghai Lake is an enclosed system, with no river input or output (Wang *et al*., 2002 and Yang *et al*., 2016). It is fed by rainfall/groundwater and drained by evaporation. Therefore, when there is a low ratio, with a dominance of long chain terrestrial acids, this implies that there has been more precipitation, which is responsible for washing the long-chain terrestrial acids in to the lake system in run-off down the surrounding slopes. Periods with high ratios suggest the opposite, when there has been less rainfall and therefore less possibility for terrestrial acid input to the lake system, so shorter aquatic chain acids dominate (Hou *et al*., 2006).

4.2 Environmental Change and Processes in and around Qinghai Lake

This section will discuss the key results from the biomarker record from Qinghai Lake, Yunnan Province, on their own merit, and the environmental changes they may infer. The following sections will then draw on existing literature and make further comparisons between the biomarker interpretations to contextualise this study within the existing literature.

A number of previous studies have shown that certain biomarkers (e.g., n-alkanes and hopanes) can indicate contributions aquatically sourced versus terrestrial sourced material into a lake, as well as environmental conditions and how they affect the precursor organism. The n-alkane, acid and hopane data (Short-to-long chain acid ratio, ACL, P_{aq}, and C31 BB) for Qinghai Lake are summarised in Figure 25. All of these proxies fluctuate throughout the 146cm long core with major changes that can be divided into three main zones: Zone I (146cm to ~95cm; approximately 8.8k cal yr BP to 7k cal yr BP), Zone 2 (95cm to 43cm; approximately 7k cal yr BP to 3.24k cal yr BP) and Zone 3 (43cm to 1cm ; approximately 3.24k cal yr BP to -67 cal yr BP).

Zone I (146 to 95 cm; approximately 8.8k to 7k cal yr BP)

In Zone 1, ACL values are generally high, and the short-to-long chain acid ratio is low across this basal section. Higher ACL values generally imply that the terrestrial plants contributing to the record (assuming the species is not changing drastically in the region due to agriculture etc., which we know it was not) were becoming stressed. Stresses that contribute to production of higher chain leaf waxes include lack of precipitation (Zhoa *et al*., 2003) or higher temperatures. In this study, the higher ACL values generally coincide with low values for the short-to-long chain acid ratios, which suggest that there is a dominance of terrestrial acids here. Given these data and the fact that precipitation is rarely limited at our site (average annual rainfall of 1482mm, Climate-Data.org, 2019), we interpret periods where the high ACL and low short-to-long chain ratio values coincide as a strong indication of increased precipitation, that also provides a means of transporting these acids and alkanes in to the lake system as seen by Hou *et al*. (2006), as well.

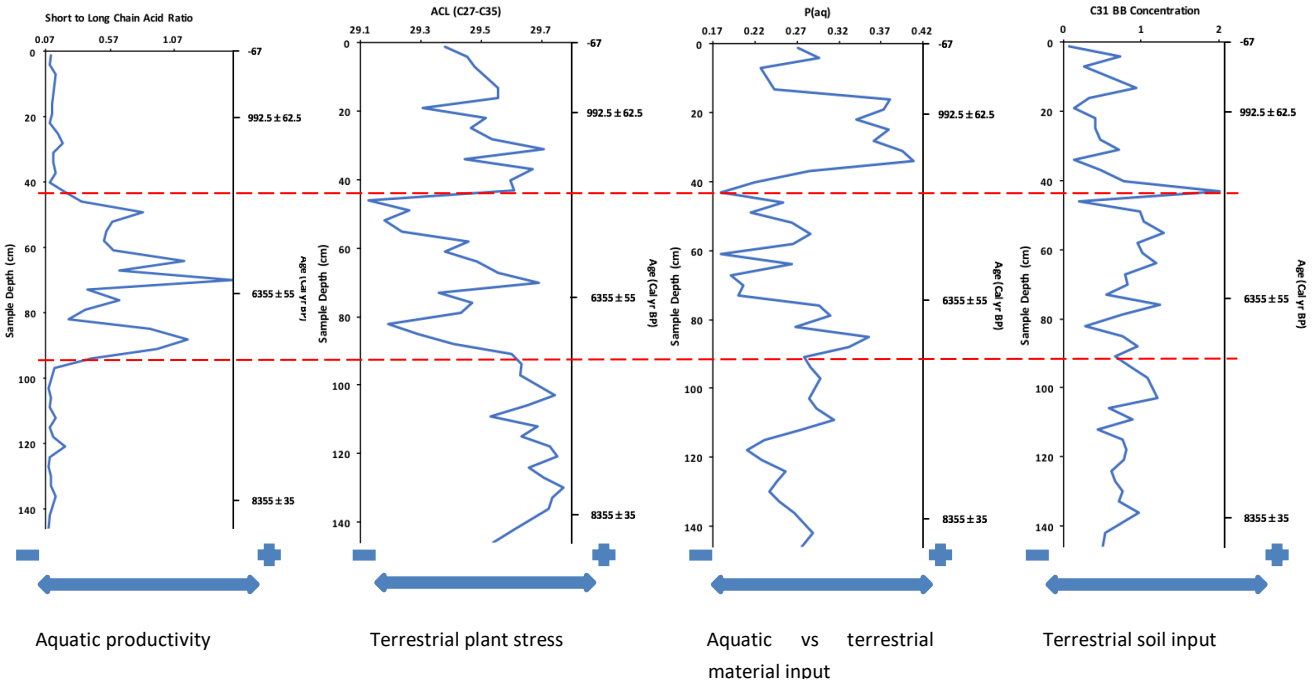

Figure 25: Displays 4 key biomarker graphs used to interpret environmental signals at Lake Qinghai, including short to long chain acid ratio, ACL, P_{Aq} and C31 BB Hopane Concentration, plotted against sample depth (cm) and age (cal yrs BP). It also includes an arrow scale showing the changes in environmental parameters that these respective biomarker proxy values/concentrations indicate. Dashed red lines indicate the approximate boundaries of the zones.

The hopane concentration across Zone 1 oscillates but steadily increases. Hopanes are sourced from terrestrial soil bacteria and are a good indicator of precipitation, which washes them in to the lake system via run-off (Cooke *et al*., 2008). This suggests that moderate intensification of precipitation either overall or in specific events influenced sedimentation into the lake from 8.88k cal yr BP – 7.08k cal yr BP (Figure 25).

Higher P_{Aq} values at the start of Zone 1 (i.e., from 146 – 118cm; 8.88k to 7.76k cal yr BP) represent a high proportion of aquatic inputs into the lake relative to terrestrial inputs (Baker *et al*., 2016)). Often this is interpreted as higher lake levels, allowing for more aquatic productivity (Baker *et al*., 2016). In this region, this could infer more precipitation, implying a stronger monsoon. The P_{Aq} values are lower in middle of Zone 1, which could indicate increasingly drier conditions as a consequence of decreasing precipitation (Figure 25); however, because the ACL and short-to-long chain acid proxies are high and low, respectively, during this interval, it is more likely that very intense precipitation washed large quantities of terrestrial material in to the lake system, thus lowering the P_{Aq} value. A marked increase in P_{Aq} values from 7.76k cal yr BP to 7.47k cal yr BP to a high value of 0.31 here, implies an increase in lake

levels and monsoon intensity here. Until 91cm the value remains fairly consistent at around 0.29, inferring stable aquatic productivity in the lake (Figure 25).

Together the proxies across the basal section of core from 8.88k cal yr BP until around 7.08k cal yr BP – 6.89k cal yr BP suggest that initially, conditions become increasingly warm and wet, potentially indicating a stronger monsoon (Figure 25).

Zone 2 (95cm to 43cm; approximately 7k cal yr BP to 3.24k cal yr BP)

Moving up core, the ACL and P_{Aq} values shift with a sharp decline in ACL values from around 6.89k cal yr BP to 6.61k cal yr BP. The P_{Aq} initially rises to a high of 0.36 at 6.7k cal yr BP before following the ACL trend and declining sharply to 0.19 at 5.65k cal yr BP. This P_{Aq} is a measure of the relative aquatic versus terrestrial inputs to the lake, so a decline possibly represents a decline in lake water level via a decline in aquatic material, or an increase in terrestrial material input. The ACL decline suggests that terrestrial plants are less stressed by environmental conditions, caused by either changes to more favourable temperature/precipitation and/or in species of vegetation. The acid ratio suggests a rapid change to increased aquatic productivity with a very high value of 1.18 at 6.8k cal yr BP, before sharply reversing back to lower aquatic productivity, with low values of 0.25 at 6.61k cal yr BP (Figure 25). The hopane data shows relatively low values at 6.61k cal yr BP implying less terrestrial input, which we interpret as drier conditions or fewer intense rainfall events before increasing sharply to a high value at 6.42k cal yr BP, suggesting a change from dry conditions to wetter conditions. A hypothesis for the proxies together indicates a change from fairly dry conditions (or fewer intense rainfall events) to wet conditions is as follows: The traditional interpretation (Baker *et al*., 2016) of lower ACL values may explain the lower ACL value here, pointing to a wet period (Figure 25). The low P_{Aq} could be explained by washing of terrestrial material in to the system by increased precipitation, while the hopane data's initial low value indicates drier conditions, but the quick following spike in values from 6.61-6.42k cal yr BP shows an increase in terrestrial soil input to the lake system, likely caused by wetter conditions here, with a slight lag in the core record.

From 6.61k cal yr BP up core, the ACL value spikes very quickly to a high value of 29.69 at 5.95k cal yr BP showing that the terrestrial vegetation has become stressed. At the same time of 5.95k cal yr BP the acid ratio value also rises rapidly to the highest recorded value of 1.53, suggesting an increase in aquatic productivity and/or that less terrestrial acids are being washed in to the lake, so aquatic, short chain acids dominate. Around the same period, the P_{Aq} retains generally very low values, implying low lake levels with less aquatic material. These proxies together imply a very hot, dry period between around 6.42-5.05k cal yr BP, as the high ACL, high acid ratio and low value

P_{Aq} data indicate this may have been a dry period (Figure 25), so the high ACL may show that terrestrial plants were likely stressed due to a rare relative lack of precipitation or higher temperatures in the area during this period.

From the peak of this probable dry period (5.95k cal yr BP) up core, the ACL, acid ratio and P_{Aq} values decline fairly rapidly towards 2.94k cal yr BP. This potentially implies that terrestrial vegetation is becoming less stressed, aquatic productivity declines (possibly more terrestrial acids being washed in to lake also) and that there is less aquatic material vs terrestrial, with possibly lower lake levels. These changes together infer a change through drier conditions at 5.95k cal yr BP to more moderate monsoon intensity at around 4.75k cal yr BP (shown by all three proxies moderate values here), back to wetter conditions around the start of zone 3 further up core from 3.84k cal yr BP to 2.94k cal yr BP (Figure 25). Due to the combined low acid ratio and ACL values, this upper region of Zone 2 likely represents a period of more intense monsoon conditions in this area, with greater precipitation resulting in terrestrial vegetation being less stressed and more terrestrial acids being washed in to the lake. The hopane data also supports this with an increase in values up core around this period suggesting more terrestrial material being washed in to the lake due to higher precipitation rates/volumes. The P_{Aq} data values drops very low to 0.18 at 3.24k cal yr BP. This could also be due to more terrestrial material being washed in to the lake system by intense precipitation here, as indicated by other proxies, particularly the hopanes. The low P_{Aq} supports the low acid ratio indicating relative lower aquatic productivity here.

Zone 3 (43cm to 1cm; approximately 3.24k cal yr BP to -15yr BP)

From 3.24-2.34k cal yr BP the ACL, P_{Aq} and hopane data values rise quickly and by a great extent indicating a sharp change in climate (Figure 25). These proxy changes potentially imply that terrestrial vegetation once again becomes more stressed, that there is a much greater aquatic versus terrestrial material input in the lake, and that more terrestrial soil material is being input to the lake system, respectively. The acid ratio data remains low here, suggesting maintained levels of low aquatic productivity and a dominance of terrestrial acids here, implying conditions are still wet. The significant and rapid P_{Aq} data rise suggests a large rise in lake level. The hopane data spike indicates a large input of terrestrial material being washed in to the lake system (perhaps due to a landslide of material) and the P_{Aq} rises regardless. This implies a change to incredibly intense monsoon conditions here, perhaps with flash flooding. The ACL rise to very high values coinciding with the low acid ratio data together suggests higher precipitation, pointing to potentially very intense monsoon conditions here. The hopane data values drop back down quickly at 2.94k cal yr BP, implying that it was possibly a rapid burst of severe monsoon intensity prior to this decline, with

a quick increase in precipitation intensity that washed great quantities of hopanes/soil material in to the lake or caused a landslide to deposit this material in to the lake. However, the ACL and P_{Aq} sustain respective high values until around 1.13-0.76k cal yr BP, with the acid ratio retaining low values, implying a prolonged period of warm, wet climate with a strong monsoon. This lasts until 1.13k cal yr BP in the ACL record, and until 0.76k cal yr BP in the P_{Aq} record. This implies that some time approximately around these dates, the climate may have shifted to drier, cooler conditions. Hopane data supports that it may become drier with lower values suggesting less terrestrial soil input and consequently less precipitation. However, the acid ratio data suggests that climate stays fairly wet, so perhaps precipitation simply declines slightly, relative to previously intense volumes. An ACL and hopane data value decline at 910 cal yr BP suggests a drier period at this time, although it is not until 755 cal yr BP that the P_{Aq} data value declines significantly (Figure 25).

The ACL rises again at 755 cal yr BP, followed by a notable rise in hopane values at 601 cal yr BP (Figure 25), showing increased terrestrial vegetation stress and soil input, implying a change to wetter conditions with a stronger monsoon in the Qinghai Lake region after this brief period of slightly weakened monsoon activity. The acid ratio values remain low, coinciding with higher ACL values indicating the monsoon intensity is likely still fairly strong. Towards the present day the ACL, P_{Aq} and hopane data declines slightly, again suggesting a mild weakening of local monsoon intensity, which remains overall fairly strong, as the acid ratios remain consistently low.

4.3 Contextualisation of Qinghai Lake in the Regional Setting

4.3.1 Bottom Core Section (Holocene Climatic Optimum, from 8877 cal yr BP to 6895 cal yr BP)

The deepest sections ACL results from 146cm- 91cm depth likely illustrates the climatic influence of the Holocene Climatic Optimum (HCO) warm period in SE Asia with ACL values ranging from 29.5 (109cm depth) to 29.8 (130cm depth) and ACL averages across this rough plateau of 29.67 (Figure 12). Generally, high or increased ACL values suggest high/increased temperature and low/decreased precipitation i.e. more arid conditions (Baker *et al*., 2016). However, in this research the ACL record is interpreted differently here. High ACL values probably indicate a period of increased temperature, humidity and precipitation in the region surrounding Qinghai Lake. Assuming that the age results from core QH4 are an accurate and comparable representation of TCQH17A, this warming period occurred between approximately 8877 cal yr BP and 6895 cal yr BP in the Qinghai Lake region. We know from previous research that ISM intensity increases drastically in a warmer climate, potentially due to increased atmospheric moisture/moisture circulation (Turner and Annamalai, 2012) and crucially due to the impact of key pressure systems controlling the monsoon, particularly when Arctic ice volume is low due to larger scale warming (Zhisheng *et al*., 2011). This implies that during a period of increased ACL such as this, ISM intensity was notably higher with increased precipitation and humidity, as opposed to the arid climate with low precipitation generally suggested by increased ACL values. The opposite can be considered of lower ACL values, were the temperature interpretation remains the same (lower) but precipitation decreases (instead of becoming wetter as insinuated by Baker *et al*., (2016) due to temperature decrease weakening the pressure systems driving the ISM (Bawiskar, 2009 and Paul *et al*., 2016). This will be explained further later, during discussion of lower ACL value periods. Low latitude regions were less affected by this warming period with increases of less than 1°C in tropical ocean reefs (Gagan *et al*., 1998). Regardless, the HCO is a well-known and long-lasting period of climate change that demands attention and the Arctic may have warmed by as much as 4°C. During periods of large scale/global climate change the poles always reflect temperature change to a much greater extent than equatorial regions, and thus it is important to examine them. Different regions of the Arctic warmed to different extents during this period however, with one study suggesting average warming of around 1.6°C higher than present in the Western Arctic (Kaufman *et al*., 2004), while another indicates rapid and severe warming as much as 6°C higher than present further south (Mangerud and Svendsen, 2017). Thus, the Arctic and Antarctic likely would have lost significant ice sheet volume, possibly increasing monsoon intensity significantly during this warm period (Zhisheng *et al*.,

2011). This warming period was most likely the result of fluctuations in solar irradiation, with a long period of severely increased solar radiation discharged by the sun, thus increasing the solar radiation received by the Earth, particularly in the Northern Hemisphere (Kutzhach and Street-Perrot, 1985 and Wang *et al*., 2005). Due to natural feedback systems such as albedo, as well as Earth's geography, land/ocean mass/volume and surface area distribution, Earth's axial tilt, seasonality and position relevant to the Sun, different parts of the world experienced this HCO warming period to differing degrees and longevity (Xiao *et al*., 2015). In the context of this study, it is interpreted to have resulted in a period of warm, wet climate with increased monsoon intensity in the Qinghai Lake region of southwestern China.

Similar climate reconstructions in other regions of southern China have suggested that in particular regional precipitation/humidity has a key influence on changes in their ACL results distribution, as pollen records do not support the hypothesis that increased ACL was not necessarily the result of increased temperature altering vegetation type, except at one period (Zhou *et al*., 2005). This leaves the possibility open that temperature still plays a role, which it very likely does considering the increased ACL, high pilot diol temperature (Figures 12 and 20) and noted temperature rise in other studies (Mangerud and Svendsen, 2017 ; Shen *et al*., 2006 ; Xioa *et al*., 2015 ; Yang *et al*., 2016 ; Zhou *et al*., 2005). This collective research records the same high value ACL profile over a period from approximately 10,450 cal yr BP and 6040 cal yr BP, which correlates fairly well with the ACL results from Qinghai Lake over the 146-91cm. Although the Qinghai record is not as long, and warming appears to occur later, this could be due to inaccurate age dating or potentially a myriad of other climate factors. One potentially stronger interpretation, assuming that the Qinghai age dating is correct, is that perhaps warming onset in the Qinghai Lake/ Yunnan Province region later than in Zhou *et al's*., (2005) Dingnan study location, and lasted for a shorter period of time, because Qinghai Lake is at a higher elevation (with subsequent cooler temperatures) than the more coastal, hilly region from which they extracted their peat core (Figure 3). There is at least 1000m difference in elevation between these locations, with Qinghai Lake located at 1849m above sea level (Yang *et al*., 2016), and Figure 3 indicating that Zhou *et al's*., (2005) site lies somewhere between 200-500m elevation.

Zhou *et al*., (2005) postulate that this period of increased ACL values represents the HCO, which agrees with this studies interpretation of the Qinghai Lake ACL over the 146cm-91cm section (8877 - 6895 cal yr BP). Furthermore, Zhou *et al's*., (2005) interpretation of these results over this stage of increased ACL, combined with low CPI values is that it represents a period of warmer temperature and higher humidity, which re-enforce each other. Qinghai Lakes CPI also record fairly moderate/high values during this period of around 6.02 on average (Figure 13), which are very similar

to Zhou *et al's*., (2005) values. They continue to state that their ACL record combined with other proxies are 'good evidence of increased East Asian summer monsoon intensity and monsoon precipitation'. Although their study site is significantly further East in China relative to the Qinghai Lake site, they have very similar latitudes and are geographically close in the context of Earth. Therefore, due to the sheer similarity in method, results and geographical location, Zhou *et al's*., (2005) results and interpretations both confirm and strengthen the validity of the ACL results and the interpretations in this study. The model created by Kutzhach and Street-Perrot, (1985) also implies increased monsoon intensity during the period of approximately 9-6k cal yr BP as a result of fluctuations in solar radiation, which supports the Qinghai record. This period of warming, which may have particularly heated the northern hemisphere (Kutzhach and Street-Perrot, 1985) and likely increased the disparity between the temperature of the land and the sea (Gagan *et al*., 1998) with land temperatures rising vastly, while ocean temperatures increased only slightly. This will have further increased the monsoons intensity as this greater temperature disparity strengthens the key pressure systems involved in the ISM development (Bawiskar, 2009 and Paul *et al*., 2016). Research from Yang *et al*., (2016) however, interprets that this warming period is probably also a response to increased ocean temperatures and sea levels in the Bay of Bengal. This point illuminates the fact that a simple slight rise in ocean temperature allows for increased atmospheric moisture from evaporation, contributing further to increased ISM intensity.

Crucially, this projects interpretation of the HCO is also partially supported by pollen records from Yang *et al*., (2016) and vegetation records from Xiao *et al*., (2015), whose respective research was also conducted from cores retrieved from Qinghai Lake. Yang *et al's*., (2016) results indicate that the climate in the region was warm and humid between roughly 8300 cal yr BP and 4600 cal yr BP, while Xiao *et al's*., (2015) record also implies the same climate from a similar time period of 8.45k cal yr BP to 4.3k cal yr BP. Although both records agree that the warming period started at a similar time, our record does not show such a prolonged, constant period of warm, wet climate. Instead, ours indicates a shorter 2000-year warm period, ended by a swift decline in temperature and precipitation (Figure 12 and 25). Evidence from other papers also points to the HCO in the Yunnan Province, China lasting for a longer period into the later Holocene. For example, records from Lake Shudu suggest the warm period lasted up until 4k cal yr BP (Cook *et al*., 2012), and the pollen record from a core from Tiancai Lake in northwest Yunnan Province suggests the HCO occurred from 6.1k cal yr BP to 3.4k cal yr BP (Xiao *et al*., 2014). Again, this late HCO onset may be due to higher elevation prolonging the onset of climate change in this northwest region. Tiancai Lake for example, lies at almost 4000m elevation (Xiao *et al*., 2014), which correlates with increased lake elevation showing results indicating

later HCO onset. In regards to a prolonged HCO period, further up core the ACL record in this project does reflect a 'second' warming period between 6513 cal yr BP and 4748 cal yr BP (79-58cm, Figure 12), which debatably could be an extension of the HCO although ACL values here are not as high or anywhere near as constant as they are between 146-91cm, so this seems unlikely, especially considering the sharp decline in temperature noted from 6894 cal yr BP to 6608 cal yr BP in our record (91-82cm). Other data, such as acid ratio also suggest this is likely a separate climate event with a weaker monsoon (Figure 24). Evidence from a sediment core from the nearby Lake Erhai in Yunnan Province aligns more closely with the data from this project. This pollen record points to a persistent warm and wet climate (HCO) occurring from 8.4k cal yr BP to 6.4k cal yr BP (Shen *et al*., 2006), which is very similar in terms of start and end date and period of time to the 8877 - 6895 cal yr BP warm period indicated by the ACL record constructed in this project. Overall, literature from other research conducted in similar regions in China supports this projects interpretation of the high ACL value record over the 146-91cm section, from 8877 - 6895 cal yr BP representing the HCO in the Yunnan Province.

The CPI values across the initial 34cm (from roughly 8.8k cal yr BP to 7.56k cal yr BP) up core from the base hold a steady plateau with low/moderate CPI values (Figure 13), suggesting relatively moderate preservation of organic matter through this stage. These values also imply a warmer climate which is consistent with the ACL record over the HCO period. The CPI spike at 109cm (approximately 7.47k cal yr BP) implies particularly good preservation of organic matter at this point, with very little degradation likely. This spike may also indicate a cooler period, but it is inconsistent with the ACL record which implies cooling later at around 6.9k cal yr BP to 6.6k cal yr BP (Figures 11 and 12). After this however the CPI declines up core to very low values at 97cm (approximately 7.08k cal yr BP) implying an increasingly labile source of organic matter, with very degraded matter at 97cm depth.

Across the first 28cm up core from the base, the moderate to low and declining P_{Aq} values point to an increasingly dry climate with lower lake levels from 8.88k cal yr BP to 7.75k cal yr BP (Figure 14). Despite traditional ACL interpretations supporting this theory of drier climate and a weaker monsoon (Baker *et al*., 2016), the acid ratio record, along with the alternative interpretation of the ACL (higher temperatures implying increasing monsoon intensity) and other research in the region (Shen *et al*., 2006; Xiao *et al*., 2015; Yang *et al*., 2016). Therefore, here we know that the common interpretation of P_{Aq} values is incorrect, and that the intense monsoon and precipitation in the warm, wet HCO must have washed increasing quantities of terrestrial organic matter in to the Qinghai Lake system, decreasing the P_{Aq} value through this period. Moving further up core, the P_{Aq} rises from approximately 7.75k cal yr BP to 6.7k cal yr BP (Figure 14). Again, this aligns with the traditional interpretation of the ACL

record (implying change to cooler, wetter climate), but the insinuated temperature decrease and the acid ratio record infer the opposite in terms of precipitation, with a change to a cool but much drier climate with a weak monsoon.

Initially the hopane concentrations hold a relatively moderate to high value plateau in all the hopanes detected from 8880 cal yr BP to 3840 cal yr BP, with a couple of distinct declines in concentration in all hopanes at 6610 cal yr BP and 6250 cal yr BP. These results are generally very consistent with the ACL record (Figures 11 and 12). The initial, relative, high moderate to high concentration plateau in each hopane between 8.88k cal yr BP to 6.89k cal yr BP supports the interpretation of a warm wet period during the HCO here. The increased monsoon intensity during the HCO likely resulted in increased soil/terrestrial material becoming unstable and being deposited in the lake, increasing the hopane concentration in the sediment record.

The bottom section of short to long chain acid ratio core record, from 146-97cm (approximately 8.88k cal yr BP to 7.09k cal yr BP) retains a low ratio plateau (Figure 24), implying a period of wet climate, supporting the ACL record and interpretation of the warm and wet HCO, with an intense monsoon during this period. In fact, it aligns remarkably well with the ACL, which retains a high ACL indicative of a warm period and corresponding intense monsoon until about 6.9k cal yr BP.

4.3.2 Mid to Late Holocene Core Section (6895 cal yr BP to 3543 cal yr BP)

From 91cm to 82cm (6895 - 6609 cal yr BP) the ACL value declines from 29.6 down to 29.2 (Figure 12). It seems likely that this period marks the end of the HCO, with a marked decrease in ACL values indicating a decline in temperature. Normally a decline in ACL would also indicate an increase in precipitation (Baker *et al*., 2016), but in this context with many factors at play influencing the monsoon, it probably shows a drier period during which the monsoon weakens significantly in this region. Again, this is probably caused by the regional decline in temperature weakening the temperature gradient between land and sea that forms the pressure systems influencing the monsoon formation. This weak monsoon hypothesis is also supported by the TAF results (Figure 23 and 24), where a shift to dominantly aquatically sourced/originated acids in the short to long chain ratio suggests there is significantly less precipitation washing terrestrial acids into Qinghai Lake from the surrounding vegetated slopes.

Numerous studies in the region also note that the end of the HCO, at the various time frames it was recorded, is marked by progressively cooler temperatures, drier climate and subsequently inferred weaker ISM in the Mid-Holocene period (Xiao *et al*., 2014: Yang *et al*., 2016: Zhou *et al*., 2005). This cooler period may well be the result of a decrease in solar radiation after the prolonged period of high intensity solar radiation causing the HCO (Wang *et al*., 2005 and Zhou *et al*., 2005). The reduction in heating

of the southeast Asian continent reduces the disparity in temperature between the continent and Indian Ocean. Therefore, the Hadley circulation pressure systems responsible for the monsoons formation are much weaker, and thus the atmospheric moisture circulation is weaker and the monsoon is less intense, with reduced precipitation (Bawiskar, 2009 and Paul *et al*., 2016). Generally, however, changes to a cooler climate are slightly more gradual in other records, while our results imply a fairly rapid change in climate conditions over approximately 300 years (Figure 12).

Closely following this cooler period however is a comparably rapid spike in temperature and precipitation indicated by high ACL values briefly reaching up to 29.7 which occurs between roughly 6600 cal yr BP and 4748 cal yr BP (82cm- 58cm, Figure 12). This short, potentially warm period, as previously mentioned could potentially be an extension of the HCO, which is noted to last further in to the mid to late Holocene in other Yunnan records than in these results (Xiao *et al*., 2014 and Yang *et al*., 2016). Alternatively, it may be an entirely separate phase of brief, sporadic climate warming. During this ascent in ACL initially, based on our understanding of how rising temperature indicated by ACL influences the monsoon, it appears likely that the ISM intensity also increased between roughly 6.6k cal yr BP and 5.95k cal yr BP, before a decline in temperature then reduced the monsoon intensity and thus precipitation, gradually, between approximately 5.95k cal yr BP and 4.75k cal yr BP (Figure 12). However, when analysed alongside other proxies this view changes. Here we must adapt and revert to Baker *et al's*., (2016) ACL interpretation (higher ACL means drier, more arid climate), due to the supporting short to long chain acid ratio which indicates a brief spike to dry climate here. For example, the highest ACL spike at 70cm (approximately 5953 cal yr BP, Figure 12), is accompanied by the highest acid chain ratio (Figure 24), indicating a very dry climate at this point. However, the sporadic nature of the ACL and acid ratio on either side of this 70cm spike (Figure 12, 24) suggests wetter climate surrounding this period and further points to a large degree of climate variation around this time, with generally drier climate but rapid and short swings to more intense spells of monsoon activity.

Between 70cm and 46cm the ACL value drops down as mentioned, from 29.7 to the lowest recorded ACL of 29.1 at 46cm, or approximately 3.54k cal yr BP (Figure 12). There is one particularly rapid section of ACL decline within this period that should be noted, between 58cm and 55cm depth (between approximately 4.75k cal yr BP and 4.45k cal yr BP). This section of declining ACL which occurred between 5953- 3543 cal yr BP likely represents another period of overall gradual, and sporadically more rapid temperature decline, as well as drier conditions due to a weakened ISM. Charcoal records from Qinghai Lake indicate that fires were more common and potentially increasingly extreme for hundreds of years after approximately 4.3k cal yr BP, supporting the interpretation of a much drier climate and weaker ISM around this

period (Xiao *et al*., 2015). The onset of this dry period in Xiao *et al's*., (2015) record correlates well with ACL values in this project, which drop below 29.24 to relatively low values at around 4450 cal yr BP, and continue to decline until around 3.54k cal yr BP. The ACL record from the peat sequence analysed by Zhou *et al*., (2005) shows their ACL values dropping to their lowest values from 6k cal yr BP to 4k cal yr BP, which aligns fairly well with the ACL decline in our Qinghai Lake record, which declines from 5.95k cal yr BP to their lowest value at 3.54k cal yr BP (Figure 12). A suite of pollen records gathered by various researchers across China, and further analysed and discussed in a study by Zhao *et al*., (2009), suggests that on a broader scale across China, moisture changes show a decrease in effective moisture from 6k cal yr BP to 5k cal yr BP, which agrees with this studies interpretation of events across this period. A further correlation noted from this study published by Zhao *et al*., (2009) is that they conclude that evidence shows an abrupt, extreme decline in moisture, and therefore precipitation at 4.5k cal yr BP, which aligns very closely with the sharp decline in ACL between 4.75k cal yr BP and 4.45k cal yr BP (from 29.5 down to 29.2, Figure 12). This abrupt decline to drier climate and inferred extreme decline in monsoon intensity is also observed at 4400 cal yr BP in a Lake Erhai study (Dearing *et al*., 2007), proving these changes were observed in a different record from a more local setting. This vastly increases the probability that this sharp climate change with weak monsoon conditions indeed occurred in the Qinghai Lake region during this period.

The overall ACL interpretation of the whole middle core section from 91cm to 43cm, from approximately 6.6k cal yr BP to 3.24k cal yr BP, is of high variability in ISM intensity, with falling and rising temperatures dictating monsoon behaviour and therefore precipitation through this mid Holocene period. Collectively, this section of core ACL results also points to an overall drier period, with a much weaker monsoon system than the previous and following core sections. Dearing *et al's*., (2007) multi proxy record also suggests significant ISM variability at periods between 5.5k cal yr BP to 3.8k cal yr BP, implying rising and falling temperatures and monsoon intensity, slightly further north of Qinghai Lake, corroborating the ACL results in this projects record.

The CPI rises and fluctuates at moderate values through the mid-section of core until it spikes again at 49cm (around 3.84k cal yr BP, Figure 13), implying an increased degree of preservation around this time and potentially varying temperature. The fluctuation of CPI values through the mid core section is fairly consistent with the increased monsoon variation reflected here by the ACL and reported by Dearing *et al*., (2007) during this period (Figures 12 and 13).

From 6.7k cal yr BP to 3.24k cal yr BP the P_{Aq} initially falls sharply, then rises and falls in several fluctuating successions (Figure 14) indicative of increasing monsoon variation also observed by Dearing *et al.*, (2007). This aligns a bit better with the other proxies which also record increased climatic and monsoon variation around a similar time period. From 43cm to 34cm depth (3.24k cal yr BP to 2.34k cal yr BP) the P_{Aq} rises sharply from 0.179 to 0.408 (Figure 14), insinuating a vast increase in lake levels and therefore precipitation.

The notable concentration decline troughs for all hopane concentrations at around 6610 cal yr BP and 6250 cal yr BP also align remarkably closely with ACL and acid ratio value declines during the same period (Figures 11, 12 and 24), and support the hypothesis of a dry period with a weaker monsoon system around these declines. The hopane concentrations do rise again after these declines, which conflicts slightly with the ACL interpretation of the driest period at around 5.95k cal yr BP. However, the hopane record through the mid core section does support the interpretation of increased monsoon variation. This is similarly noted in the ACL and acid ratio record in the mid to late Holocene period from 6.89k cal yr BP to 3.54k cal yr BP and by other records in the region (Dearing *et al.*, 2007).

In the mid-section of the short to the long chain acid ratio from 97cm to 40cm (7085 cal yr BP until 2940 cal yr BP), the values generally indicate a much drier climate overall. However, there is significant variability here, with the ratio dropping to 0.246 at 82cm (around 6610 cal yr BP) and 0.519 at 58cm (approximately 4750 cal yr BP), pointing to periods of wetter climate. Particularly dry and arid climates with a weak monsoon are inferred at around 6.8k cal yr BP, 5953 cal yr BP and 3844 cal yr BP (Figure 24). This roughly aligns with Dearing et al's (2007) findings of high monsoon variability between the periods of 5.5k cal yr BP to 3.8k cal yr BP. Again, although the TAF ratio record is more sporadic, it does generally support the ACL record, which experiences sharp oscillation in values along this section of core, but with two periods of distinct low values, and overall has fairly low ACL values. There are however periods were the two do not align well, and this may be due to the sheer sporadic values of the acid ratios.

The acid data from the short, mid and long-chain supports the acid ratio data, as several of these chains were incorporated into the equation. The mid-chain length acid data overall does not reveal much that the short to long chain ratio does not already cover. The C_{24} data does reinforce some points such as increased monsoon variation through the mid Holocene, with a spike at 64cm (5351 cal yr BP) in concentration, that is not as prominent in the C_{22} indicating a wetter period here after a very dry period implied by all proxies (except perhaps hopanes) including this at 70cm (5953 cal yr BP).

4.3.3 Late Holocene (3543 cal yr BP to -16 cal yr BP)

From 46cm up core, the ACL value spikes up again to about 29.6 at 43cm and then oscillates between 43cm and 22cm holding a generally fairly high ACL value with a generally gradual ACL decline towards 22cm (Figure 12). This insinuates a sharp change in climate at around 3.54k cal yr BP to 3.24k cal yr BP with temperatures rising rapidly and subsequently a stronger ISM with increased precipitation, followed by a generally gradual decrease in temperature and ISM intensity from approximately 3.24k cal yr BP towards 1.13k cal yr BP. These implications, particularly over the period from 3.24k cal yr BP to 1.13k cal yr BP are well supported by the P_{Aq}/ P_{Wax} and acid ratio data (Figures 14, 15 and 24) discussed later. Zhou *et al's*., (2005) peat record also shows increasing ACL values at the similar time of 3.8k cal yr BP to a high value period, suggesting this climate change event was widespread and experienced across different environments in China. This higher temperature and corresponding warm, wet climate due to a stronger, more intense ISM was also noted at the base of a 3500-year old sediment core record constructed by Xu *et al*., (2015) from nearby Lake Erhai. This record, combining organic and inorganic analysis techniques, also interpreted a consistent long-term decrease in ISM intensity up core from their results, implying the same monsoon and climate changes were universal across the Yunnan province at this time, also supporting this records interpretation of climate events based on ACL changes. Other studies have suggested that the Roman Warm Period (RWP), which is considered to have mainly influenced climate in Europe and the North Atlantic, may have also influenced climate in Asia (Ji *et al*., 2005). The initial 46-43cm ACL spike does not coincide that well with this warming period, which likely occurred around 2.5k cal yr BP to 1.6k cal yr BP at latest (Wang *et al*., 2012). However, the initial period or proposed warming does coincide with the one ACL anomaly in the gradual decline, an ACL spike between 2.34k cal yr BP to 2.04k cal yr BP from 29.4 to 29.7 (Figure 12), which could represent some warming influence of the RWP in the Yunnan Province.

The ACL value decreases very abruptly from 22cm-19cm depth (1133 cal yr BP - 910 cal yr BP), with values decreasing from 29.5 to 29.3 (Figure 12). This is a very distinct trough in the ACL record and probably indicates a short period of much drier climate, very possibly influenced by human activity and this could represent some influence of the Medieval Warming Period (MWP). The P_{Wax}/P_{Aq} data supports the hypothesis of a dry climate around this point in time (Figures 14 and 15), indicating a low lake level, however the acid ratio contradicts this, unless it is interpreted here as containing a higher proportion of terrestrial acids, relatively, due to the lake level decline. Sediment core analysis from Lake Huguangyan in the more tropical, coastal setting of southern China suggests a distinct drought period occurring from 1260 cal yr BP to 880 cal yr BP (Chu *et al*., 2002). Analysis of the Total Organic Content, grain size, pollen

contents and several elements present in a sediment core retrieved from the nearby Lake Erhai also suggest a significant and abrupt dry spell just before and slightly during the MWP as a consequence of a weaker ISM (Xu *et al*., 2015). This Lake Erhai cores results also imply an overall decrease in monsoon intensity through 3500 years from the RWP which generally corresponds with this cores ACL results interpretation. Despite regional differences this time scale from both these records closely resembles that of dry period inferred from the ACL and P_{Wax}/P_{Aq} record in this project (Figures 12, 14 and 15), and supports the interpretation that this represents some of the impact of the MWP. The ACL value drops due to initial lower temperatures and likely weakened the ISM, potentially as a consequence of relative temperature rise in the Bay of Bengal waters compared to the relatively cooler southeast Asian continent weakening vital pressure systems influencing the monsoon (Bawiskar, 2009 and Chu *et al*., 2002). Eventually it seems likely that MWP warming cascaded slightly and propelled temperatures upwards briefly to the extent that they increased the ACL values in our record from 19-16cm (29.305 to 29.555) or 910 cal yr BP to 755 cal yr BP (Figure 12). Increased temperature eventually raised the disparity between land and sea temperatures, strengthening the key pressure systems and thus the ISM, increasing precipitation later after the drought period.

From 16cm up core, the ACL value consistently declines (Figure 12). This could be due, at least partially to the influence of the Little Ice Age (LIA). During this period the ACL record indicates that temperature declined consistently from 600 cal yr BP towards the present day. It is likely during this period that the interpretation of how ACL represents precipitation is different to previously in this project, and does align with Baker *et al's*., (2016) interpretation, i.e. that decreased ACL points to increased precipitation, and thus in this context a stronger monsoon. The reason for this alternative interpretation compared to previous ACL interpretations is due to the supporting evidence from the short to long chain acid ratios and P_{Aq}/P_{Wax} data, which indicates increased precipitation and run-off during this period (Figures 14, 15 and 24). This interpretation is supported by data from nearby Lake Erhai, which points to a cold, wet climate during the period from approximately 570 cal yr BP to 170 cal yr BP (Xu *et al*., 2015). The ACL record from this project's continual decline points to continually decreasing temperatures from 600 cal yr BP towards present and also implies progressively more intense precipitation up core. $\delta^{18}O$ analysis from carbonates from Dongge cave in southern China also imply increasing monsoon intensity over the last 500 years towards present (Wang et al. 2005). There are several potential reasons for this cooler period with some that are slightly more unique than previous natural reasons. Many temperature changes throughout this roughly 8900 year, 146cm record may likely be attributed to fluctuations in solar radiation (Kutzhach and Street-Perrott, 1985 and Mayewski *et al*., 2004) and a decrease in solar

radiation likely played a role in this LIA cool period with a well-known period of minimal solar irradiation (a.k.a. the Maunder Minimum) occurring between 305 cal yr BP-235 cal yr BP (Lean *et al*., 2005). However, some of the more unique reasons firstly include a decline in human population cooling the planet. The plague or 'Black Death' wiped out large percentages (at least one third) of Europe's population in the 1300's (Fowler, 2018), and overall almost a quarter of the world's population is estimated to have perished in this outbreak. Another factor that could be considered for this period more locally was the dynastic changes from the Ming to Qing dynasties. This brutal period resulted in massive population decline in China during the 1600's, which may have contributed to continued temperature decline. Zhang *et al*., (2006) found that there is a strong correlation in China between cold climate phases and population decline, war, harvest levels and dynastic changes. Whether the LIA caused these or these changes exacerbated the LIA, or both, remains plausible and up for debate. Increases in volcanic activity may also have played a role, with a spike in activity noted at around 600 cal yr BP that may have contributed to the cooling onset (Mayewski *et al*., 2004). The large spread ash clouds would have decreased the overall solar radiation received by Earth.

This LIA period is particularly interesting in context of the ISM, as generally we attribute a decrease in regional temperature, as observed here, with a weaker land/ocean temperature disparity and thus weaker pressure systems driving the monsoon. However, this period illustrates just how complex climate can be and how global changes can influence more regional climate. Research suggests that polar ice volume distribution may be a crucial control on the ISM and although Arctic warming may stoke monsoon intensity, the opposite can be said of the Antarctic (Zhisheng *et al*., 2011). Increased Antarctic ice volume has been linked to enhanced ISM intensity by increasing the cross equatorial pressure gradient (XEPG) and thus strengthening the Mascarene High and improving the southern hemisphere atmospheric meridonial circulation, providing more moisture to southeast Asia (Zhisheng *et al*., 2011). This shows the importance of pressure system interaction (and the factors which effect this) on monsoon variability, as Zhisheng *et al*., (2011) overall conclude that during the past 0.92My, ISM intensity is amplified during interglacial periods by northern Indian lows, as reduced global ice volume in general allows for intense Indian lows and an increased range of the Intertropical Convergence Zone's northern migration, which enhances the XEPG and ISM intensity. Meanwhile during glacial periods ISM intensity is amplified predominantly by southern Mascarene High pressure systems, influenced by Antarctic ice volume. Therefore, it seems probable that during the LIA, an increase in Antarctic ice volume may be responsible for the observed increase in ISM intensity.

CPI values decline initially at the top core section, and reach a fairly low, gradually oscillating plateau over the last 37cm (2.64k cal yr BP up to the present, Figure 13). This implies that over the last 3.84k cal yr BP to 2.64k cal yr BP, organic matter became increasingly labile, until there reached a degree of fairly poor preservation that was roughly maintained over the last 2.64k cal yr BP. This low plateau again may point to a period of warmer wetter climate, which is consistent with ACL records from about 3.24k cal yr BP to 1.13k cal yr BP. It does not really reflect changes around the MWP or LIA as effectively but there is a slight CPI increase potentially reflecting aridity around the MWP.

The period of P_{Aq} rise observed towards the near the start of the Late Holocene and the following high value plateau (and respective corresponding P_{Wax} record) until at least 1.13k cal yr BP is the section that best aligns with the ACL record, supporting each other thoroughly. The hike in P_{Aq} values that are then maintained indicate a fairly long period of high lake levels and high monsoon intensity that corroborates the interpretation of the possible influence of the Roman Warm Period (RWP) here at this time. The P_{Aq} then drops sharply from 755 cal yr BP to about 600 cal yr BP and stays low until 300 cal yr BP (Figure 14), which points to a rapid change to a dry and arid climate with a weaker monsoon that then becomes stronger towards the present day as the P_{Aq} rises again. This initial P_{Aq} decline lags a few hundred years behind the corresponding ACL records change but the very likely occurred, as it was also recorded in other studies (Chu *et al*., 2002 and Xu *et al*., 2015) and may well represent the MWP here in the Yunnan Province. The rise is P_{Aq} over the last couple hundred year at the top of the core (Figure 14) corroborate roughly with the ACL record and indicates a slightly wetter climate in southwest China during the LIA.

From 3.54k cal yr BP to 3.24k cal yr BP the hopane concentration spikes to its high values in all hopanes. This implies a distinct and rapid change in climate from dry to wet, with a marked increase in monsoon intensity, which is also observed in the ACL, P_{Aq}/P_{Wax} and to a lesser extent the acid ratio data (Figures 11, 12, 14, 15 and 24). The spike here is very large and rapid, and it could be possible that extreme precipitation weakened the slopes surrounding the lake that a landslide or large slump deposited a large concentration of terrestrial material in to the lake system at this time. However, the timing with the P_{Aq}/P_{Wax} data may be interpreted support this with initial low values. Or the following P_{Aq} rise could be interpreted to dispute this and points to a more intense monsoon simply washing terrestrial hopanes in to the lake system with run-off. The hopane concentration drops after this spike and then fluctuates to to slightly different relative degrees in different hopanes from 3.24k cal yr BP towards the present. Concentration spikes at around 2.04k cal yr BP, 600cal yr BP and 140cal yr BP (Figure 11) support ACL and acid ratio results implying a wetter climate with a more intense monsoon during the RWP and the LIA.

The top 40cm of acid ratio from this core displays another low value plateau (Figure 24), which again points to a period of wet climate with an intense monsoon, with terrestrial acids being washed in to Qinghai Lake and preserved in the sediment record. Again, it also aligns with the ACL fairly well in a similar value to the bottom core section, as the ACL spikes up at 46-43cm indicating a warmer temperature which should produce a more intense monsoon, at the same point where the acid ratio is dropping to this low value plateau. This suggests a progressively increasing monsoon intensity from 3.54k cal yr BP to 2.94k cal yr BP, which then holds a strong monsoon intensity up core over approximately the last 3000 years.

4.4 Temperature Proxies for Qinghai Lake

Alkenone paleothermometry is one of the most explored biomarker techniques for reconstructing past temperatures from lake archives (Brassell *et al*., 1986, Theroux *et al*., 2013). Unfortunately, no alkenones were detected in the sediments from Qinghai Lake, suggesting that alkenone-producing haptophytes are likely not present. Another novel, but promising paleotemperature proxy is the long-chain diol index (LDI), also derived from algae within lake systems.

4.4.1 The Long-chain Diols and LDI

Diols are chemical compounds that contain two hydroxyl groups (an oxygen and hydrogen atom together) within their structure. They were first discovered in the Black Sea (De Leeuw *et al*., 1981) and have since been located in quaternary marine sediment worldwide (Rampen *et al*., 2014b). Rampen *et al's*., (2012) results indicate that there is very likely a strong relationship between the C28 1,13, the C30 1,13 and C30 1,15 diols and SST (Sea Surface Temperature), with SST likely controlling the abundance of these diols and therefore diol isomers. The C32 diol, despite being calculated and very abundant (the most abundant diol isomer detected), is not thought to be related to temperature (Rampen *et al*., 2012). However, the C32, 1,15 diol isomer, due to its abundance is required to calculate the fractional abundance of the respective diol isomers used in the LDI. Therefore, here we investigate Rampen *et al's*., (2012) LDI in Qinghai Lake with four pilot samples to determine if the calibration provides reasonable temperatures for reconstructing quantifiable temperature changes during the Holocene in Qinghai Lake.

There are limitations with applying the LDI to lake sediments. First, the LDI is a marine calibration, and Qinghai Lake is a freshwater lake. Second, unlike alkenones, where the algal producers, alkenones are well known, the sources of long chain diols remain largely unknown and likely have producers that span algal classes. We do know that diols are produced by eustigmatophyte algae, and that they produce different quantities and distributions of long chain diols under different growth temperatures (Rampen *et al*., 2014a). In order to accurately apply the LDI in Qinghai Lake, a site-specific calibration may be required for accurate quantifiable temperature change to be obtained. Despite the marine calibration being derived in the ocean, this calibration has been shown to be a potentially valid paleoclimate proxy in lacustrine environments (Rampen *et al*., 2014a).. However, more research is needed to refine this technique for use in freshwater lakes. Here we determine if the LDI produces realistic temperatures for the pilot samples in our study and discuss what further information may need to be gathered for an appropriate lake calibration..

Firstly, we confirm the presence of diols in Qinghai Lake (Figure 17 and 18). Secondly, we confirm that the SIM data extraction method works well overall, and

that future quantifiable temperature reconstruction for Qinghai Lake is possible. Finally, based on the four pilot samples, and on the calibration by Rampen et al. (2012), the LDI is applicable over a surface water temperature range between -3°C and 27°C (Rampen *et al*., 2012), which Qinghai Lake and the values calculated fall within. If we apply the Rampen et al. (2012) calibration, it suggests that a gradual, yet fairly drastic temperature decrease of approximately 12°C occurred over the record (Figure 20). The resolution of the pilot samples is low, the data lacks uncertainty values and the temperature change/range is unrealistic, but the results show that there were likely higher temperatures in Qinghai Lake during the HCO period. During the mid-Holocene period the results imply lower lake surface temperatures (19.6 -17.4°C from approx. 7.15k cal yr BP until 3.94k cal yr BP). The final sample at approximately 1.94k cal yr BP has a much lower value implying colder temperatures in the region at this time. This does not align well with the ACL record, but does appear around the time that the ACL record implies cooling begins after the RWP (Figure 12). The quantitative temperature values cannot be taken at face value given the limitations discussed above, but do indicate a future potential for this proxy. This illuminates some of the problems with the marine LDI being used in a freshwater lake environment, and highlights the need for species/site- specific calibrations being developed. These results cannot yet be considered as quantitatively accurate indications of lake surface temperature change. However, they do provide a strong qualitative indication that lake surface temperatures were higher in the basal section of the core record, becoming progressively cooler up core towards the present.

4.5 Synthesis of Biomarker results

There are several key periods of climate from which many of the paleoclimate proxies confirm each other's implications of climate conditions and monsoon intensity in the Qinghai Lake region. During the HCO period from 8.88k cal yr BP to 6.89k cal yr BP the ACL, short to long chain acid ratio and hopane concentrations indicate a warm, wet period of climate (Figure 26). Although the P_{Aq} may be interpreted as indicating a moderately wet period, is it important to remember that intense monsoon precipitation may be sweeping terrestrial material in to the lake system in larger quantities, thus lowering the P_{Aq} value. Therefore, it can be interpreted as supporting the rest of the data suggesting wet conditions and an intense monsoon during the HCO period. Following on up core, from 6.89k cal yr BP to 3.54k cal yr BP the ACL, acid ratio and P_{Aq} data certainly suggest an overall drier climate with a weaker monsoon intensity than during the HCO, however they also point brief periods in which the monsoon intensity abruptly increases such as the acid ratio drop/ P_{Aq} rise at 6.61k cal yr BP / 4.75k cal yr BP. Significant dry periods likely occurred at around 6.8-6.7k cal yr BP, 5.95k cal yr BP, 5.35k cal yr BP and 3.84k cal yr BP. Overall, the often rapid changes in the data from generally high acid ratio/ ACL values which suggest a very dry, arid climate, imply a period of weaker intensity yet markedly increased monsoon variability during this Mid-Holocene period. The CPI, hopane and P_{Aq} data also point to an increasingly varied climate regime here (Figures 13 and 26).

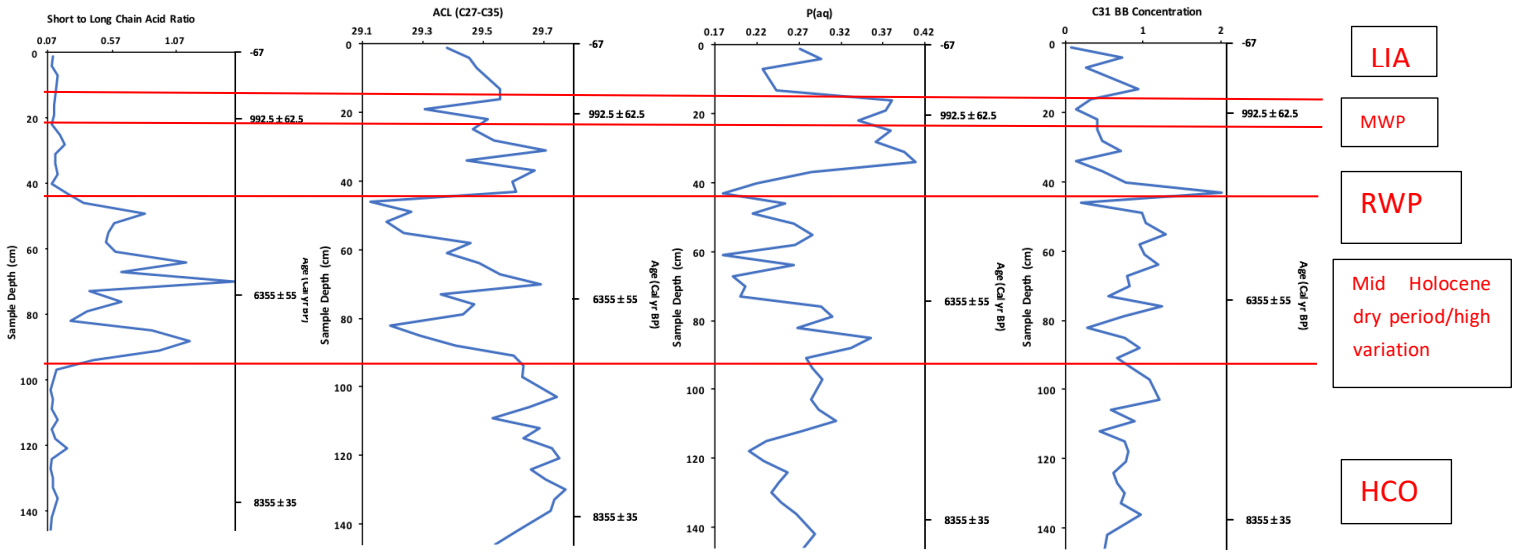

Figure 26: Annotated graph combining the P_{Aq}, Short to long chain acid ratio, ACL and C31 BB hopane concentration, plotted against sample depth (cm) and age (cal years BP). The annotations divide the graphs in to sections, illustrating periods of climate indicated by the various results.

From around 3.54k cal yr BP to 3.24k cal yr BP the climate abruptly changes to warmer, wetter conditions, with almost all proxies (except debatably, the CPI) indicating a rapid change from drier, arid conditions to a moist, wet climate with a strong and intense ISM system. This is noted in the sharp rise in P_{Aq}, ACL and hopane data, and by the decline in the acid ratio, indicating increased precipitation and temperature, the latter of which further increases the monsoons intensity (Figure 26). The P_{Aq} and ACL hold high value plateaus from about 2.34 to 0.75k cal yr BP and from 3.24 to 1.13k cal yr BP respectively (and the acid ratio holds a low value plateau throughout) indicating a prolonged warmer, wet period with a strong monsoon during the RWP here, with monsoon intensity slightly declining towards the present during this section. The hopane data shows the same sharp spike but the concentration increase does not hold (Figure 26), implying perhaps a large deposition of terrestrial material in to the lake around this time due to increased slope instability caused by the more intense monsoon rains. The P_{Aq} data may support this with low values around the same 3.24k cal yr BP period indicated a potentially large deposit of terrestrial material in to the lake, but the following rise and high value plateau in P_{Aq} suggests less terrestrial material being deposited and a persistent, consistent strong monsoon that may wash hopanes into the lake system with run-off.

A brief cool, dry period during the MWP is indicated by the ACL and hopane decline at 1.13k cal yr BP and the following, lagging P_{Aq} decline at 755 cal yr BP. The acid ratio data disputes that this period was dry, but there was likely a relative decrease in

monsoon intensity. From around 755 cal yr BP towards the present the monsoon intensity increased here during the LIA as indicated by the alternatively interpreted decreasing ACL, hopanes spikes, low acid ratio values and later spike in the P_{Aq} data (Figure 26).

4.6 Potential Future of the Monsoon

Based upon the various controls of the monsoon pressure systems that we currently understand, the future of the monsoon looks increasingly chaotic. With global temperature rise, loss of Arctic ice rapidly (which strengthens monsoon) in comparison to a slower decline in Antarctic ice volume , with a larger relative volume that may also strengthen monsoon (Zhisheng *et al*., 2011), increases in greenhouse gases such as CO_2 which increase atmospheric moisture (Kitoh *et al*., 1997) and a rise in solar radiation over the last 200 years towards the present (Lean *et al*., 2004), many factors point towards an increase in monsoon intensity on a longer term scale. Recent events would seem to corroborate these finding, with horrific flooding occurring more regularly in southeast Asia, and a particularly extreme monsoon downpour in 2017 that claimed many lives. However, we also know that more regular and extreme El Nino patterns/warm cycles may be weakening the ISM in some years by re-distributing atmospheric pressure systems and thus moisture (Wang *et al*., 2001). Some models have concluded that the future of the monsoon will likely be one of increasingly extreme variability in a warmer planet (Kitoh *et al*., 2007 and Turner and Annamalai, 2012), with desirable monsoon conditions becoming considerably rare, which is of grave concern for the population living in southeast Asia.

4.7 Future Work

The first key and obvious piece of future work to be conducted is to use the newly obtained radiocarbon dates from TCQH17A to create a chronology with age errors propagated throughout the core. Knowing that diols are present in the core opens the window to extracting quantifiable data and constructing a high-resolution record of lake surface temperature change. Samples would be taken as close to every 3cm as possible, or at an even higher resolution if possible, and analysed with the GC-MS. Unfortunately, in this project time constraints combined with technical problems due to GC-MS maintenance prevented this from occurring, but with more time this would have been possible. Furthermore, if considerable time was available, a species/site-specific diol calibration could be developed to drastically improve the accuracy of the LDI here. This would not only allow for the diol temperature reconstruction, but would also enable the search for sterols in N3 samples, which was also disrupted by the GC-MS needing maintenance. We hope to undertake these steps in order to write a future paper on the results produced in this project.

Given more time and resource, the GC-IRMS (Isotope Ratio Mass Spectrometer) could be used to determine carbon and hydrogen stable isotope values from the n-acids. Given the fairly high concentration of the TAF samples acquired from Qinghai Lake sediment, the samples would certainly be very appropriate for this type of analysis. Research indicates that analysis of hydrogen isotope ratios in FAME's provides insight to changes in the hydrological cycle and other climate parameters and therefore act as effective paleoclimate proxies (Hou *et al*., 2006 and Huang *et al*., 2004). GC-IRMS analysis of low to mid chain aquatic FAMEs produced by algae (C16 palmitic acid) and macrophytes (C22 behenic acid) has been proven to accurately reveal changes in lake hydrogen isotope ratios. Lake water hydrogen isotope ratios are acutely sensitive to rapid environmental changes as data from Hou *et al*., (2006), shows at the 8.2ka cooling event. These isotope ratios clearly capture changes in environmental factors such as temperature and precipitation/moisture (Hou *et al*., 2006 and Huang *et al*., 2004) and due to their robust nature and slow degradation rate (Huang *et al*., 2004) are ideal as paleoclimate proxies throughout the Holocene for high-resolution climate reconstruction.

Oxygen isotopes used in climate reconstructions are typically extracted from carbonates, for example in speleothems and calcite in lake sediment, or from alternative sources such as ice cores to investigate changes in paleotemperature and precipitation (Leng and Dean, 2014). The same principle applies to FAME's preserved within the sediment layers, which could be analysed to investigate such factors in greater depth.

One final additional improvement to this body of work would be to increase the resolution, sampling at every centimetre of core to produce a three-fold higher resolution.

5 Conclusion

This multi proxy climate reconstruction has produced results that infer several key periods of climate change through approximately the last 9000 years of the Holocene in the Qinghai Lake regions of the Yunnan Province, in south west China. Firstly, the ACL record combined with the short to long chain acid ratio, long and short chain acid data, and one pilot diol result indicate a prolonged period of significantly warm temperatures and associated wet climate with a very strong monsoon from approximately 8.88k cal yr BP to 6.89k cal yr BP. This period most likely represents the HCO here in the southwest China. In the Mid-Holocene period from 6.89k cal yr BP until around 3.24k cal yr BP the ACL record, long to short chain acid ratio, CPI and P_{Wax}/P_{Aq} data infers several successions of declines and spikes in temperature, and in turn decreases and increases in precipitation/monsoon intensity. During this section, the ACL implies two distinct lower temperature periods, with relatively cool and dry conditions and weak ISM intensity inferred by the ACL, P_{Wax}/P_{Aq} and acid ratio data from around 6.8k cal yr BP-6.25k cal yr BP in the first cool period and 4.45k cal yr BP-3.54k cal yr BP in the second period. However, there were short periods of increased monsoon activity through these dry periods, indicated by changes in the acid ratio result at 6.61k cal yr BP and 4.15k cal yr BP. Between these two periods there is a warm spike indicated by the ACL record which was likely very dry and arid and this theory is supported by the acid ratio which implicates the driest conditions recorded here at around 5.95k cal yr BP. The multiple proxies together indicate an exceedingly varied Mid-Holocene climate with several abrupt changes in monsoon intensity and an overall drier, yet more volatile climate from around 7k cal yr BP to 3.54k cal yr BP.

From about 3.54-3.24k cal yr BP the climate changed drastically and the proxies point to a rapid rise in temperature and monsoon intensity that may represent the RWP influence in Asia. The ACL, P_{Wax}/P_{Aq} and acid ratio/acid data suggest that the period between approximately 3.54k cal yr BP and 3,24k cal yr BP may represent the most abrupt and drastic period of climate change implied by this record in the Yunnan region, from dry to wet conditions. This warm, wet period with a strong monsoon was likely maintained with a gradual decrease in monsoon intensity for 2000 years, as indicated by a high plateau in ACL and corresponding P_{Wax}/P_{Aq} values between roughly 3.24k cal yr BP and 1.13k cal yr BP. The acid ratio also indicates high proportions of terrestrial acids being washed into Qinghai Lake by intense monsoon precipitation during this period. From 1133 cal yr BP to 755 cal yr BP, the MWP was likely, contradictory to its name, mostly cool and dry in the Yunnan Province, with temperature decline and rise indicated by the ACL record (low temperatures also loosely inferred by diols) and supporting P_{Wax}/P_{Aq} data. A quick rise in temperature towards the end of the MWP likely gave rise to an increase in monsoon intensity.

Following this the ACL declined, indicating a cooler, wetter period which likely represents the influence of the LIA period and its climate controls. This interpretation is supported by P_{Aq}/P_{Wax} and acid ratio data, which implies a generally higher monsoon intensity over the last few hundred years. The pilot long-chain diol results and the CPI data also points to probable lower temperatures during this period. Furthermore, the results of N2 and N3 analysis prove there are no alkenones present in Qinghai Lake but that there are abundant diols present throughout the lacustrine sediment record, which provide the potential for future calculation of quantifiable lake surface temperatures throughout the Holocene.

6 References:

Baker, A., Routh, J. and Roychoudhury, A. (2016). Biomarker records of palaeoenvironmental variations in subtropical Southern Africa since the late Pleistocene: Evidences from a coastal peatland. *Palaeogeography, Palaeoclimatology, Palaeoecology*, 451, pp.1-12.

Bawiskar, S. (2009). Weakening of lower tropospheric temperature gradient between Indian landmass and neighbouring oceans and its impact on Indian monsoon. *Journal of Earth System Science*, 118(4), pp.273-280.

Brassell, S., Eglinton, G., Marlowe, I., Pflaumann, U. and Sarnthein, M. (1986). Molecular stratigraphy: a new tool for climatic assessment. *Nature*, 320(6058), pp.129-133.

Castañeda, I. and Schouten, S. (2011). A review of molecular organic proxies for examining modern and ancient lacustrine environments. Quaternary Science Reviews, 30(21-22), pp.2851-2891.

Cranwell, P.A, Eglinton, G, Robinson, N. (1987). Lipids of aquatic organisms as potential contributors to lacustrine sediments II. Organic Geochemistry, 11, pp. 513-527

Chen, X., Chen, F., Zhou, A., Huang, X., Tang, L., Wu, D., Zhang, X. and Yu, J. (2014). Vegetation history, climatic changes and Indian summer monsoon evolution during the Last Glaciation (36,400–13,400yr BP) documented by sediments from Xingyun Lake, Yunnan, China. *Palaeogeography, Palaeoclimatology, Palaeoecology*, 410, pp.179-189.

Chu, G., Liu, J., Sun, Q., Lu, H., Gu, Z., Wang, W. and Liu, T. (2002). The 'Mediaeval Warm Period' drought recorded in Lake Huguangyan, tropical South China. *The Holocene*, 12(5), pp.511-516.

Climate-Data.org (2019). *Tengchong climate: Average Temperature, weather by month, Tengchong weather averages - Climate-Data.org*. [online] En.climate-data.org. Available at: https://en.climate-data.org/asia/china/yunnan/tengchong-4677/ [Accessed 20 Apr. 2019].

Cooke, M., Talbot, H. and Wagner, T. (2008). Tracking soil organic carbon transport to continental margin sediments using soil-specific hopanoid biomarkers: A case study from the Congo fan (ODP site 1075). *Organic Geochemistry*, 39(8), pp.965-971.

Cook, C., Leng, M., Jones, R., Langdon, P. and Zhang, E. (2012). Lake ecosystem dynamics and links to climate change inferred from a stable isotope and organic

palaeorecord from a mountain lake in southwestern China (ca. 22.6–10.5ka yr BP). *Quaternary Research*, 77(01), pp.132-137.

Dearing, J., Jones, R., Shen, J., Yang, X., Boyle, J., Foster, G., Crook, D. and Elvin, M. (2007). Using multiple archives to understand past and present climate–human–environment interactions: the lake Erhai catchment, Yunnan Province, China. *Journal of Paleolimnology*, 40(1), pp.3-31.

De Leeuw, J.W., Rijpstra, W.I.C., Schenck, P.A., 1981. The occurrence and identification of C30, C31 and C32 alkan-1,15-diols and alkan-15-one-1-ols in Unit I and Unit II Black Sea sediments. Geochimica et Cosmochimica Acta 45, 2281–2285.

Eglinton G, Hamilton R J (1967). Leaf epicuticular waxes. Science, 156: 1322–1335

Fowler, D. (2018). *Black Death Consequences • History Of The Plague*. [online] History in Numbers. The Black Death. Available at: https://blackdeath.info/consequences/ [Accessed 14 Sep. 2018].

Gagan, Michael K.; Ayliffe, LK; Hopley, D; Cali, JA; Mortimer, GE; Chappell, J; McCulloch, MT; Head, MJ (1998). Temperature and Surface-Ocean Water Balance of the Mid-Holocene Tropical Western Pacific. Science. 279 (5353): 1014–8.

Gautam, R., Hsu, N., Lau, K. and Kafatos, M. (2009). Aerosol and rainfall variability over the Indian monsoon region: distributions, trends and coupling. *Annales Geophysicae*, 27(9), pp.3691-3703.

Ghosh S, Vittal H, Sharma T, Karmakar S, Kasiviswanathan KS, Dhanesh Y, et al. (2016) Indian Summer Monsoon Rainfall: Implications of Contrasting Trends in the Spatial Variability of Means and Extremes. PLoS ONE11(7): e0158670. https://doi.org/10.1371/journal.pone.0158670

Google Maps (2018). *Google Maps, CNES/Airbus Maps data*. [online] Google Maps. Available at: https://www.google.com/maps/@25.1198621,98.5715103,1600a,35y,38.72t/data=!3m1!1e3 [Accessed 1 Oct. 2018].

Goswami, B.N. and Ajaya Mohan, R.S. (2001). Intraseasonal Oscillations and Interannual Variability of the Indian Summer Monsoon: Journal of Climate: Vol 14, No 6. [online] Available at: http://journals.ametsoc.org/doi/full/10.1175/1520-0442(2001)014%3C1180%3AIOAIVO%3E2.0.CO%3B2 [Accessed 13 Oct. 2017].

Häggi, C., Sawakuchi, A., Chiessi, C., Mulitza, S., Mollenhauer, G., Sawakuchi, H., Baker, P., Zabel, M. and Schefuß, E. (2016). Origin, transport and deposition of leaf-

wax biomarkers in the Amazon Basin and the adjacent Atlantic. Geochimica et Cosmochimica Acta, 192, pp.149-165.

Hou, J., Huang, Y., Wang, Y., Shuman, B., Oswald, W., Faison, E. and Foster, D. (2006). Postglacial climate reconstruction based on compound-specific D/H ratios of fatty acids from Blood Pond, New England. Geochemistry, Geophysics, Geosystems, 7(3), pp.1525-2027.

Huang, Y., Shuman, B., Wang, Y. and Webb, T. (2004). Hydrogen isotope ratios of individual lipids in lake sediments as novel tracers of climatic and environmental change: a surface sediment test. *Journal of Paleolimnology*, 31(3), pp.363-375.

IBEF (India Brand Equity Foundation) (2018). Agriculture in India: Industry Overview, Market Size, Role in Development...| IBEF. The Economic Survey 2016–17, Agricultural and Processed Food Products Export Development Authority (APEDA), Department of Commerce and Industry, Union Budget 2017–18, Press Information Bureau, Ministry of Statistics and Programme Implementation, Press Releases, Media Reports, Ministry of Agriculture and Farmers Welfare, Crisil

Ishiwatari R, Hirakawa Y, Uzaki M, Yamada K, Yada T (1994). Organic geochemistry of the Japan Sea sediments. 1. Bulk organic matter and hydrocarbon analyses of core KH-79-3, C-3 from the Oki Ridge fro paleoenvironment assessments. Journal of Oceanogrphy, , 50: 179– 195

Ji, J., Shen, J., Balsam, W., Chen, J., Liu, L. and Liu, X. (2005). Asian monsoon oscillations in the northeastern Qinghai–Tibet Plateau since the late glacial as interpreted from visible reflectance of Qinghai Lake sediments. *Earth and Planetary Science Letters*, 233(1-2), pp.61-70.

Kaufman, D. Ager, T.A., Anderson, N.J., Anderson, P.M., Andrews, J.T., Bartlein, P.T., Brubaker, L.B., Coats, L.L., Cwynar, L.C., Duvall, M.L., Dyke, A.S., Edwards, M.E., Eisner, W.R., Gajewski, K., Geirsdóttir, A., Hu, F.S., Jennings, A.E., Kaplan M.R., Kerwin, M.W., Lozhkin, A.V., MacDonald, G.M., Miller, G.H., Mock, C.J., Oswald, W.W., Otto-Bliesner, B.L., Porinchu, D.F., Rühland, K., Smol, J.P., Steig, E.J., Wolfe, B.B (2004). Holocene thermal maximum in the western Arctic (0–180°W). *Quaternary Science Reviews*, 23(5-6), pp.529-560.

Kitoh, A. , Yukimoto, S. , Noda, A. , Motoi, T. (1997) Simulated changes in Asian Summer Monsoon at times of increased atmospheric CO2 :Journal of the Meteorological Society of Japan, Vol. 75, No. 6, pp. 1019-103

Kutzhach, J.E., Street-Perrott, F.A. Milankovitch forcing of fluctuations in the level of tropical lakes from 18 to 0 Kyr BP Nature, 317 (1985), pp. 130-134

Lean, J., Beer, J. and Bradley, R. (1995). Reconstruction of solar irradiance since 1610: Implications for climate change. *Geophysical Research Letters*, 22(23), pp.3195-3198.

Leng, P. and Dean, D. (2014). Oxygen isotopes and lakes - Climatica. [online] Climatica. Available at: http://climatica.org.uk/oxygen-isotopes-lakes [Accessed 3 Sep. 2018].

Madhusudhan, L. (2015). Agriculture Role on Indian Economy. *Business and Economics Journal*, [online] 06(04). Available at: https://www.omicsonline.org/open-access/agriculture-role-on-indian-economy-2151-6219-1000176.php?aid=62176.

Mangerud, J. and Svendsen, J. (2017). The Holocene Thermal Maximum around Svalbard, Arctic North Atlantic; molluscs show early and exceptional warmth. The Holocene, 28(1), pp.65-83.

Mayewski, P., Rohling, E., Stager, J., Karle´n, W., Maasch, K., Meeker, L., Meyerson, E., Gasse, F., van Kreveld, S., Holmgren, K., Lee-Thorp, J., Rosqvist, G., Rack, F., Staubwasser, M., Schneider, R. and Steig, E. (2004). Holocene Climate Variability. *Quaternary Research*, 62, pp.243-255.

Müller, P.J., Kirst, G., Ruhland, G., von Storch, I., Rosell-Melé, A., 1998. "Calibration of the alkenone paleotemperature index $U^{K'}_{37}$ based on core-tops from the eastern South Atlantic and the global ocean (60°N–60°S)." *Geochimica et Cosmochimica Acta* Vol.62, p.1757–1772

Paul, S., Ghosh, S., Oglesby, R., Pathak, A., Chandrasekharan, A. and Ramsankaran, R. (2016). Weakening of Indian Summer Monsoon Rainfall due to Changes in Land Use Land Cover. *Scientific Reports*, 6(1).

Rampen, S., Willmott, V., Kim, J., Uliana, E., Mollenhauer, G., Schefuß, E., Sinninghe Damsté, J. and Schouten, S. (2012). Long chain 1,13- and 1,15-diols as a potential proxy for palaeotemperature reconstruction. *Geochimica et Cosmochimica Acta*, 84, pp.204-216.

Rampen, S., Datema, M., Rodrigo-Gámiz, M., Schouten, S., Reichart, G. and Sinninghe Damsté, J. (2014a). Sources and proxy potential of long chain alkyl diols in lacustrine environments. *Geochimica et Cosmochimica Acta*, 144, pp.59-71.

Rampen, S., Willmott, V., Kim, J., Rodrigo-Gámiz, M., Uliana, E., Mollenhauer, G., Schefuß, E., Sinninghe Damsté, J. and Schouten, S. (2014b). Evaluation of long chain 1,14-alkyl diols in marine sediments as indicators for upwelling and temperature. Organic Geochemistry, 76, pp.39-47.

Rao, Z., Zhu, Z., Wang, S., Jia, G., Qiang, M. and Wu, Y. (2009). CPI values of terrestrial higher plant-derived long-chain n-alkanes: a potential paleoclimatic proxy. *Frontiers of Earth Science in China*, 3(3), pp.266-272.

Shen, J., Jones, R., Yang, X., Dearing, J. and Wang, S. (2006). The Holocene vegetation history of Lake Erhai, Yunnan province southwestern China: the role of climate and human forcings. The Holocene, 16(2), pp.265-276.

Theroux, S., Toney, J., Amaral-Zettler, L., Huang, Y., 2013. Production and temperature sensitivity of long chain alkenones in the cultured haptophyte Pseudoisochrysis paradoxa, Organic Geochemistry (2013)

Turner, A. and Annamalai, H. (2012). Climate change and the South Asian summer monsoon. Nature Climate Change, 2(8), pp.587-595.

UNICEF (2018). *16 Million Children Affected by Massive Flooding in South Asia, with Millions More at Risk*. [online] UNICEF USA. Available at: https://www.unicefusa.org/press/releases/16-million-children-affected-massive-flooding-south-asia-millions-more-risk/32783 [Accessed 25 Sep. 2018].

U.S. Geological Survey, EROS Data Center (2018). Elevation Map - high resolution. IIASA LUC Project [online] China-food-security.org. Available at: http://www.china-food-security.org/data/maps/dem/dem_h.htm [Accessed 10 Sep. 2018].

Versteegh, G., Bosch, H. and De Leeuw, J. (1997). Potential palaeoenvironmental information of C24 to C36 mid-chain diols, keto-ols and mid-chain hydroxy fatty acids; a critical review. Organic Geochemistry, 27(1-2), pp.1-13.

Wang, B., Wu, R. and Lau, K. (2001). Interannual Variability of the Asian Summer Monsoon: Contrasts between the Indian and the Western North Pacific–East Asian Monsoons*. *Journal of Climate*, 14(20), pp.4073-4090.

Wang, Y.F., Zhu, Y.X, Pan, H.X., Yin, Y. (2002). Environmental characteristics of an acid Qinghai Lake in Tengchong, Yunnan Province J. Lake Science., 14 (2), pp. 117-124

Wang, Y., Cheng, H., Edwards, R. and Li, X. (2005). The Holocene Asian Monsoon: Links to Solar Changes and North Atlantic Climate. *Science*, 308(5723), pp.854-857.

Wang, T., Surge, D. and Mithen, S. (2012). Seasonal temperature variability of the Neoglacial (3300–2500 yr BP) and Roman Warm Period (2500–1600 yr BP) reconstructed from oxygen isotope ratios of limpet shells (Patella vulgata), Northwest Scotland. *Palaeogeography, Palaeoclimatology, Palaeoecology*, 317-318, pp.104-113.

Xavier, P., Marzin, C. and Goswami, B. (2007). An objective definition of the Indian summer monsoon season and a new perspective on the ENSO–monsoon relationship. *Quarterly Journal of the Royal Meteorological Society*, Vol. 133(624), pp.749-764.

Xiao, X., Haberle, S., Shen, J., Yang, X., Han, Y., Zhang, E. and Wang, S. (2014). Latest Pleistocene and Holocene vegetation and climate history inferred from an alpine lacustrine record, northwestern Yunnan Province, southwestern China. *Quaternary Science Reviews*, 86, pp.35-48.

Xiao, X., Shen, J., Haberle, S., Han, Y., Xue, B., Zhang, E., Wang, S. and Tong, G. (2015). Vegetation, fire, and climate history during the last 18 500 yr BP in south-western Yunnan Province, China. *Journal of Quaternary Science*, 30(8), pp.859-869.

Xu, H., Zhou, X., Lan, J., Liu, B., Sheng, E., Yu, K., Cheng, P., Wu, F., Hong, B., Yeager, K. and Xu, S. (2015). Late Holocene Indian Summer Monsoon Variations Recorded at Lake Erhai, Southwestern China. *Quaternary Research*, 83(02), pp.307-314.

Yamada K, Ishiwatari R (1999). Carbon isotopic composition of longchain n-alkanes in the Japan Sea sediments: implication for paleoenvironmental changes over the past 85 kyr. Organic Geochemistry, 30: 367–377

Yang, Y., Zhang, H., Chang, F., Meng, H., Pan, A., Zheng, Z. and Xiang, R. (2016). Vegetation and climate history inferred from a Qinghai Crater Lake pollen record from Tengchong, southwestern China. Palaeogeography, Palaeoclimatology, Palaeoecology, 461, pp.1-11.

Zhang, D., Jim, C., Lin, G., He, Y., Wang, J. and Lee, H. (2006). Climatic Change, Wars and Dynastic Cycles in China Over the Last Millennium. *Climatic Change*, 76(3-4), pp.459-477.

Zhao, M., Dupont, L., Eglinton, G. and Teece, M. (2003). n-Alkane and pollen reconstruction of terrestrial climate and vegetation for N.W. Africa over the last 160 kyr. *Organic Geochemistry*, 34(1), pp.131-143.

Zhao, Y., Yu, Z., Chen, F., Zhang, J. and Yang, B. (2009). Vegetation response to Holocene climate change in monsoon-influenced region of China. *Earth-Science Reviews*, 97(1-4), pp.242-256.

Zhisheng, A., Clemens, S., Shen, J., Qiang, X., Jin, Z., Sun, Y., Prell, W., Luo, J., Wang, S., Xu, H., Cai, Y., Zhou, W., Liu, X., Liu, W., Shi, Z., Yan, L., Xiao, X.,

Chang, H., Wu, F., Ai, L. and Lu, F. (2011). *Glacial-Interglacial Indian Summer Monsoon Dynamics*. Vol. 333, Issue 6043, pp. 719-723

Zhou, W., Xie, S., Meyers, P. and Zheng, Y. (2005). Reconstruction of late glacial and Holocene climate evolution in southern China from geolipids and pollen in the Dingnan peat sequence. *Organic Geochemistry*, 36(9), pp.1272-1284.

7 Appendices: Respective sample n-alkane concentrations

	Depth (cm)	Age (cal yr B	C16 n-alkane (ug/g)	C17 n-alkane (ug/g)	C18 n-alkane (ug/g)	C19 n-alkane (ug/g)	C20 n-alkane (ug/g)	C21 n-alkane (ug/g)	C22 n-alkane (ug/g)	C23 n-alkane (ug/g)	C24 n-alkane (ug/g)
2693	1	-15.568	0.06125099	0.03419847	0.127946513	0.036240169	0.067546231	0.166922284	0.155022873	0.54538964	0.240301981
2694	4	138.728	0.380326114	0.190163057	0.309934264	0.268959904	0.223783045	1.075648848	0.93073221	3.767832589	1.881875215
2695	7	293.024	0.08807824	0.062277543	0.176749599	0.129596602	0.111506458	0.282882443	0.270783602	1.00017092	0.509879761
2696	13	601.616	0.4474239	0.179836241	0.60125972	0.286004624	0.390006305	1.252271276	1.163875657	4.45976947	2.275134873
2697	16	755.912	0.130201524	0.0581021	0.224749488	0.18539852	0.17958831	0.822460403	0.755760558	2.555630237	1.328353078
2698	19	910.208	0.132710479	0.044236826	0.099532859	0.104559771	0.115618978	0.542985718	0.531266602	1.765680178	0.959014344
2699	22	1133.04	0.108679122	0.064203178	0.171447592	0.191533502	0.183642609	0.888435703	0.962297808	3.291044568	1.765025596
2700	25	1434.3	0.170923567	0.090732554	0.29779855	0.208195446	0.234925784	1.157084031	1.200236975	3.850851722	2.031114004
2701	28	1735.56	0.612904434	0.219260791	0.739844892	0.219260791	0.393643642	1.350132771	1.327713592	4.12512891	2.239426866
2702	31	2036.82	2.126154233	0.61025921	2.769852303	0.606079352	1.279036426	3.673097068	3.424073538	9.641541456	5.191599245
2703	34	2338.08	0.029385892	0.013271048	0.050240396	0.037443314	0.073938695	0.484334332	0.441978098	1.310280902	0.710848107
2704	37	2639.34	0.078962735	0.050429982	0.256794777	0.147308631	0.210346109	0.901082846	0.895926435	2.923685115	1.622980406
2705	40	2940.6	0.208253367	0.085751386	0.349538984	0.331572027	0.209070047	0.707618267	0.677473094	2.759076606	1.415236534
2905	43	3241.86	0.285501949	0.212382989	0.326449722	0.291782495	0.288893559	1.041103963	1.038297753	5.126945931	4.184059323
2906	46	3543.12	0.034349264	0.037415508	0.045500736	0.041709008	0.046764645	0.243087954	0.186612975	1.028826794	0.967440947
2907	49	3844.38	0.263708564	0.100460405	0.235168676	0.191788047	0.117584338	0.805065481	0.645383071	3.719269453	1.843444704
2908	52	4145.64	0.158681777	0.114159552	0.151832204	0.163248159	0.121009125	0.751838011	0.541145943	3.17812351	1.623437829
2909	55	4446.9	0.23786359	0.112550089	0.187970252	0.284275998	0.11835164	0.694283991	0.67850481	3.606670085	1.767268342
2910	58	4748.16	0.206220069	0.089129013	0.133693519	0.687691502	0.075147991	0.480416248	0.487206583	2.514121776	1.327510621
2911	61	5049.42	0.240074452	0.117646046	0.276420385	0.337634588	0.182686137	0.434810885	0.793436957	2.140607435	1.057296554
2912	64	5350.68	0.435357143	0.142893295	0.339204645	0.47141433	0.209665863	0.573366974	0.848375568	4.57136927	1.590379888
2913	67	5651.94	0.253971426	0.109290983	0.200887235	0.24980796	0.105127517	0.378136817	0.48126504	2.048409601	0.960507957
2914	70	5953.2	0.047185948	0.032667195	0.322134837	0.130668779	0.238652006	0.278534345	0.423090145	1.531938899	0.879674926
2915	73	6254.46	0.145602354	0.075834559	0.112235148	0.085945834	0.054600883	0.316259883	0.320188577	1.400579482	0.734665815
2916	76	6418.496	0.558605102	0.112687494	0.414429215	0.114550098	0.155527368	0.588011796	0.569919126	2.636102115	1.291816685
2917	79	6513.734	0.263651485	0.125632587	0.187564143	0.098205754	0.128286796	0.709865933	0.531110347	2.755242351	1.270195944
2918	82	6608.972	0.09861333	0.038172902	0.083503223	0.034196558	0.054873546	0.24256376	0.191579021	1.028964739	0.392427994
2919	85	6704.21	0.142489146	0.079160636	0.153664765	0.085679748	0.099649272	0.550017188	0.421559226	2.525736824	0.810551646
2920	88	6799.448	0.213875438	0.07308693	0.261574277	0.070009586	0.163868591	0.709940664	0.553006412	3.238824039	0.993916929
2921	91	6894.686	0.729099003	0.212336766	0.896533012	0.105787851	0.419346086	0.526360535	0.514532208	1.970894924	0.764405608
2922	94	6989.924	0.541824851	0.177354081	0.558095868	0.103320955	0.244878799	0.567402789	0.482055294	2.094174638	0.918275823
2970	97	7085.162	0.141557844	0.11122402	0.381195052	0.12740206	0.192114217	0.624662378	0.538231105	2.915091097	1.094141335
2971	103	7275.638	0.181421835	0.100880303	0.275793731	0.099253201	0.159455962	0.47099173	0.412512891	2.271191664	0.815542727
2972	106	7370.876	0.202862422	0.084711781	0.299277804	0.051830234	0.161063846	0.271760461	0.283670282	1.285177957	0.605235449
2973	109	7466.114	0.399006451	0.164891555	0.644788202	0.117446343	0.346116707	0.574193768	0.566638587	2.49774289	1.220917275
2974	112	7561.352	0.232119695	0.086605265	0.268168587	0.038246995	0.127489984	0.288673617	0.261343571	1.417746168	0.587596002
2975	115	7656.59	0.185291162	0.065599977	0.210610451	0.046035071	0.13235083	0.374503573	0.294013253	1.530434005	0.696464854
2976	118	7751.828	0.206128089	0.099338838	0.261385317	0.067053716	0.148387389	0.429399384	0.307575401	1.713979	0.777984838
2977	121	7847.066	0.181539831	0.103737046	0.553804543	0.068077436	0.272850043	0.519577305	0.3736758	1.799102023	0.868061478
2978	124	7942.304	0.09930996	0.08339842	0.173929599	0.052124012	0.105345372	0.375205524	0.290997466	1.687358932	0.753608822
2979	127	8037.542	0.11747335	0.071270442	0.230031497	0.040304664	0.098795579	0.433520492	0.328482487	2.083572056	0.802108399
2980	130	8132.78	0.147836619	0.108451574	0.413257577	0.08904445	0.281974093	0.450215682	0.429146475	2.013772608	0.969183513
2981	133	8228.018	0.099680315	0.069599273	0.19523186	0.048365597	0.096731193	0.323135098	0.273862725	1.570986593	0.689813223
2982	136	8323.256	0.083322022	0.075258601	0.152309073	0.055548015	0.109304158	0.466470273	0.348112144	2.104337912	0.884204847
2983	142	8645.054	0.032172237	0.031099829	0.126544133	0.031636033	0.072923738	0.266675	0.232298926	1.600050002	0.758357032
2984	146	8877.102	0.026617714	0.02480287	0.056260169	0.029642455	0.046581	0.257379838	0.253854087	1.909781903	0.808572276

Respective sample N-alkane concentrations

	C25 n-alkane (ug/g)	C26 n-alkane (ug/g)	C27 n-alkane (ug/g)	C29 n-alkane (ug/g)	C30 n-alkane (ug/g)	C31 n-alkane (ug/g)	C32 alkane (ug/g)	C33 alkane (ug/g)	C34 n-alkane (ug/g)
2693	0.82998387	0.303104424	1.342230403	2.302810129	0.368375872	1.385742268	0.140122954	0.391606783	0.03355576
2694	6.257949467	2.204365761	9.736443473	13.33637732	3.292539116	10.53566977	1.040588089	2.955543412	0.257300775
2695	1.673096977	0.570950105	3.090236447	5.609730388	0.766131831	3.487442379	0.33550404	1.061786733	0.091267383
2696	7.658849033	2.677124476	12.29843065	23.01905576	4.010255736	14.65809518	1.526151188	4.890727575	0.457845356
2697	4.613063934	1.40634059	5.595011596	6.591524659	1.243208715	5.077580345	0.683993745	2.185918086	0.19231958
2698	3.281352542	1.136754274	4.506059212	5.046437686	0.862862402	3.418765427	0.442325928	1.27686204	0.115484109
2699	5.973075172	2.060474018	8.344112635	10.25640228	1.916176416	7.648381239	1.047872539	3.072101093	0.040422383
2700	6.410040739	2.281986206	8.25818475	9.587360025	2.011305741	7.238252832	1.060729194	2.899054482	0.263550407
2701	6.6933704	2.613079847	8.49245572	10.94348515	2.328755855	8.145087603	1.147704258	3.304165527	0.352926007
2702	14.58141039	5.483931215	16.39665037	20.10174982	4.780091628	16.89791077	2.572734092	7.959773551	0.782087007
2703	1.983376713	0.777144821	2.313293012	2.746778647	0.620439156	2.020536125	0.300974624	0.813555979	0.074986852
2704	5.259539361	1.983929185	7.514093419	11.58968017	2.312471238	9.018350207	1.163426139	3.516164289	0.325011505
2705	5.10564032	1.696062617	9.520690998	15.86250841	2.568232504	12.20928174	1.221282169	3.773584906	0.27257602
2905	9.254881052	3.485312998	20.4425995	35.40044642	6.045123986	30.36649542	2.454364166	7.478923461	0.403843083
2906	1.681972204	0.527918283	2.766638179	5.546972586	0.523195933	2.462581903	0.169833235	0.438279315	0.021913966
2907	5.271737322	1.809733974	9.750654415	22.58658314	1.303880963	10.39393535	0.744721385	2.107982127	0.108862927
2908	4.64187893	1.468191042	8.335436367	14.49608836	1.578512438	7.368040814	0.549262949	1.548822548	0.08659551
2909	4.956917199	1.816860056	9.872780448	12.76722016	2.107333167	8.57267156	0.699091433	2.092244863	0.138309456
2910	3.795797631	1.22735317	7.268402523	9.864801653	1.878649115	7.573304245	0.710174817	2.213851628	0.181804753
2911	2.188919755	0.8844871	7.487469061	12.4936257	1.382652786	7.421134895	0.611518099	2.091599192	0.17620013
2912	5.448283466	1.426931384	9.704579068	17.22685792	1.94496783	10.79283488	0.949329536	3.221352968	0.251803871
2913	2.804683235	0.936242493	6.253214585	12.32821707	1.955821445	8.242873772	0.694801621	2.3235249	0.203026448
2914	2.222986135	0.712201743	4.525233932	8.413277166	0.839754406	6.11231076	0.534925523	1.976471144	0.143564571
2915	2.386681727	0.777881452	4.435386672	10.28422414	0.929152149	4.796967107	0.390068591	1.295115377	0.08984726
2916	4.678764632	1.503500932	7.425662638	10.12223379	1.085894672	7.215749913	0.61157265	2.504823956	0.145324194
2917	4.341698178	1.528016501	6.824282865	8.686148182	1.372909956	7.165592882	0.580994017	2.017180549	0.141892928
2918	1.504822307	0.500577441	2.438852033	4.886321918	0.60324962	2.023471581	0.184422027	0.530859665	0
2919	3.649291672	0.971576414	5.074236442	6.76564859	0.66203244	4.410185611	0.427899016	1.225163692	0.108993146
2920	3.235834815	1.077615197	5.023776653	7.718241661	0.847022416	5.300559568	0.508546923	1.45394399	0.118383054
2921	3.203997974	0.943309048	4.879038443	7.204746424	1.035847242	6.2084857	0.559159578	1.773146155	0.156696637
2922	3.6920694	1.085809794	5.538188108	7.708678258	1.541030375	6.75126465	0.666486821	2.128173526	0.220399081
2970	3.940480283	1.22575259	5.86417724	8.48289615	3.878771941	7.707141761	0.663993163	2.171674008	0.192842899
2971	3.660459217	1.066843684	5.504687448	7.391303581	1.087889864	7.558806883	0.752883261	2.579550844	0.169266494
2972	2.786898114	0.77955192	4.007667472	4.993278279	0.562861074	4.807268397	0.468648276	1.695830359	0.108707074
2973	5.794823945	1.473260325	7.533347156	10.19842253	0.439965005	7.937912678	0.837787768	2.789816412	0.20902552
2974	2.876487406	0.752430346	4.020736328	6.062546269	0.998514614	5.336527056	0.574527016	1.773125665	0.117192078
2975	3.123471592	0.932346209	5.028453414	8.698775437	1.215957857	6.768208501	0.713361943	2.191218415	0.119725081
2976	3.319401977	1.068673747	5.868137132	10.0018031	1.582419002	8.911871641	0.898857052	2.800181924	0.162816921
2977	3.940390313	1.192403675	6.356053767	10.21441728	1.678007562	9.18747197	0.981277276	3.074981059	0.185014093
2978	3.51009031	1.038210739	5.522319374	7.961224851	1.291395099	7.099105655	0.751530113	2.315235965	0.148641241
2979	3.937970284	1.198388144	6.313809207	10.04542278	1.604284911	8.465638902	0.927843398	2.907100612	0.190681938
2980	4.117366571	1.163241996	6.060448614	10.7217612	1.223841971	9.069024044	0.978529262	3.097645097	0.204117988
2981	3.619800619	0.985447462	5.050621261	8.357621312	1.33583883	7.328578003	0.664723628	2.38150023	0.131666411
2982	4.715178995	1.30193942	6.642705548	9.434933136	1.401939025	9.35532164	0.953396207	3.031062076	0.176698686
2983	3.261560257	0.90836172	4.60425702	6.410167018	1.072622219	5.540913042	0.601969999	1.786154225	0.109237799
2984	4.389560251	1.1705494	6.45188358	9.338908096	1.490711569	7.264760601	0.820743573	2.378320832	0.152086668

Respective sample n-alkane, hopane and acid concentrations

	C35 n-alkane (ug/g)	C29 BA Hopane (ug/g)	C29 BB (ug/g)	C30 BB (ug/g)	C31 BB (ug/g)	C16 acid (ug/g)	C18 acid (ug/g)	C20 acid (ug/g)	C22 acid (ug/g)
2693	0.072273945	0.070061477	0.064899052	0.034293249	0.077805114	1.751350218	2.211178942	0.673085033	3.024827917
2694	0.560141509	0.546479521	0.633005446	0.268685765	0.728639362	5.310582822	8.025322594	2.556506705	10.48958421
2695	0.237166649	0.171608388	0.210814799	0.082911918	0.269945779	2.990940353	4.395960616	1.116658806	4.381825695
2696	1.155179053	0.709073321	0.805338242	0.319317787	0.943865811	8.497141188	17.12585177	4.423461212	17.69384485
2697	0.569517804	0.185451024	0.251847069	0.130502572	0.331980228	1.44675396	2.156712432	1.015417137	2.760927588
2698	0.248399782	0.098052546	0.145989346	0.296336583	0.139452509	2.033370515	3.100393323	1.265075483	3.16748066
2699	0.760251738	0.291507568	0.381680576	0.173349834	0.410442656	2.890620682	4.610117413	2.091363523	5.698538211
2700	0.635621571	0.276605536	0.387574129	0.196642874	0.407156821	3.585258669	5.658446368	2.338744746	6.065184584
2701	0.728083573	0.283452383	0.397389126	0.177852476	0.475199584	5.963071634	10.28561371	2.737941142	7.266544682
2702	1.974845183	0.465024707	0.79114593	0.374435478	0.721694188	3.436226913	6.016579462	2.370771377	5.976734565
2703	0.148946486	0.083204589	0.145864835	0.060605812	0.146892052	0.730353491	2.259063362	1.106941047	3.185279341
2704	0.770823746	0.290497009	0.428554993	0.212839393	0.470260009	3.81390593	5.703381968	2.403643417	8.012144725
2705	0.792948423	0.552231937	0.569931679	0.332755142	0.785868526	4.700330345	5.319804594	2.620976898	12.6377797
2905	1.339882479	1.715550463	1.055000924	0.889080897	2.016084851	9.273402613	11.13610663	4.733275616	25.2154501
2906	0.043827932	0.158876252	0.117787566	0.098612846	0.210921921	2.125328659	3.147628285	0.888564922	4.141616164
2907	0.33648541	0.601220254	0.482460698	0.353804512	0.979766341	5.039910284	4.815448612	2.720592436	7.168761069
2908	0.242467428	0.593797782	0.457719124	0.442874179	1.039146119	3.766739231	5.373170062	1.754782121	8.039350649
2909	0.369663455	0.729268041	0.633708781	0.570840846	1.2875353	3.902242784	6.650287511	1.534681733	6.484375972
2910	0.513219667	0.58139645	0.655254631	0.46587468	0.952581154	2.544876165	3.758783945	0.832971511	3.279825326
2911	0.516162734	0.659195781	0.671633437	0.482995651	1.019887812	5.156690433	6.621701401	1.390443323	4.456256881
2912	0.865394912	0.694631368	0.720680044	0.509396336	1.198239109	8.534938457	15.0058639	1.432160924	4.407873066
2913	0.527868764	0.480495926	0.460193281	0.356424208	0.798570694	3.711054974	6.784277344	1.017021467	3.162688707
2914	0.652923801	0.635224059	0.424793798	0.344161642	0.831887854	2.013528394	2.486900522	0.454129661	1.719205143
2915	0.271733176	0.302412728	0.306795521	0.197225692	0.547849144	3.196026877	3.951854842	1.421703876	5.494042097
2916	0.575241601	0.607535867	0.5994623	0.472303631	1.237274041	2.793025509	4.050460976	1.143006796	4.250209736
2917	0.347062433	0.446770977	0.385411873	0.270363553	0.751649026	2.239263804	2.740996879	1.275617779	4.828371426
2918	0.09996708	0.14995062	0.136162057	0.091349228	0.280941966	1.355667379	1.724672194	0.758097668	2.454341199
2919	0.256335731	0.35725531	0.320924262	0.248262165	0.756896844	2.061134431	2.652219653	1.165201103	2.718802573
2920	0.288454484	0.515216391	0.403502805	0.536892161	0.960403369	3.231972971	4.290255985	1.145901705	2.796000161
2921	0.420606762	0.409060694	0.33648541	0.232570798	0.66307419	2.242892011	2.339709495	0.761765882	1.86814014
2922	0.571274418	0.521905024	0.38613919	0.373796841	0.853385242	2.642032767	3.160265191	1.250534385	3.664356571
2970	0.525935178	0.578528696	0.512786799	0.458001885	1.082549909	4.820333041	7.45792118	2.7952144	9.361558573
2971	0.507799483	0.613591042	0.440798162	0.444324547	1.214839735	3.530545566	5.341429816	1.76431983	5.923073717
2972	0.322497654	0.304379808	0.205335585	0.258481266	0.591849627	2.5151764	3.944644813	1.195346913	3.333689724
2973	0.564706041	0.51919242	0.352309142	0.348937763	0.890044148	3.959639542	4.661779984	1.751642976	4.541296605
2974	0.388734697	0.293456585	0.191509005	0.1362477	0.435420972	1.567402101	1.927734069	0.675754606	1.870111583
2975	0.391600787	0.306795521	0.319266883	0.288088477	0.764494529	1.502984355	1.86504353	0.726818435	2.550721299
2976	0.526127406	0.322942653	0.353891324	0.286611605	0.8154302	2.220787142	2.663316806	0.9913457	3.499302359
2977	0.697901261	0.307966496	0.316163323	0.256443584	0.784553431	1.988791583	1.944289037	0.585861928	1.879908606
2978	0.503001958	0.243771635	0.263986843	0.206908607	0.621914951	1.585263392	2.020198058	0.83030794	2.726286699
2979	0.694550971	0.269511343	0.299338685	0.213052445	0.674310988	1.627471029	1.938611041	0.661821896	2.208025264
2980	0.7496697	0.315455072	0.332774174	0.246178664	0.766988802	2.391318689	2.686585031	0.795773288	2.632173182
2981	0.553510252	0.304238891	0.302960577	0.254384619	0.71713453	1.826857532	2.649630317	0.723904304	2.551235557
2982	0.578639653	0.417474918	0.421358405	0.330096446	0.976697133	3.27198364	3.779212835	1.046222762	2.145824237
2983	0.409060694	0.221961911	0.2463661	0.163856699	0.536892161	1.63599182	2.19151965	0.830605115	1.271464753
2984	0.479859661	0.343506096	0.312039889	0.163886496	0.507392592	1.555590513	2.667110705	0.836175248	1.391222611

Respective sample acid concentrations and calculated ACL and CPI values

	C24 acid (ug/g)	C26 acid (ug/g)	C28 acid (ug/g)	C30 acid (ug/g)	C32 acid (ug/g)	C34 acid (ug/g)	ACL (C27--C35)	CPI (C27--C33) (woC28)	CPI (woC28 and C29)
2693	15.36428746	21.64018468	22.86194836	14.3618147	6.244569939	2.739396066	29.37984028	8.34224274	4.799413368
2694	51.65345352	79.94067659	84.5222904	51.58557776	21.39783341	8.908693527	29.45203631	6.779126332	4.306505649
2695	20.34907707	29.81376408	31.27593688	18.46220678	7.056045508	3.130627242	29.47934042	9.514032564	5.485776223
2696	82.8472136	124.6476001	126.2212096	72.25305413	27.59357435	12.18993245	29.55716681	7.91657167	4.595189068
2697	14.577417	21.12050521	18.21906973	11.45445665	5.359821224	2.555640563	29.55575252	7.505628438	4.9620065
2698	16.82701801	25.20041861	25.82981202	16.75914225	6.571607693	2.961851355	29.30512551	7.931945502	5.122588447
2699	29.34434217	44.33571278	45.4804283	30.74588489	12.56251908	5.591495057	29.51388997	7.797349308	5.069858474
2700	28.40576495	37.36343975	34.65996266	22.09765175	9.319678848	4.205408803	29.46718367	6.807849592	4.475374517
2701	36.43649505	49.94082021	48.54789156	32.76923658	14.44081391	6.5632909	29.5342827	6.568577801	4.241147589
2702	33.0250313	45.98021577	43.45758909	30.26296887	15.0160422	7.952687495	29.70566919	6.161017376	4.14251781
2703	16.41623743	21.13845104	15.04902569	9.105048405	4.421620951	2.210810475	29.44291188	6.285123371	4.098211218
2704	35.79767593	45.63966116	40.12814944	27.06885317	13.08644657	6.230994787	29.66950657	7.059308356	4.473355354
2705	49.20470494	68.61926084	61.85256967	41.03455189	19.51480318	8.922007619	29.59842982	8.862159855	5.463816754
2905	78.21503927	86.74799199	62.16865547	30.03156084	11.1260838	6.848525683	29.60826882	9.170064165	5.705129973
2906	13.82726201	14.91327417	10.45286707	4.693123992	1.648411319	0.639971453	29.12506083	12.4354404	6.284544745
2907	18.60233738	15.62456209	9.020907486	2.872677335	1.173593789	1.331240716	29.25981708	16.20231358	8.040810478
2908	19.86351279	19.68834954	11.78848687	3.801042572	1.191110115	1.156077464	29.17865429	11.58315953	6.294371215
2909	21.6134224	21.63122588	13.99353378	5.358846904	1.887168677	1.388671291	29.23717422	9.25686318	5.708305768
2910	14.26564126	12.53606633	8.379723483	3.75411612	1.112827278	1.233495297	29.45726909	8.385305298	5.312561344
2911	17.28813957	17.18540869	12.9000634	6.824265621	2.186700167	2.113320966	29.37756441	11.91749491	6.869227985
2912	39.26036424	24.17913873	14.40502926	5.983312296	1.700736029	1.495828074	29.48442475	11.24508909	6.513996259
2913	16.57765626	14.27786579	10.52473552	5.79738846	1.772755149	1.405427505	29.55400988	9.170248557	5.291647182
2914	4.399741585	3.480808216	2.102408162	0.835393972	0.278464657	0.334157589	29.69176343	11.9628401	7.17636143
2915	19.92056597	21.96847462	12.89251582	5.135286087	1.334243515	1.163584461	29.35734331	12.34692666	6.24561816
2916	11.73178929	14.84692944	8.059353423	2.615002972	0.61445425	0.714481686	29.46872055	11.65809533	7.330534404
2917	15.2856212	17.2947437	9.90986099	3.461663771	0.950260643	0.814509123	29.43265181	9.437042699	6.117443116
2918	9.249406964	12.76369352	8.871133065	3.63631039	1.000595476	0.53690489	29.18963731	10.10580489	5.107557006
2919	9.002469249	8.173670492	4.001097444	1.34322557	0.314371942	0.50013718	29.28821855	11.52633807	7.063842666
2920	12.04056964	9.63245571	4.757205455	1.617213765	0.436765761	0.672855362	29.40940502	10.6200674	6.41581768
2921	6.352587278	6.632848481	3.468232393	1.389628467	0.338648954	0.385359155	29.59919485	9.679906996	6.20421166
2922	11.8837193	15.39141376	9.524451501	4.13183938	1.073529265	1.048563468	29.63295269	7.915908114	5.158050892
2970	44.4489264	78.68933846	60.95631128	28.82586571	10.11542758	4.406106491	29.62735724	4.65768019	3.026754816
2971	34.26555619	78.14294417	66.03453269	34.00341532	12.33310365	5.317714731	29.7422109	9.690860398	6.581239548
2972	17.70969441	45.40728022	38.19000253	20.56582089	7.362649391	3.044254568	29.65191178	11.0791043	7.510935305
2973	25.41984514	77.89452077	58.56111742	32.6042333	12.17288359	5.131705827	29.52909746	14.74341044	9.460129436
2974	8.903950656	25.19413311	15.33233321	8.202427271	2.934256466	1.288374678	29.68574216	8.782618946	5.685705433
2975	13.01448723	30.60258665	20.26339768	12.46706646	4.529465364	1.827679007	29.63236963	9.499799435	5.85727835
2976	15.96628409	35.42876522	24.16853385	15.69001783	6.316018108	2.838873901	29.72736847	9.100618874	5.800545691
2977	8.257008509	18.87671524	11.58136635	6.358559765	2.072542296	0.953369456	29.75006939	8.811440782	5.689879724
2978	13.13317035	34.61769004	22.52001967	13.70564188	5.859414463	2.087837337	29.65948473	8.939909966	5.831647751
2979	11.25983444	30.54409209	22.39900087	16.24493194	7.624710397	2.933741191	29.70706389	8.8094352	5.618371015
2980	14.11815812	41.25094588	27.16782041	18.5497884	8.075025924	3.406925254	29.77127504	10.31543766	6.494921521
2981	14.73356502	43.49478714	26.11859253	16.49833478	6.570373588	2.488777874	29.73517658	9.292268897	5.932973677
2982	19.6032069	53.29707794	30.46332853	19.2045442	7.657073101	3.148060575	29.72380825	9.512207533	6.359208256
2983	13.64919833	39.39262302	24.22136219	13.86310981	5.561698655	2.089750678	29.61183762	8.69152984	5.653927445
2984	18.44364247	53.42808557	32.00487128	17.19983366	6.618176688	2.422642518	29.54095624	8.814242672	5.577794889

Respective sample's calculated P_{Aq} P_{Wax} and short to long chain acid ratio values

	P(aq)	P(Ter)	Short to Long Chain Acid Ratio
2693	0.271602218	0.78530441	0.106451601
2694	0.295764723	0.770231484	0.097980415
2695	0.227117062	0.820111299	0.148515816
2696	0.243366427	0.804834936	0.129099826
2697	0.380548391	0.706595601	0.12143708
2698	0.373515737	0.719893991	0.120542144
2699	0.34098247	0.739134526	0.098400904
2700	0.378819355	0.709690694	0.162862818
2701	0.36173716	0.718264783	0.199818731
2702	0.395653679	0.687926025	0.128224835
2703	0.40859309	0.682516546	0.123764498
2704	0.284226044	0.774600028	0.141632625
2705	0.218850344	0.826986324	0.097389593
2905	0.17943915	0.857027226	0.221360752
2906	0.252864703	0.799006401	0.348142087
2907	0.214216822	0.826167288	0.828628126
2908	0.263440499	0.794316378	0.58628513
2909	0.286374281	0.784706068	0.545283315
2910	0.265702909	0.796562021	0.51951075
2911	0.178579269	0.863558541	0.597150444
2912	0.263402343	0.790137639	1.154620757
2913	0.190884903	0.846796356	0.643012657
2914	0.20540589	0.835351806	1.531903345
2915	0.200719228	0.837483378	0.396492138
2916	0.296714847	0.771969894	0.641114671
2917	0.309252647	0.761631377	0.372452714
2918	0.268307877	0.786761925	0.246280512
2919	0.355891727	0.724637628	0.881936603
2920	0.332145182	0.735914005	1.180064991
2921	0.278397788	0.779483664	0.943337333
2922	0.285794261	0.775591069	0.424880958
2970	0.297478417	0.7628633	0.136756031
2971	0.284058935	0.775200864	0.088686099
2972	0.293533252	0.77225895	0.109943506
2973	0.313768874	0.755829869	0.094569038
2974	0.273634716	0.782173879	0.148509528
2975	0.231297209	0.814949217	0.102901929
2976	0.210187884	0.831180667	0.122535911
2977	0.228288661	0.817779058	0.219236166
2978	0.256565591	0.798392969	0.099527829
2979	0.245450598	0.804789546	0.092280516
2980	0.236523303	0.808296302	0.11107107
2981	0.248636804	0.799796909	0.105040136
2982	0.266285736	0.788558353	0.141966951
2983	0.289163136	0.773001718	0.100500579
2984	0.275044281	0.785407433	0.085819054